



Glycerol to value-added chemicals: State of the art and advances in reaction engineering and kinetic modelling

Aya Sandid, Vincenzo Spallina, Jesús Esteban*

Department of Chemical Engineering, School of Engineering, The University of Manchester, Manchester M13 9PL, United Kingdom

ARTICLE INFO

Keywords:

Glycerol
Kinetic models
Thermodynamics
Process intensification
Value-added chemicals
Biofuels

ABSTRACT

The boom of the biodiesel industry has led to an oversupply of by-product glycerol as a direct consequence, which has been detrimental to its market value. The chemical reactivity that this compound possesses makes it an exceptional building block from which many synthetic routes can originate. In the past two decades, as a way to upgrade glycerol, there have been great developments in experimental approaches to obtain different products with applications as fuel additives, green solvents or precursors to other materials. These works have focused mainly on the development of catalytic and biotechnological processes and optimization of operation conditions to obtain chemicals like glycerol carbonate, acetals, esters, ethers, 1,2- and 1,3-propanediol, acrolein, halogenated products and different organic acids. Throughout these years an increasing amount of articles have reported thermodynamic information and kinetic models for different reactions using glycerol of substrate, whose knowledge is essential for subsequent reactor and process design. For the first time, these aspects for transformation reactions from glycerol are compiled and presented in a systematic way in this comprehensive review that also touches on process intensification strategies to enhance glycerol conversion.

1. Introduction

Over the past decades, there has been a growing consciousness about the declining availability of fossil resources as well as the pernicious effects that their use inflict on climate change and the environment in general. The energy total final consumption reached values of about 475 EJ in 2020, with estimations to increase to over 500 EJ by 2050 [1]. At the same time, CO₂ emissions from energy combustion and industrial processes reached a maximum of 36.3 Gt in 2021 after a brief circumstantial decrease in 2020, thus following the ever-growing trend observed in the last decades [2]. For these reasons, with the ambition to achieve carbon neutrality, throughout the years different policies have been implemented all over the world to make a transition to the use of renewable sources of energy. This has been met with notable increases in clean energy investments in the period 2015–2023, with projection to reach as much as USD 1.7 trillion by the end of 2023 [3]. In particular, regarding the context of fuels, biofuels have been an important target of legislative efforts [4–10].

Among biofuels, biogas [11,12] and bioethanol [13,14] have attracted a great deal of attention as alternatives to replace their fossil counterparts natural gas and gasoline, respectively. The other big player

in the biofuel business is biodiesel, which in addition to being a transportation fuel, in some regions is used for electricity generation in turbines and engines [15]. The history of the use of biodiesel runs as far back as the beginning of the 20th century, when Otto used it to operate a small diesel engine on peanut oil in the Paris Exposition. Despite the interest of several countries in the use of vegetable oils as source of fuel for Diesel engines, their properties (high viscosity and low cetane numbers) and, more importantly, their higher price compared to petrodiesel led to the use of the latter being predominant [15]. In the past two decades, the global biodiesel supply has undergone continuous growth from 3.9 billion litres in 2005 to 18.1 billion litres in 2010, 30.8 in 2016, 41.0 in 2018, 47.0 in 2019 [15,16]. Further to these data, the OECD and UN's FAO foresee a gradual increase over the next decade [17]. Over the years, Indonesia has taken over as the world leader in the biodiesel production (17% of the totals share), followed by the USA (14%), Brazil (12%), Germany (8%), France (6.3%) and Argentina (5.3%) [16]. This geographical distribution is a clear indication that the production as well as the challenges associated to it have a global impact.

Despite in some contexts hydrotreated vegetable oils being considered biodiesel [16], the vast majority of the production corresponds to the transesterification of oils and fats from different sources. Throughout

* Corresponding author.

E-mail address: jesus.estebanserrano@manchester.ac.uk (J. Esteban).

<https://doi.org/10.1016/j.fuproc.2023.108008>

Received 9 October 2023; Received in revised form 22 November 2023; Accepted 24 November 2023

Available online 21 December 2023

0378-3820/© 2023 The Authors. Published by Elsevier B.V. This is an open access article under the CC BY license (<http://creativecommons.org/licenses/by/4.0/>).

the years, different generations of biodiesel have appeared depending on the source of the oils and fats. The first generation used edible oils as source of triglycerides, but competition with food products led to a second generation of biodiesel, originating from non-food crops like *Jatropha curcas*. A third generation would have waste oils and fats or, alternatively, oil from microalgae cultures as feedstock. Last, a fourth generation stems from taking advantage of the use of synthetic biology in algae and cyanobacteria to obtain photobiological solar biodiesel [18]. Regardless of the origin of the triglycerides source, the transesterification chemical reaction is conducted with short chain alcohols, mostly methanol to yield fatty acid methyl esters (FAMES) or ethanol in some regions. In addition, the chemical reaction generates glycerol (Gly) as a byproduct of the reaction in approximately 10% w/w. The purification of Gly from the process to obtain different qualities has proven challenging as it features different steps to neutralize the product, remove the excess methanol by stripping, filtration or centrifugation to remove precipitates and vacuum distillation [19,20]. Fig. 1 presents a scheme of the biodiesel cycle.

The ongoing context of increase of biodiesel production has caused an oversupply of Gly, which has inevitably led to the decline of its retail

prices as a general rule with occasional remarkable volatility of prices [21]. The traditional uses of Gly in established markets include its application in the formulation of different fast moving consumer goods, food products and pharmaceuticals among others [21]. However, the demand for these applications has been clearly exceeded in light of the price collapse. Landfilling and burning of Gly can cause environmental issues and is not regarded as the best alternative [22,23]; therefore, considering the wide availability of this material and its rich chemical reactivity, the door to its chemical valorisation has been opened leading to many interesting by-products.

Throughout almost the last two decades, countless works have been published on the synthesis of a plethora of value-added products using Gly as building block by different chemical reactions. The publication of many reviews bear witness of all these efforts focusing on different aspects of the reactions and the processes. The supplementary information of this work (section S1) contains a summary of the aspects covered in the most significant review works published to date [20,21,23–44]. Nevertheless, little attention has been paid to systematically analyse the kinetics and thermodynamics of reactions involving Gly as feedstock, a feature that is of paramount importance to the ulterior reactor and

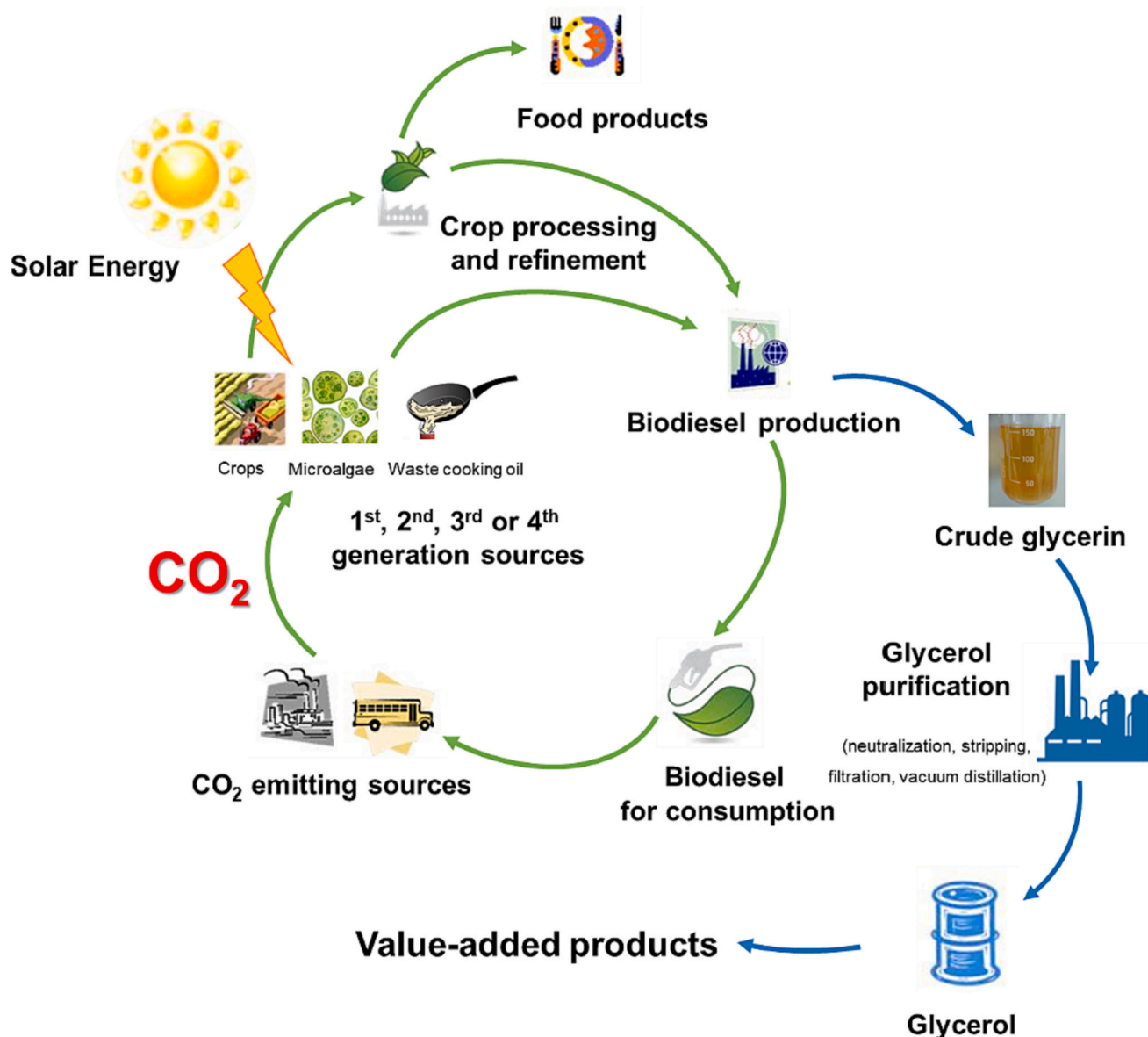


Fig. 1. Scheme of the biodiesel cycle and the concomitant production of value-added products from glycerol.

process design. This work will provide first an overview of the properties and market of Gly. Then, there is a wide systematic account and a critical review of kinetic studies to yield the most common value-added products derived therefrom (glycerol carbonate, acetals, esters, ethers, glycols, acrolein, halogenated products, hydrogen and organic acids) and aspects of process intensification [45] to improve the performance of these reactions.

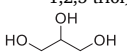
2. Properties of glycerol

Glycerol (propane-1,2,3-triol, Gly) is the simplest trihydric alcohol in nature and was discovered in the late 18th century by C.W. Scheele, though given a name in the 19th century by M.E. Chevreul [24]. Whilst Gly is the term used for the molecule, the word “glycerin” is most commonly employed when referring to purified commercial products with >95% content [28]. When pure and at room temperature, it is a highly viscous liquid of clear colourless appearance with no odor. It is non-toxic and highly hygroscopic owing to its chemical structure [24,38]. These properties make this compound useful for its application in the formulation of many consumer goods. A comprehensive compilation of physicochemical properties from different sources can be found in Table 1.

All of the properties above have been measured for pure Gly; however, its composition will vary significantly depending on different

Table 1

Compilation of physicochemical properties of glycerol. Note: Properties at 25 °C unless otherwise noted.

Property	Value	Units	Ref.
Name	Glycerol (propane-1,2,3-triol)	–	–
Chemical structure		–	–
CAS number	56–81-5	–	–
Canonical SMILES code	C(C(CO)O)O	–	–
Molecular formula	C ₃ H ₈ O ₃	–	–
Molecular mass, MW	92.09	g mol ⁻¹	–
Melting point, T _m	291.22	K	[33]
Boiling point, T _b	563.15	K	[33]
Flash point, T _f	433.15(closed cup)	K	[33]
Autoignition temperature, T _{ig}	673.15	K	[33]
Triple point, T _{triple}	291.8	K	[46]
Critical temperature, T _c	850	K	[47]
Critical pressure, P _c	75	bar	[47]
Enthalpy of fusion, ΔH _{fus}	8.475 (at 291.22 K)	kJ mol ⁻¹	[48]
Enthalpy of vaporization, ΔH _{vap}	91.7	kJ mol ⁻¹	[49]
Constant pressure heat capacity of liquid, C _p	223.8	J mol ⁻¹ K ⁻¹	[50]
Density, ρ	1.258	g cm ⁻³	[51]
Viscosity, η	906	mPa s	[51]
Surface tension, σ	62.9	mN m ⁻¹	[52]
Refraction index, n ^D	1.4730	–	[53]
Thermal conductivity, λ	0.30	W m ⁻¹ K ⁻¹	[50]
Thermal expansion coefficient, α	5 × 10 ⁻⁴	K ⁻¹	[50]
Dielectric constant, ε	42.5	–	[31]
Dielectric permittivity, ε	41.01	F m ⁻¹	[31]
Specific electric conductivity ε ₀	0.1	μS cm ⁻¹	[38]
Dipole moment, μ	2.67	D	[54]
Hildebrand solubility parameter, δ	36.1	MPa ^{1/2}	[55]
Hansen solubility parameter (global), δ _t	36.2	MPa ^{1/2}	[56]
Hansen solubility parameter (London dispersion), δ _d	17.4	MPa ^{1/2}	[56]
Hansen solubility parameter (polar interactions), δ _p	12.1	MPa ^{1/2}	[56]
Hansen solubility parameter (hydrogen bonding), δ _H	29.3	MPa ^{1/2}	[56]
Normalized solvent polarity, E _T ⁺	0.40	–	[57]
LD50 (rat, oral)	12,600	mg kg ⁻¹	[54]
LD50 (rabbit, dermal)	>10,000	mg kg ⁻¹	[33]
LC50 (rat, 1 h)	570	mg m ⁻³	[33]

factors, namely the production process, the feedstock used and the subsequent purification processes.

Crude glycerol composition may contain fractions of Gly of about 75%, although on occasions it can reach values as low as 40%, if obtained by transesterification, 83–84% if it originates from saponification or 88–90% if derived from hydrolysis. In addition, it contains mostly ash, water, soap, methanol, organic matter and compounds like trimethylene glycol, showing a dark brownish appearance in most cases [29,32,38]. Many works have also measured its elemental composition, being carbon, hydrogen and oxygen represent the major components, although sometimes small fractions of nitrogen and metals like potassium, magnesium or sodium may be found [21].

Crude glycerol purification is indeed one of the most challenging issues to tackle to render it useful for further applications in the markets [20]. Concerning its quality, purified Gly can be classified commercially into different categories, as summarized in Table 2.

3. State of the market

At this point, a few reviews have shed some light on the uses, applications, and the market of Gly. Owing to the properties discussed above, the traditional uses of Gly in established markets include its application in the formulation of cosmetics (37–40%) and food products (23–25%) mainly, followed by tobacco products (9–10%), polyurethanes (7–10%), pharma products (6–8%), alkyd resins (3–9%) and other products [21]. Among its functions, Gly has served the purpose of being a humectant, flavorant, sweetener, emulsifier, lubricator or plasticizer in these formulations [38].

Considering that a very large share of the origin of Gly is from the transesterification of oils, the state of the Gly market is undoubtedly related to that of biodiesel. The first reviews of Gly give initial estimates of the global Gly production. For example, Zhou et al. [26] commented in their review of 2008 on the global Gly production increasing from approximately 0.75 Mtons in 2001 to a projected 1.2 Mtons by 2010 as estimated by Procter & Gamble. Probably the most comprehensive reviews on the market of Gly production and consumption are Ayoub and Abdullah published in 2012 [28], Quispe et al. in 2013 [21] and Anitha et al. in 2016 [39]. In addition, Attarabachi et al. have recently provided some new data previously unavailable in the open literature regarding Gly prices [20].

In their work, Ayoub and Abdullah talk about the Gly production remaining stable up to 2003 with marked increases afterwards. The crude Gly production showed a dramatic increase escalating from about 20 million lbs. in 2004 to 62 million lbs. in 2005 and further to 213 million lbs. in 2006. Most of these amounts were solely produced in the EU prior to 2005, but as other regions started implementing policies for biodiesel production, countries like the USA, Canada, Brazil, Argentina, Indonesia, China, India or Malaysia would show their prominence in future years. In addition, this work gives an overview of the Gly supply drivers and their change in trends before and after the boom of the

Table 2

Specifications of glycerol content for different qualities. Based on [19,28].

Type of glycerol	Glycerol content (% w/w)	Source and usage
Crude glycerol	70–90	As obtained from biodiesel production
Technical grade	99.5% technical grade (not certified mostly >96.0%)	Adequate for industrial application as building block for chemicals, but not for food or drug formulation
United States Pharmacopeia (USP)	96–99.5%	Prepared from animal fat or plant oils. Suitable for food products, cosmetics and pharmaceuticals
Food Chemical Codex (FCC) / Kosher grade	99.5–99.7%	Prepared from plant oils and suitable for use in kosher foods and drinks

biodiesel industry comparing 1999 and 2009. Figures for 2011 and estimations for 2012, 2013 and 2014 are further given in another reference, confirming a more or less stable share of about 60% of biodiesel production as the main driver [39]. Other drivers include the production of fatty acids, soap or fatty alcohols. Also included in this work is an analysis of the market of crude Gly featuring the supply and demand as well as imports and exports, covered as well by Anitha et al. [39]. Finally, the prices of Gly and how they affect and relate to that of biodiesel with price trends between 2005 and 2009. Their main conclusion is that crude Gly prices will continue to decline in that context [28].

Quispe et al. give in their work an extensive overview on global Gly production in relation with biodiesel manufacture [21]. The authors cover extensively the production and framework in areas like the EU and the USA forecasting that Asian nations would take over as the leaders in the production, as explained by Ayoub and Abdullah [28]. Most relevantly, they comment on the price volatility of Gly and provide information on the projection Gly production and prize evolution crude and refined Gly, although these data only reach until 2011 [21].

More recently, Vivek et al. gave some figures to the expected size of the Gly market, which would exceed 3 billion USD in 2022, representing an increase of almost 8% with respect to 2015. The major players in these markets would be companies like Procter & Gamble, Dow Chemicals, Solvay, BASF, Cargill, Archer Daniels Midland or Evonik Industries [35].

Only very recently, further information on recent prices has become available [20]. The historical price development of kosher grade glycerol (99.7%) from 1995 to 2020 in the US and EU markets show similar trends in both with prices ranging between 400 and 800 €/tonne [58]. In addition, high-grade glycerol prices increased significantly as a consequence of the enormous demand by the pharma, health and fast-moving consumer goods industries owing to the COVID-19 pandemic. Table 3 compiles Gly prices in different regions in 2020 [20,59,60].

4. Description of reaction kinetic models and thermodynamics for the conversion of glycerol into value-added products

Fig. 2 presents many of the products that can be obtained from Gly by different chemical transformations. The most interesting products considered so far are glycerol carbonate (GC), glycidol, acetals, esters, ethers, glycols (1,2- and 1,3-propanediol), acrolein (Acr), halogenated products, syngas (as the main product of reforming) and oxidation products (mainly organic acids). The vast majority of the existing reviews feature comprehensive information on the reaction pathways to these products. Among the aspects covered are reaction conditions and catalysts used, but information on reaction kinetics and thermodynamics often lack in the discussions. The supplementary information (sections S2-S3) includes a detailed survey of previous review works dedicated to the production of each of the chemicals mentioned [22–27,29,31–44,61–82]. In addition, considering the focus of this review, section S4 includes a general description of thermodynamic and kinetic equations often used as a basis for many of the works discussed in the following sections, including pseudohomogeneous, Langmuir-

Table 3
Refined and crude glycerol prices in different regions (June–December 2020) [20,59,60].

Glycerol quality	US price (€ ton ⁻¹)	EU price (€ ton ⁻¹)	China price (€ ton ⁻¹)
Refined (99.7% kosher grade)	705	650	565
Refined (99.5% technical grade)	660	520	505
Crude (80% vegetable based)	200–280	395	295
Crude (75% non-vegetable based)	180–240	150–250	145–175

Hinshelwood-Hougen-Watson (LHHW) and Eley-Rideal (ER) mechanisms.

4.1. Glycerol carbonate

The synthesis of GC has attracted a lot of interest due to its application as a multipurpose green solvent, a solvent for Li and Li-ion batteries or in the formulation of adhesives, protective coatings and building block to many other chemicals [62]. This chemical can be produced by different routes starting from Gly, which appeared as alternatives to the traditional phosgenation reaction to produce organic carbonates. In this way, a greener approach can be followed neglecting the use of hazardous phosgene as co-substrate and avoiding the production of HCl as by-product, as shown in Fig. 3.

In the following subsections, a comprehensive description of different pathways, such as the direct addition of CO or CO₂ to Gly, the glycerolysis of urea (U) and the transesterification with organic carbonates (OC) is discussed.

4.1.1. Carbonylation of glycerol

The carbonylation of Gly occurs via its reaction with CO in the presence of O₂ [83] or else by the direct addition of CO₂ [84,85]. These typically take place at temperatures between 373 and 453 K and varying pressures that can reach up to 50 bar. In the two cases, the mechanisms have been well presented for molecular catalysts. A PdCl₂ (1,10-phenantroline) aided by KI organometallic complex has proven to catalyse the oxidative carbonylation of Gly [83]. The mechanism starts by the complexation of one of the hydroxyl moieties of Gly with the iodized form of the organometallic complex, which liberates HI; subsequently, CO is introduced and the second –OH coordinates to form the cyclic structure liberating yet another HI. Finally, GC is released and the catalyst remains in a Pd(0) until HI forms coordinates and the cycle starts again [83]. For the direct addition of CO₂, a dibutyltin (IV)oxide (tBu₂SnO) in methanol (MeOH) starts by the coordination of Sn with two molecules of MeOH, which will render two bonds for the subsequent substitution of two hydroxyl moieties of Gly. Then, CO₂ is inserted forming a cyclic intermediate from which GC is then liberated leading to a regenerated catalyst by a subsequent coordination of two MeOH molecules to start the cycle again [84].

Whilst these relatively complex mechanisms have been established, these carbonylation routes have not retained much interest throughout the years in comparison with the rest of the routes, and as a consequence kinetic studies have not been reported in the open literature. In part, this is due to the hazards associated with working with CO in one case and the severe thermodynamic constraints that activating a molecule like CO₂ represents in the other. Concerning the latter aspect, Table 4 summarizes the reaction enthalpies (ΔH_{rxn}^0), entropies (S_{rxn}^0) and Gibbs free energies (ΔG_{rxn}^0) as well as the thermodynamic equilibrium constants at standard conditions for the oxidative addition of CO to Gly and the direct addition of CO₂ together with transesterification cases. It is clearly seen that for the former two cases, the equilibrium constant is very low and the values of the free Gibbs energy are positive, thus indicating the non-spontaneity of the reactions [86].

4.1.2. Glycerolysis of urea

The glycerolysis of urea (U), otherwise known as carbamoylation of Gly, follows a mechanism where U provides the carbonyl moiety and ammonia is hence released. The mechanism requires the presence of both acid and basic sites to attract a proton from the hydroxyl functions of glycerol, thereby allowing the glyceroxide anion to perform a nucleophilic attack on the carbamoyl group of urea [87,88].

As in the case of the addition of CO₂ to Gly, at standard conditions this reaction shows unfavourable spontaneity (Table 4), but further thermodynamic analysis of the equilibrium position at relevant reaction temperatures (373–453 K) shows that the Gibbs free energy of reaction

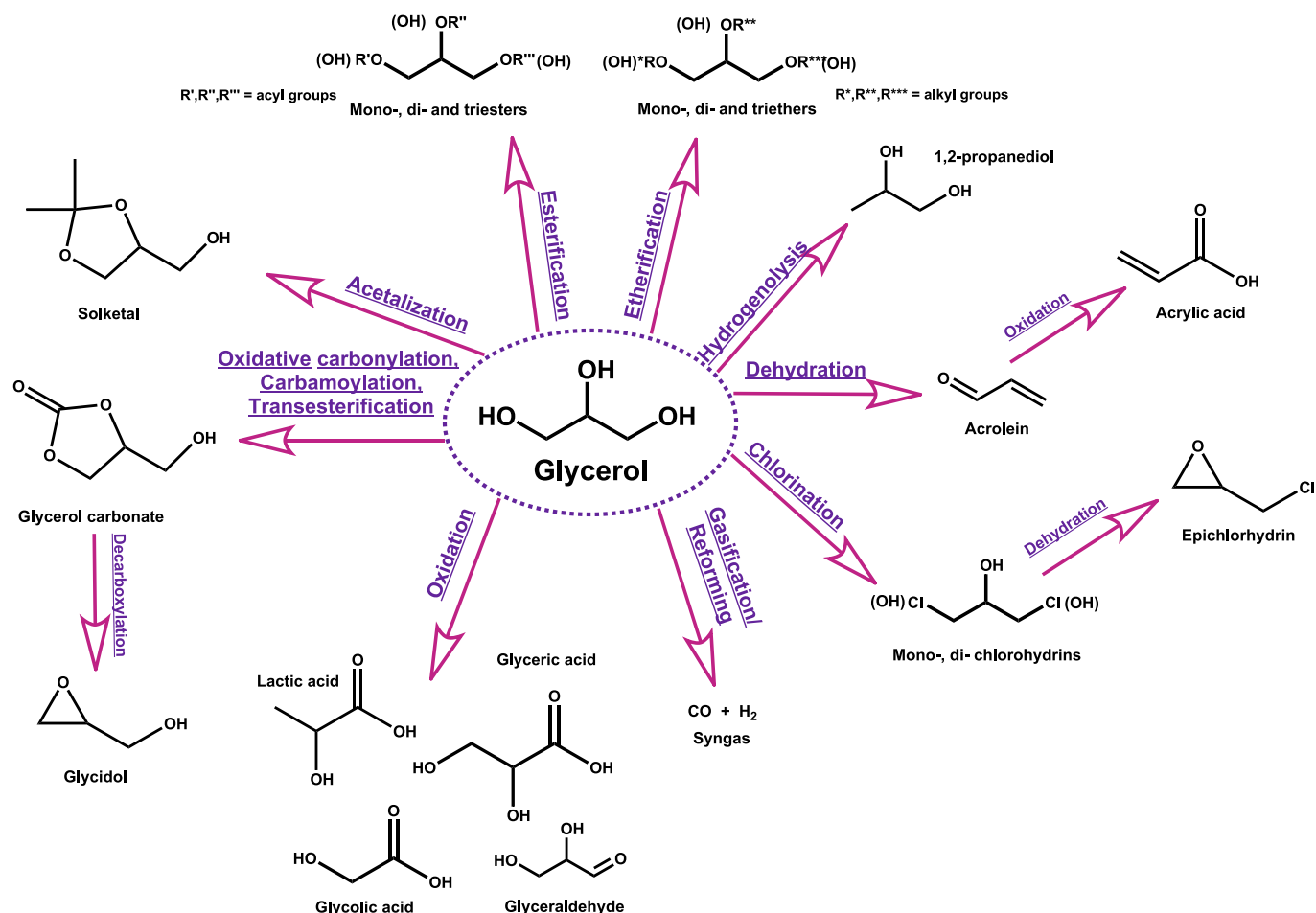


Fig. 2. Glycerol as a building block for a large number of value-added products.

acquires negative values, hence making this a spontaneous reaction at these conditions [89]. As featured in Table 5, the kinetics of the glycerolysis of U has been studied only on two occasions. A kinetic model was first reported using $\text{Co}_3\text{O}_4/\text{ZnO}$ considered a power law model with the presence of the reaction equilibrium through the consideration of an equilibrium constant expressed as a function of temperature, leading to an E_a of the reaction of $31.89 \text{ kJ mol}^{-1}$ [89]. In a second study, MgO was employed as a bifunctional catalyst consisting of vacant basic and acid sites, onto which Gly and U would adsorb, respectively. Considering the nature of the sites, models based on Langmuir-Hinshelwood-Hougen-Watson (LHHW) equations were proposed accounting for a balance of the active sites. The first model would assume that the formation of the products GC and NH_3 through an intermediate occurs after the adsorption and that this is the rate limiting step. The second model considers that the rate is limited by the adsorption of the reactants Gly and U onto the acid sites with the formation of the products taking place very fast. The evolution of the concentration profiles observed confirmed that the latter model was the appropriate following a zero-order kinetics [87].

4.1.3. Transesterification of glycerol with organic carbonates

The production of GC has mostly been approached via the base-initiated transesterification of Gly with acyclic dialkyl or cyclic organic carbonates, which yield two molecules of alcohol or a single molecule of glycol as by-product.

Transesterification with dimethyl carbonate (DMC) has been reported, although the extent to which further reactions take place is subject of discussion. Whilst most studies treat the reaction only as a forward reaction, some studies have considered the presence of a reverse reaction in [90], which in principle goes against the thermodynamic

studies reported.

In addition to DMC, transesterification with diethyl carbonate (DEC), ethylene carbonate (EC), propylene carbonate (PC) and butylene carbonate (BC) have been reported, which have the advantage of obtaining glycols as by-products of interest. These reactions have been observed to proceed until completion, thus achieving total conversion of Gly, typically used as limiting reactant. This is supported by the values of K_{eq} compiled in Table 4, calculated for the transesterification of Gly with DMC and EC. Fig. 4 shows a general scheme for the reaction mechanism, in agreement with previous observations and assumptions for the case of the reaction between Gly and DMC [91,92]. The mechanism can be summarized in four steps, namely: (1) proton removal by a Bronsted base to obtain the glyceroxide anion, reportedly the active species; (2) nucleophilic attack on the carbonate group; (3) catalyst regeneration giving a proton to the anionic species (and liberating a first molecule of alcohol in the case of transesterification with a dialkyl carbonate); (4) intramolecular cyclization to yield GC and either a second molecule of alcohol or a glycol.

Table 5 features a compilation of kinetic models developed for the production of GC via transesterification with OCs with a range of different catalysts and considerations. Reactions of Gly with DMC are by far the most frequently reported, both with heterogeneous and homogeneous catalysis. For the development of kinetic models, most have in common a previous analysis of external and internal mass transfer limitations through studies of the influence of stirring rates and particle sizes (e.g. Weisz-Prater criterion) on the performance of the reaction, so as to ensure that the intrinsic kinetics of the reaction was being analysed. Yadav et al. [93] used a calcined hydrotalcite supported on hexagonal mesoporous silica for the reaction of Gly and DMC, where both are

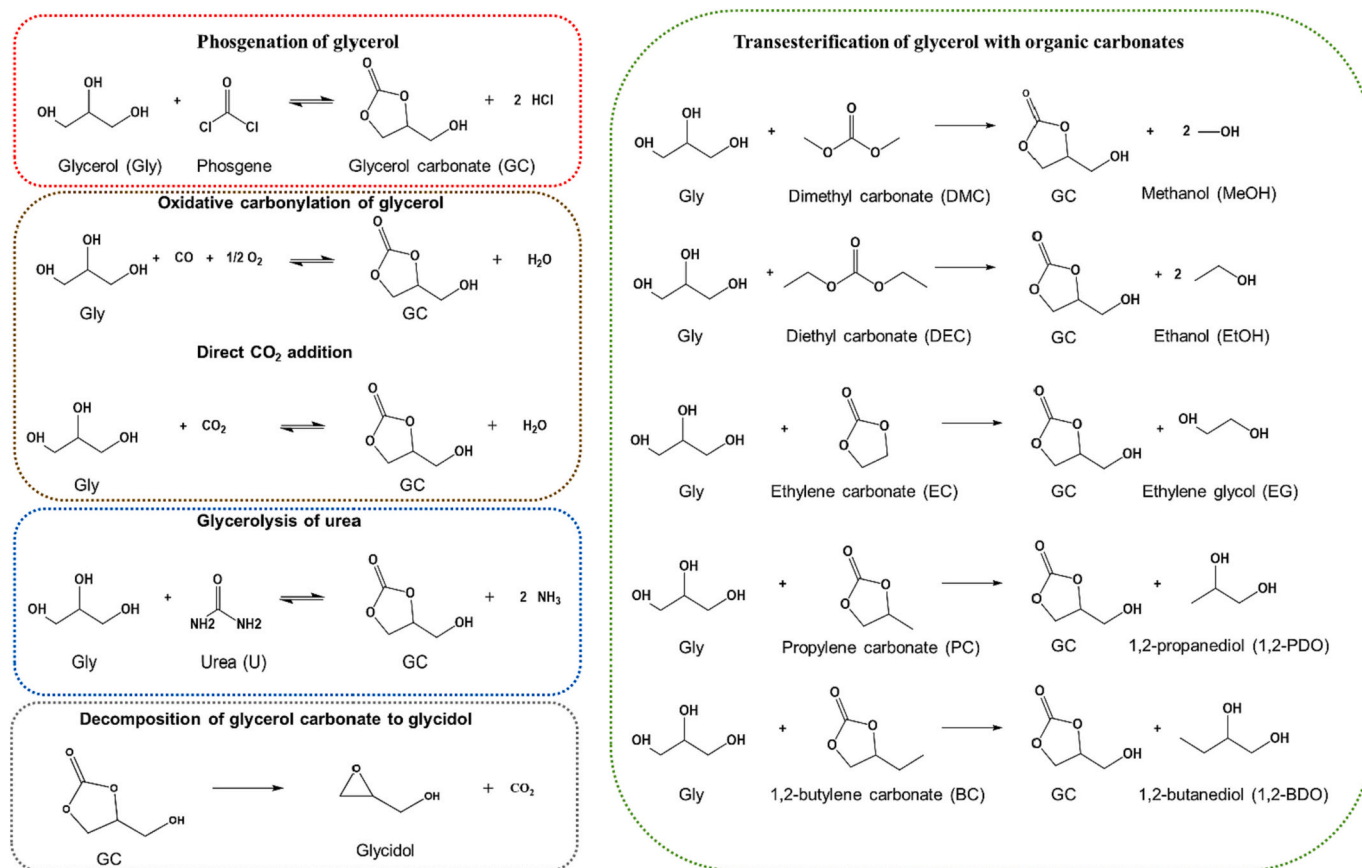


Fig. 3. Overall reactions reported for the production of GC using Gly as starting material.

Table 4

Summary of the thermodynamic analysis for reactions to obtain GC at standard conditions [86].

Reaction	ΔH_{rxn}^0 (kJ mol ⁻¹)	ΔS_{rxn}^0 (J K ⁻¹ mol ⁻¹)	ΔG_{rxn}^0 (kJ mol ⁻¹)	K_{eq}
Oxidative carbonylation of Gly	-9.13	-110.85	23.92	6.41×10^{-5}
Addition of CO ₂ to Gly	126.2	314.52	32.43	2.07×10^{-6}
Transesterification of Gly with DMC	13.57	51.66	-1.83	2.100
Transesterification of Gly with EC	-6.1	-14.76	-1.70	1.985

adsorbed onto the surface of the catalyst with the intermediate rearranging to form GC and MeOH. A complex LHHW model was used to describe the progress of the reaction accounting for the presence of intermediate reactions to yield the adsorbed intermediate species, each of which with the associated adsorption constants [93]. In a reaction with ZnO/La₂O₃ as catalyst [94], there was the unusual consideration of a reverse reaction from the products GC and MeOH in addition to the in-series reaction to generate glycidol and CO₂ from GC. The latter was explained by the decomposition of GC at the operating temperature in this case, somewhat higher than usual (393–413 K). The model reported here was based on power-law, with E_a of 98.3 kJ mol⁻¹ for the forward reaction, 77.5 kJ mol⁻¹ for the reverse reaction and 127.7 kJ mol⁻¹ for the decomposition of GC to glycidol [94]. Similarly, Qing et al. [90] investigated the reaction with DMC in the presence of 1,8-diazabicycloundec-7-ene (DBU) as catalyst at 303–333 K with crude glycerol as feedstock. To develop the kinetic model, the system is assumed to be pseudo-homogeneous, which was considered valid as it was observed that the system has a quick reaction rate and therefore is in the heterogeneous state for a short time before turning into a homogeneous system. A power law model was developed in which the forward and backward reactions for the formation of DMC has E_a values of 30.95 kJ mol⁻¹ and 55.16 kJ mol⁻¹, respectively. Additionally, the E_a for the decomposition

of DMC to glycidol is 26.58 kJ mol⁻¹ [90]. A Ti-SBA-15 catalyst was also employed for the reaction [95] and in this case a mechanism based on LHHW was proposed under the assumptions that surface reaction controls the rate of reaction, and the adsorption of reactants and desorption of products occur very fast. Further simplification of the model included the consideration that the reaction was away from equilibrium, thus simplifying the rate equation significantly. The apparent reaction constant gave an E_a of 39.2 kJ mol⁻¹ [95]. Remarkably, a study in 2021 [96] published for the first time the kinetics of the production of GC using crude Gly as feedstock catalysed by CaO under microwave irradiation, which allowed operation as low as 318–338 K. Here, they optimised the reaction conditions in the first place through a Box-Behnken design of experiments, which led to a power-law second order kinetic model with an E_a value of only 4.53 kJ mol⁻¹ [96]. This low value hints towards process intensification via microwave-assisted operations as a promising alternative to reduce operational costs. Interestingly, there is no account of deactivation in the kinetic model, which could be expected to some extent owing to the presence of impurities (up to 30%) in the starting material potentially leading to pore blockage or other type of deactivation mechanism [96]. The use of deep eutectic solvents (DES) as catalyst has also been reported [97], with the reaction moving forward to glycidol production. The DES that provided the best activity was

Table 5
Summary of the most relevant aspects of kinetic studies for the production of GC through different routes.

Reactants and Catalyst	Reaction conditions ^a	(Best) X _{Gly} /Sel/ Yield ^b	Kinetic rate type and equation ^c	Kinetic parameters ^d	Notes	Ref.
Gly + U Catalyst: MgO	T = 408–423 K MR = 1.5:1 Cat _{load} = 0.03 g cm ⁻³ ω = 1000 rpm t _{rxn} = 180 min	S _{GC} = 100%	Power law (zero order derived from LHHW): – r _{Gly} = kC _{TS1} C _{TS2} = kw C _{Gly0} $\frac{dX_{Gly}}{dt}$ = kw Where w = C _{TS1} C _{TS2}	E _a = 117.4 kJ mol ⁻¹ ln k ₀ = 26.42°	Two LHHW based models were tested assuming different r.d.s. Model assumed the adsorption of Gly and urea on different sites S1 (basic) and S2 (acidic), respectively. Model selected assumed that the r.d.s is the adsorption of reactants onto catalytic sites.	[87]
Gly + U Catalyst: Co ₃ O ₄ /ZnO	T = 373–453 K MR = 1:1 Cat _{load} = 1.5 wt% of Gly ω = 1163 rpm t _{rxn} ≈ 360 min	X _{Gly} = 45%	Power law: – r _{Gly} = – r _{urea} = r _{GC} = $\frac{r_{NH_3}}{2} = k \left(x_{Gly}x_{urea} - \frac{x_{NH_3}^2 x_{GC}}{K_{eq}} \right)$ Where lnK _{eq} = – 8041 + 291370 $\left(\frac{1}{T}\right)$ + 1316.80ln (T) + – 1.4475(T)	E _a = 31.89 kJ mol ⁻¹ k ₀ = not available	Study in batch experiment. The study features the simulation of a reactive distillation.	[89]
Gly (crude glycerol) + DMC Catalyst: 1,8-diazabicycloundec-7-ene (DBU)	T = 303–333 K MR = 3:1 Cat _{load} = 4.0 wt% of Gly ω = not available t _{rxn} = 90–150 min	S _{GC} = 84%	Power law (second order main reaction with first order decomposition of GC to glycidol): r _{GC} = k ₁ C _{Gly} C _{DMC} – k ₋₁ C _{GC} C _{methanol} ² r _{glycidol} = k ₂ C _{GC}	E _{a1} = 30.95 kJ mol ⁻¹ E _{a-1} = 55.16 kJ mol ⁻¹ E _{a2} = 26.58 kJ mol ⁻¹ lnk ₀₁ = 6.529* lnk ₀₋₁ = 11.483* lnk ₀₂ = 4.4708*	Uses crude Gly as reactant.	[90]
Gly + DMC Catalyst: calcined hydrotalcite supported on hexagonal mesoporous silica (CHT-HMS)	T = 423–453 K MR = 1:1–4:1 Cat _{load} = 0.001–0.004 g cm ⁻³ ω = 1000 rpm t _{rxn} = 150 min	S _{GC} = 84.3%	Power law (second order derived from LHHW): $\frac{dX_{Gly}}{dt} = k_r C_{Gly}^2 w(1 - X_{Gly})(MR_0 - X_{Gly})$ Upon integration ln $\left(\frac{MR_0 - X_{Gly}}{MR_0(1 - X_{Gly})} \right) = k_1 C_{Gly_0} (MR_0 - 1)t$	E _{a1} = 52.55 kJ mol ⁻¹ ln k ₀₁ = 9.4566°	Weak adsorption of all species is considered.	[93]
Gly + DMC Catalyst: ZnO/La ₂ O ₃ (mole ratio Zn:La of 4:1)	T = 393–413 K MR = 2:1–6:1 Cat _{load} = 0.25–1.0 wt% ω = 1000 rpm t _{rxn} = 240 min	S _{GC} = 97.2%	Power-law (second order, decomposition of GC is first order): r _{Gly} = r _{DMC} = $\frac{-r_{methanol}}{2} = k_2 x_{GC} x_{methanol}^2 - k_1 x_{Gly} x_{DMC}$ r _{GC} = k ₁ x _{Gly} x _{DMC} – k ₂ x _{GC} x _{methanol} ² – k ₃ x _{GC} r _{glycidol} = k ₃ x _{GC}	E _{a1} = 98.3 kJ mol ⁻¹ E _{a2} = 77.5 kJ mol ⁻¹ E _{a3} = 127.7 kJ mol ⁻¹ k ₀₁ = 1.18 × 10 ¹⁰ kmol (kg s) ⁻¹ k ₀₂ = 1.04 × 10 ⁷ kmol (kg s) ⁻¹ k ₀₃ = 2.78 × 10 ⁹ kmol (kg s) ⁻¹	Model features a reverse reaction and further conversion of GC to glycidol (observed if T is high due to decomposition)	[94]
Gly + DMC Catalyst: Ti-SBA-15	T = 338–383 K MR = 3:1 Cat _{load} = 5.5 wt% ω = not available t _{rxn} = 420 min	S _{GC} = 87.17%	Power law (derived from LHHW): – $\frac{dX_{Gly}}{dt} = k(1 - X_{Gly})$ Upon integration – ln(1 – X _{Gly}) = kt	E _a = 39.2 kJ mol ⁻¹ k ₀ = not available	Model developed assuming surface reaction is the r.d.s. Reaction is far from equilibrium and adsorption and desorption constants are very small.	[95]
Gly (crude glycerol) + DMC Catalyst: CaO	T = 318–338 K MR = 2.5:1 Cat _{load} = 1 wt% ω = not available; microwave reactor (1200 W, 24550 MHz) t _{rxn} = 20 min	Y _{GC} = 97.1%	Power-law (irreversible second order): – r _{Gly} = – $\frac{dC_{Gly}}{dt} = kC_{Gly}C_{DMC}$	E _a = 4.53 kJ mol ⁻¹ ln k ₀ = – 2.0465°	Model developed for microwave assisted transesterification of crude glycerol	[96]

(continued on next page)

Table 5 (continued)

Reactants and Catalyst	Reaction conditions ^a	(Best) X _{Gly} /Sel/ Yield ^b	Kinetic rate type and equation ^c	Kinetic parameters ^d	Notes	Ref.
Gly + DMC Catalyst KOH:MEA(1:2) DES	T = 333–343 K MR = 1:1–5:1 Cat _{load} = 1–5 wt% of Gly ω = 600 rpm t _{rxn} = 170 min	Y _{GC} = 18.4% Y _{glycidol} = 80.2%	Power-law (homogeneous model): $r_{GC} = k_1 C_{Gly} C_{DMC}$ $r_{Gly} = k_2 C_{GC} C_{methanol}^2$ $r_{glycidol} = k_3 C_{GC}$	$E_{a1} = 51.22 \text{ kJ mol}^{-1}$ $E_{a2} = 100.65 \text{ kJ mol}^{-1}$ $E_{a3} = 199.92 \text{ kJ mol}^{-1}$ $\ln k_1 = 12.88-$ $\left(\frac{6160.42}{T}\right) L \text{ min}^{-1} \text{ mol}^{-1}$ $\ln k_2 = 32.58-$ $\left(\frac{12106.43}{T}\right) L \text{ min}^{-1} \text{ mol}^{-1}$ $\ln k_3 = 69.93 - \left(\frac{24046.55}{T}\right) \text{ min}^{-1}$	Model considers the reversible reaction and the decomposition of GC to glycidol.	[97]
Gly + DMC Catalyst: K ₂ CO ₃	T = 339–343 K MR = 1.5:1–3:1 Cat _{load} = 0.75–1.25% wt ω = 1500 rpm t _{rxn} = 180 min	X _{Gly} = 99%	Power law in two stages (X_{crit} = 0.30): $r_{GC_1} = k C_{cat} C_{Gly} C_{DMCsol}$ for $X < X_{crit}$ $r_{GC_2} = k C_{cat} C_{Gly} C_{DMC}$ for $X \geq X_{crit}$ Power law in two stages with first order deactivation (X_{crit} = 0.34): $r_{GC_1} = k_1 C_{cat} ((1 - a) * e^{(-k_d t)} + a) C_{Gly} C_{ECsol}$ for $X \leq X_{crit}$ $r_{GC_2} = k_1 C_{cat} a C_{Gly} C_{EC}$ $r_{Gly} = k_3 C_{cat} a C_{GC} C_{EG}$ for $X > X_{crit}$	$E_a = 179.2 \text{ kJ mol}^{-1}$ $\ln k_0 = 55.43$ $C_{DMCsol} = 3.34 \text{ mol L}^{-1}$ (concentration of DMC dissolved in Gly rich phase) $E_{a1} = 91.8 \text{ kJ mol}^{-1}$ $\ln k_{01} = 32.71$ $E_{a3} = 93.9 \text{ kJ mol}^{-1}$ $\ln k_{03} = 31.91$ $k_d = 0.36 \text{ min}^{-1}$ $a = 0.08$ $C_{ECsol} = 1.10 \text{ mol L}^{-1}$ (concentration of EC dissolved in Gly rich phase) $E_a = 28.3 \text{ kJ mol}^{-1}$ $\ln k_0 = 4.84$ $k_d = 0.03 \text{ min}^{-1}$ $a = 0.32$	Model discrimination. 1st step considers partial first order with respect to Gly. 2nd step is partial first orders for Gly and DMC.	[100]
Gly + EC Catalyst: K ₂ CO ₃	T = 313–323 K MR = 2:1–3:1 Cat _{load} = 125–500 ppm ω = 800 rpm t _{rxn} = 240 min	X _{Gly} = 96%	$r_{GC_1} = k_1 C_{cat} ((1 - a) * e^{(-k_d t)} + a) C_{Gly} C_{ECsol}$ for $X \leq X_{crit}$ $r_{GC_2} = k_1 C_{cat} a C_{Gly} C_{EC}$ $r_{Gly} = k_3 C_{cat} a C_{GC} C_{EG}$ for $X > X_{crit}$	$E_{a1} = 91.8 \text{ kJ mol}^{-1}$ $\ln k_{01} = 32.71$ $E_{a3} = 93.9 \text{ kJ mol}^{-1}$ $\ln k_{03} = 31.91$ $k_d = 0.36 \text{ min}^{-1}$ $a = 0.08$ $C_{ECsol} = 1.10 \text{ mol L}^{-1}$ (concentration of EC dissolved in Gly rich phase) $E_a = 28.3 \text{ kJ mol}^{-1}$ $\ln k_0 = 4.84$ $k_d = 0.03 \text{ min}^{-1}$ $a = 0.32$	Model discrimination studies. Biphasic system.	[101]
Gly + DMC Catalyst: CH ₃ OK	T = 323–343 K MR = 1.5:1–3:1 Cat _{load} = 1000–2500 ppm ω = 1500 rpm t _{rxn} = 240 min	X _{Gly} = 96%	Power law in two stages with first order deactivation (varying X_{crit}): $r_{GC_1} = k C_{cat} ((1 - a) * e^{(-k_d t)} + a) C_{Gly} C_{DMCsol}$ for $X \leq X_{crit}$ $r_{GC_2} = k C_{cat} a C_{Gly} C_{DMC}$ for $X > X_{crit}$ Power law in two stages with first order deactivation (varying X_{crit}): $r_{GC_1} = k_1 C_{cat} ((1 - a) * e^{(-k_d t)} + \beta) C_{Gly} C_{ECsol}$ for $X \leq X_{crit}$ $r_{GC_2} = k_1 C_{cat} a C_{Gly} C_{EC}$ $r_{Gly} = k_3 C_{cat} a C_{GC} C_{EG}$ for $X > X_{crit}$	$E_{a1} = 83.0 \text{ kJ mol}^{-1}$ $\ln k_{01} = 31.03$ $E_{a3} = 58.7 \text{ kJ mol}^{-1}$ $\ln k_{03} = 15.94$ $k_d = 0.11 \text{ min}^{-1}$ $a = 0.022$ $C_{ECsol} = 1.11 \text{ mol L}^{-1}$ (concentration of EC dissolved in Gly rich phase)	Model discrimination. Model described the change from biphasic to single phase reaction.	[102]
Gly + EC Catalyst: CH ₃ OK	T = 313–333 K MR = 1.5:1–3:1 Cat _{load} = 50–150 ppm ω = 800 rpm t _{rxn} = 420 min	X _{Gly} = 95%	$r_{GC_1} = k_1 C_{cat} ((1 - a) * e^{(-k_d t)} + \beta) C_{Gly} C_{ECsol}$ for $X \leq X_{crit}$ $r_{GC_2} = k_1 C_{cat} a C_{Gly} C_{EC}$ $r_{Gly} = k_3 C_{cat} a C_{GC} C_{EG}$ for $X > X_{crit}$	$E_{a1} = 83.0 \text{ kJ mol}^{-1}$ $\ln k_{01} = 31.03$ $E_{a3} = 58.7 \text{ kJ mol}^{-1}$ $\ln k_{03} = 15.94$ $k_d = 0.11 \text{ min}^{-1}$ $a = 0.022$ $C_{ECsol} = 1.11 \text{ mol L}^{-1}$ (concentration of EC dissolved in Gly rich phase)	Model discrimination. Model described the change from biphasic to single phase reaction.	[102]
Gly + EC Catalyst: None (thermal reaction)	T = 373–413 K MR = 2:1–3:1 Cat _{load} = none ω = 750 rpm t _{rxn} = 360 min T = 378–408 K	Y _{GC} = 96.9%	Power-law (overall second order): $r_{GC} = k C_{Gly} C_{EC} = k C_{Gly_0}^2 (1 - X)(MR_0 - X)$	$E_a = 61.82 \text{ kJ mol}^{-1}$ $\ln k_0 = 11.72$	Model discrimination studies.	[103]
Gly + PC Catalyst: Na ₂ CO ₃	T = 378–408 K MR = 2:1–3:1 Cat _{load} = 0.025–0.05 wt% ω = 900 rpm t _{rxn} = 240 min	Y _{GC} = 93%	Power law with first order deactivation: $r_{GC} = k C_{cat} ((1 - a) * e^{(-k_d t)} + a) C_{Gly} C_{PC}$	$E_a = 67.13 \text{ kJ mol}^{-1}$ $\ln k_0 = 17.04$ $k_d = 0.14 \text{ min}^{-1}$ $a = 0.34$	Operation in homogeneous regime after finding thermomorphic behaviour. Overall second order model.	[104]

(continued on next page)

Table 5 (continued)

Reactants and Catalyst	Reaction conditions ^a	(Best) $X_{Gly}/Sel/Yield^b$	Kinetic rate type and equation ^c	Kinetic parameters ^d	Notes	Ref.
Gly + BC Catalyst: Na ₂ CO ₃	$T = 408-438$ K MR = 2:1-3:1 Cat _{load} = 0.0125-0.025 wt% $\omega = 900$ rpm $t_{run} = 240$ min	$Y_{GC} = 91\%$	Power law with first order deactivation: $r_{GC} = k_{GCcat}((1-a)^{j_{GC}}e^{-k_{GC}t} + a)C_{Gly}C_{GC}$	$E_a = 58.56$ kJ mol ⁻¹ $\ln k_0 = 14.44$ $k_d = 0.39$ min ⁻¹ $a = 0.12$	Operation in homogeneous regime after finding thermomorphic behaviour. Overall second order model.	[104]

^a Reaction conditions used for kinetic studies. Temperature (T), cosubstrate to Gly molar ratio (MR), catalyst loading (Cat_{load}), stirring speed (ω), reaction time (t_{run}).

^b Best Gly conversion (X_{Gly}), selectivity (S) or yield (Y) with respect to GC, achieved at optimum operating conditions which are different than the reaction conditions^a for kinetic study presented in the table.

^c Rate of reaction (r_i), reaction rate constant (k_i), deactivation rate constant (k_d), overall equilibrium constant (K_{eq}), concentration (C_i), initial concentration ($C_{i,0}$), concentration of Gly dissolved in Gly rich phase ($C_{DMC(Gly)}$), concentration of EC dissolved in Gly rich phase ($C_{EC(Gly)}$), concentration of total active sites (C_{cat}), catalyst loading unless stated otherwise (w), catalytic activity (a), conversion (X), initial molar ratio (MR₀), molar fraction (x_i), time (t), *i*, components, *j*=reactions, Subscripts: DMC = dimethyl carbonate, EC = ethylene carbonate, GC = glycerol carbonate, EG = ethylene glycol.

^d Activation energy (E_a), pre-exponential factor (k_0), deactivation rate constant (k_d), catalytic activity (a), $\ln k_0$ obtained from Arrhenius plot provided, values taken as equal to the y-intercept of line equation.

based on KOH as hydrogen bond acceptor and monoethanolamine (MEA) as hydrogen bond donor (KOH:MEA (1:2)). As a case of homogeneous catalysis, it considered power-law model of first partial order with respect to each component as well as reversible reaction to yield GC and irreversible to yield glycidol [97].

Esteban et al. have worked very extensively on the production of GC through the transesterification of Gly with different OCs, focusing on the use of homogeneous catalysts and the progress of the reaction. Despite the reaction of Gly with DMC and EC having been reported long before, there had been no mention of the limited miscibility between Gly and these components. They observed that, as the reactions progressed and GC and either MeOH or ethylene glycol (EG) were produced, they acted as cosolvents between Gly and the OC, up to a point where there was no longer a biphasic reacting system, but only a single phase. By artificially adding the reaction products in inert systems (i.e. in the absence of catalyst), detailed liquid-liquid equilibria (LLE) studies were made to determine the composition of the systems at which the transition, which were to compositions of the systems corresponding to approximately 30% of conversion of Gly in systems with 3:1 M ratio of DMC:Gly and EC:Gly [98,99]. This was validated in kinetic studies in which the evolution of the reacting dispersion of DMC with Gly [100] or EC with Gly [101] were assessed by chemical analysis (HPLC) and optically by focused beam reflectance measurement to visualize the disappearance of the biphasic system. As Fig. 5 shows, no droplets were observed at the aforementioned conversion value. This realization led to the development of kinetic models for homogenous catalysts like K₂CO₃, which is only soluble in Gly and not in DMC. The model was based on power-law equations divided into two parts, the first of which were of first order for Gly and zero order with respect to the concentration of DMC since the reaction only took place in the Gly-rich phase [100]. Once the reaction is in a single phase, the model switched to a first order also with respect to DMC. Although simpler alternatives disregarding this phase behaviour were tested, model discrimination through information criteria proved for this model to adequately represent the reaction progress for the transesterification of Gly with DMC [100] and with EC [101] catalysed by K₂CO₃ as well as with CH₃OK [102]. Interestingly, the miscibility between Gly and cyclic OCs was also studied as a function of temperature, and it was found that the mixtures of Gly with EC, propylene carbonate (PC) and butylene carbonate (BC) exhibited thermomorphic behaviour achieving an upper critical solution temperature (UCST), beyond which the systems would turn monophasic [103,104]. Determination of such UCST would allow operation in the absence of external mass transfer limitations caused by the presence of two liquid phases without having to use excessive agitation rates. In this way, the reaction with EC was studied in the absence of catalyst between at higher temperatures than the UCST, leading to a power-law model of first partial order with respect to the concentrations of Gly and EC only with direct reaction with E_a of 61.82 kJ mol⁻¹ [103]. In the case of the reaction of Gly with PC and BC, Na₂CO₃ was used as basic catalyst. The models developed were based on direct reactions described by power-law equations of first order with respect to Gly and each of the OCs. A deactivation constant was considered in this case considering that no complete conversion of Gly was observed and this was expected according to other thermodynamic studies with other OCs, reaching values of 0.14 and 0.39 min⁻¹ [104].

Considering the immiscibility of Gly with OCs, an interesting way forward to intensify these reactions would be to devise less energy intensive mixing strategies in reactors than mechanical stirring. This could entail the use of ultrasound or designing reactors where mixing occurs thanks to alternative designs as is the case of static mixer reactors (Fig. 6) [105].

4.2. Acetals and ketals

Gly acetals are oxygenate products that have been extensively used as fuel additives owing to the improvement of certain performance

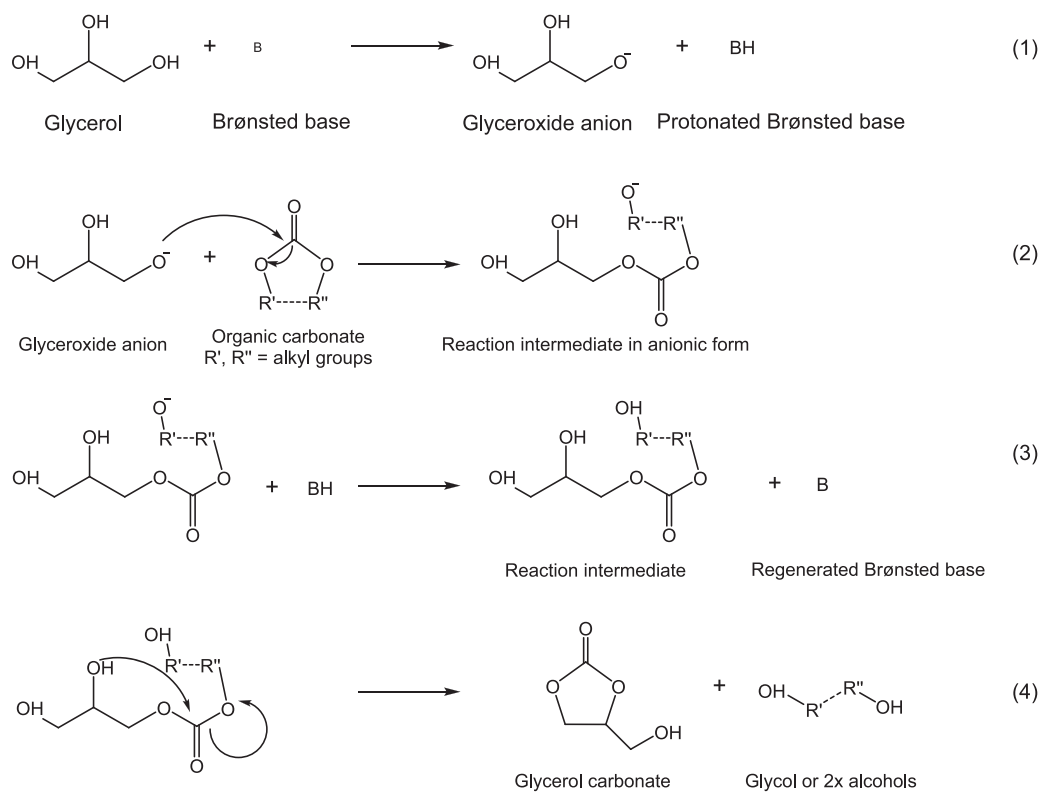


Fig. 4. General mechanism for the production of glycerol carbonate via transesterification of glycerol with an organic carbonate in the presence of a basic catalyst. The dashed lines represent the presence of a bond if transesterification occurs in the presence of cyclic carbonates, which would yield a glycol as by-product.

parameters. In addition, solketal (Slk), the most common acetal, has also been used as green solvents, as plasticizer in food and pharmaceutical formulations or as building block for active pharmaceutical ingredients [106]. Acetals originate from the reaction of the hydroxyl group of an alcohol with a carbonyl moiety, which could be from an aldehyde or a ketone. In the latter case, they are referred to as ketals. This is an equilibrium reaction that initiates in the presence of an acidic medium and release H_2O as a by-product. In the particular case of Gly acetalisation, it could be summarized by the following steps: (1) nucleophilic attack on the carbonyl group; (2) the proton supplied by the catalyst adds to the hydroxyl group; (3) a H_2O molecule is released and (4) intramolecular cyclation leading to the acetal and catalyst regeneration, which could lead to a 5 (step 4a) or 6-membered ring (step 4b). The latter isomer, also referred to as dioxane form is normally less stable and the vast majority of the works report selectivities clearly favoured towards the 5-membered ring (dioxolane). Fig. 7 shows the general mechanism.

Acetalisation reactions occur in liquid phase atmospheric pressure and typically require mild temperatures, in some cases being performed even at temperatures as low as 298 K, although some authors reach higher temperatures, which are determined by the boiling point of the corresponding ketones or aldehydes. To overcome the thermodynamic limitations of the acetalisation reaction, it is quite common to use a large stoichiometric excess of the aldehyde or ketone with respect to the alcohol. The equilibrium of the reaction has been studied in detail for the case of the production of Slk. A recent work compiled available experimental data and estimated enthalpies (ΔH_f^0), entropies (S_f^0) and Gibb's free energy (ΔG_f^0) of formation of Gly, Slk, Acetone and H_2O by the use of group contribution methods. With this information, they reached a value of ΔH_{rxn}^0 of $-6.43 \text{ kJ mol}^{-1}$, indicating an exothermic reaction and a ΔG_{rxn}^0 of 3.36 kJ mol^{-1} (positive, hence not spontaneous) leading to a value of the equilibrium constant K_{eq} of 0.2577 [107]. This

value was compared with previously reported values of experimental work, where two cases showed negative values of ΔG_{rxn}^0 [106,108] and other three cases reported positive values [109–111]. In addition, a van't Hoff type equation is given to show the estimated dependence of K_{eq} as a function of temperature [107]. The thermodynamics of the production of Gly ethyl acetal by acetalisation of Gly with acetaldehyde was also reported, indicating the values of ΔH_f^0 and ΔG_f^0 for the compounds involved. In this case, ΔH_{rxn}^0 was reported to be $-8.77 \text{ kJ mol}^{-1}$ and ΔG_{rxn}^0 had a value of $-12.3 \text{ kJ mol}^{-1}$, indicating an exothermic and spontaneous reaction. Likewise, the dependence of K_{eq} with T is provided [112].

In addition to these reaction equilibrium considerations, as in the case described for the production of GC, Gly shows limited miscibility with aldehydes and ketones at the start of the reaction prior to the generation of the products, with the LLE for Gly + Ac + Slk having been studied in detail [113]. However, no consideration of this phase transition has been made in any of the models reported in literature, mostly because studies have mostly been conducted using heterogeneous catalysts.

Table 6 displays a summary of the most relevant information obtained from kinetic studies for the production of different Gly acetals. A common thread of many of these works is the consideration of an analysis of the effect of stirring and/or particle size to assess that the studies were being performed in the absence of mass transfer limitations.

Acetalisation of Gly with formaldehyde has been studied with Amberlyst 47 as catalyst in a stirred tank reactor [114], realizing that conversions of Gly of only about 50% could be achieved at 353 K with an equimolar ratio of reactants. The kinetic model proposed was based on a power-law model of first order with respect to the concentrations of reactants (Gly being formally analysed) or products for the direct and reverse reactions, respectively, with apparent E_a values of 59.1 and 46.3 kJ mol^{-1} [114]. Another effort with formaldehyde used Amberlyst 15 [115]. In this case, the work very notably approached the philosophy

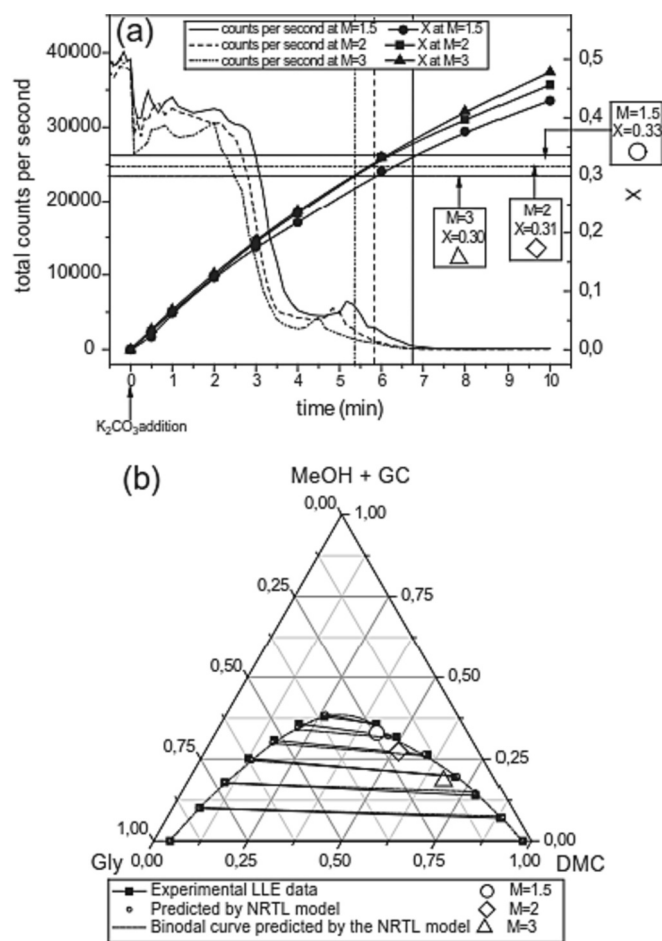


Fig. 5. Evolution of the number of droplets of the reacting dispersion of DMC and Gly at different initial molar ratios of DMC:Gly (M) and correspondence to the liquid-liquid equilibrium of the quaternary system including the products. Reproduced by permission of Elsevier publishing [100].

of process intensification through the use of reactive distillation as a strategy to remove both products and enhance the limited equilibrium position, for which toluene was used as an entrainer. For the kinetic model, the authors make use of a rate equation for the direct and reverse based on the activities of the reactants and products, whose coefficients are estimated by UNIQUAC. The estimated E_a for the forward reaction and backward reaction were similar to the previously mentioned study. This work also included process simulation efforts to estimate the utility cost in the reactive distillation column, of great relevance for process designs and techno-economic analysis [115].

Acetalisation with acetaldehyde has also been reported. Following a very similar approach to their study with formaldehyde [114], these

authors also performed the reaction with acetaldehyde [116]. They realized that, at 303 K, using an excess of Gly with respect to this aldehyde (molar ratio of 1:1 and above) did not cause any thermodynamic limitations, which enabled them to model the reaction with a simple power-law rate equation disregarding the reversible reaction [116]. This is not consistent with a different thermodynamic at a similar temperature of 313 K, where a ratio of Gly to acetaldehyde 1:1 provided an approximate Gly conversion of 90% [112]. In this study, apart from the thermodynamic analysis, the kinetics of the reaction were studied with Amberlyst 15. In their model, even though the authors discarded external mass transfer limitations, internal diffusion within the ion exchange resin (IER) pores was considered through a mass balance for the bulk and intraparticle fluid that featured an effective internal diffusion coefficient. This consideration was applied to a power-law pseudohomogeneous (PH) and a LHHW model and the fitting of the model was compared to neglecting such internal diffusion. After model discrimination, the LHHW model with consideration of internal diffusion gave the best results, with an E_a of 77.7 kJ mol^{-1} and $0.345 \text{ dm}^3 \text{ mol}^{-1}$ for the water adsorption constant (K_{a,H_2O}) [112]. The kinetics of the reaction with longer-chain aldehydes like butyraldehyde has also been analysed [117]. In this case, again Amberlyst 47 was used and a PH model considering the forward and backwards reaction following a similar approach to what the same authors reported for the acetalisation with formaldehyde and acetaldehyde [117].

Regarding kinetic studies for the formation of Gly ketals, thus far only studies of the reaction to yield Slk have been reported, possibly owing the interest that using acetone as reactant attracts. Most of these studies have been performed using either IERs or zeolites as catalyst, with a notable variety in the models considered.

Xu et al. [108] were the first to report the kinetics of Slk production, for which they used Amberlyst 35 to catalyse the reaction between Gly and acetone, to which ethanol was added as cosolvent to prevent limitations caused by the immiscibility of the two components at the initial stages of the reaction. With the consideration of the study of the thermodynamic equilibrium, where K_{eq} was obtained as a function of temperature, a LHHW model was put forward where the surface reaction for the formation of H_2O , by-product of the reaction, would be the rate-limiting step. This leads to an equation that considers the adsorption constant of H_2O in addition to the intrinsic reaction constant, which, represented by Arrhenius-type equations, lead to values of E_a of 55.6 kJ mol^{-1} and ΔH_a of $-64.7 \text{ kJ mol}^{-1}$ [108]. Esteban et al. [118] made catalyst screening settling for Lewatit GF101 after observation of its performance in a solventless operation. When contemplating a statistical discrimination analysis for different assumptions of PH, LHHW and ER based models were proposed. For the latter two types, a common thread with previous works is the assumption of H_2O as the only compound adsorbing onto the surface of the catalyst, which is a usual consideration when using IER. After correlation of 12 different models and statistical analysis based on goodness of fit and information criteria, the conclusion was that the data were best described with an ER model of zero order with respect to the reactant species (owing to their excess

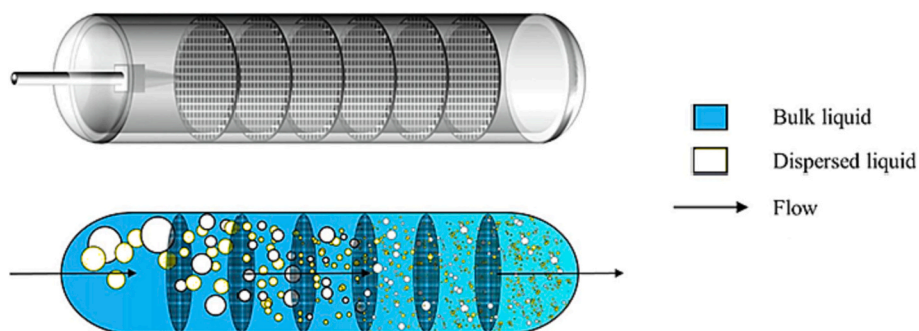


Fig. 6. Schematic representation of a static mixer reactor. Based on the original figure by Vorholt et al. [105].

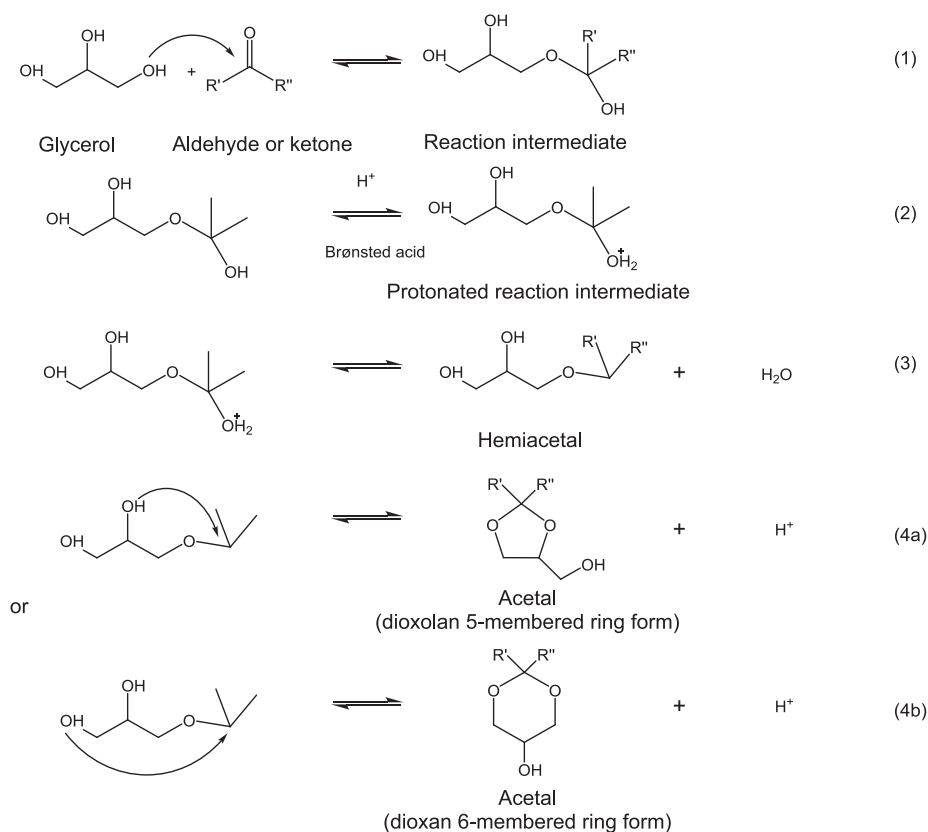


Fig. 7. General mechanism for the production of glycerol acetals by reaction with aldehydes or ketones in the presence of an acid catalyst.

and constant value at the surface) and first order for the products for the reverse reaction [118]. Rodrigues et al. [109] conducted a catalyst and solvent screening for the production of SLk, settling for Amberlyst 35 in the presence of ethanol to enhance productivity. Similarly to their study for the acetalisation of Gly with acetaldehyde [112], they performed a thermodynamic study of the reaction and assumed internal diffusion in their study, which they incorporated into PH, ER and LHHW models. The results revealed that the latter is the most adequate, a value of 14.4 for the adsorption constant of H_2O ($K_{a,\text{H}_2\text{O}}$), given at a constant temperature [109].

Last, a power-law PH model was also found appropriate to describe the reaction despite the use of heterogeneous catalysts. For the reaction catalysed by zeolite H-BEA, a kinetic analysis was made based on the correlation of data with an inverse stochastic routine known as random restricted window and a fractional factorial design to identify the best stirring rate ($\omega = 700$ rpm), T (313–353 K), catalyst amount (5%) and MR of Acetone:Gly (4:1). With a power-law model, the forward E_a was $44.77 \text{ kJ mol}^{-1}$ and that for the reverse reaction was $41.40 \text{ kJ mol}^{-1}$, which are significantly lower values than in other cases [119]. Using Puro-lite CT-275 as catalyst, a lab scale and a scaled-up reaction study was made, validating the reaction kinetics for both as well as the reaction thermodynamics. A power-law model was tested together with others based on the assumption of ER and LHHW mechanisms. The former gave the best fit and was validated, also for scaled-up operation, although in this article the authors fail to provide details about the ER and LHHW and the values obtained for the adsorption constants and for which particular components they were assumed [106].

In terms of process intensification, here novel mixing strategies could be an option, such as the aforementioned potential use of ultrasound or static mixers. In addition, to overcome the thermodynamic limitations of the reaction, the use of hybrid operations would be key to remove water as by-product and enhance the equilibrium position. These could include using pervaporation membranes [120] or reacting distillation

devices, which can effectively separate the product directly, as shown in Fig. 8 [121]. Another alternative to shift the reaction towards the products on a more localized level would be to modify the surface of heterogeneous catalysts to confer them a certain level of hydrophobicity [122]. In this way, water could be removed from the active sites as it is produced, which is oftentimes problematic due to its high affinity to active sites in materials like IER. These approaches are also applicable to the subsequent esterification and etherification reactions, which show similar characteristics in terms of thermodynamic limitations.

4.3. Esters

The esterification of Gly with organic acids leads to a wide range of products with applications such as fuel additives, solvents, plasticizers, food additives and pharmaceuticals [123]. The reaction is acid-catalysed and occurs in three steps where monoglycerides (MGs), diglycerides (DGs) and triglycerides (TGs) are generated along with water as a by-product, as shown in Fig. 9. The three steps are in equilibrium and thus makes the reaction thermodynamically limited.

Consequently, reaction conditions such as molar ratio (MR) and temperature (T) affect product yields and distribution. Apart from the obvious positive effect of temperature on reaction rates, strategies to shift the equilibrium towards the products must be followed. It was observed that a molar excess of acid had a greater impact on equilibrium compared to temperature [124,125]. Additionally, it was observed water removal leads to higher conversions due to the suppression of the reverse reactions [126], which leads to logically think that in situ water removal would be a very interesting approach to overcome thermodynamic limitations. In relation with thermodynamics, to investigate the effect of water in the esterification of ibuprofen and Gly with *Candida antarctica* lipase B (CALB), an open system where water is removed and a closed system in which water remains in the reaction mixture were studied. In the former, no enzymatic inhibition by water occurred and

Table 6

Summary of the most relevant aspects of kinetic studies for the production of glycerol acetals. a, b, c, d

Reactants and Catalyst	Reaction conditions ^a	(Best) $X_{\text{Gly}}/\text{Sel}/\text{Yield}^b$	Kinetic rate type and equation ^c	Kinetic parameters ^d	Notes	Ref.
Gly + Formaldehyde Catalyst: Amberlyst 47	$T = 353\text{--}373\text{ K}$ MR = 1:3–1:1 Cat _{load} = 5.0 wt% $\omega = 1250\text{ rpm}$ $t_{\text{rxn}} \approx 600\text{--}750\text{ min}$	$S_{\text{acetals}} = 100\%$	Power law (pseudo homogeneous): $r = wk_1 C_{\text{Gly}} C_{\text{formaldehyde}} - wk_{-1} C_{\text{acetal}} C_{\text{H}_2\text{O}}$	$E_{a1} = 59.062\text{ kJ mol}^{-1}$ $E_{a-1} = 46.301\text{ kJ mol}^{-1}$ $k_{01} =$ $7463.6\text{ L}^2\text{ mol}^{-1}\text{ g}_{\text{cat}}^{-1}\text{ min}^{-1}$ $k_{0-1} =$ $34.5\text{ L}^2\text{ mol}^{-1}\text{ g}_{\text{cat}}^{-1}\text{ min}^{-1}$	–	[114]
Gly + Formaldehyde Catalyst: Amberlyst 15	$T = 333\text{--}353\text{ K}$ MR = 1:1–2:1 Cat _{load} = 0–10 wt% $\omega = 1200\text{ rpm}$ $t_{\text{rxn}} = 120\text{ min}$	$X_{\text{Gly}} = 60\%$	Power law (pseudo homogeneous): $r = k_1 (a_{\text{Gly}} a_{\text{formaldehyde}}) - k_{-1} (a_{\text{acetal}} a_{\text{H}_2\text{O}})$	$E_{a1} = 39.05\text{ kJ mol}^{-1}$ $E_{a-1} = 46.30\text{ kJ mol}^{-1}$ $\ln k_{01} = 18.53$ $\ln k_{0-1} = 25.5$	Reactive distillation study.	[115]
Gly + acetaldehyde Catalyst: Amberlyst 15	$T = 303\text{--}358\text{ K}$ MR = 0.5:1–2:1 Cat _{load} = 0.15–0.3 wt % $\omega = 500\text{ rpm}$ $t_{\text{rxn}} \approx 420\text{ min}$	$X_{\text{Gly}} \approx 90\%$	LHHW: $r = k \frac{C_{\text{Gly}} C_{\text{acetaldehyde}} - C_{\text{acetal}} C_{\text{H}_2\text{O}}/K_{\text{eq}}}{(1 + K_{a,\text{H}_2\text{O}} C_{\text{H}_2\text{O}} + K_{a,\text{solvent}} C_{\text{solvent}})^2}$	$E_a = 77.7\text{ kJ mol}^{-1}$ $k_0 = 5.97 \times 10^8\text{ dm}^6\text{ mol}^{-1}\text{ g}_{\text{cat}}^{-1}\text{ s}^{-1}$ $\Delta G_{\text{K}_{\text{eq}}} = 12.95\text{ kJ mol}^{-1}$ Adsorption constants $K_{a,\text{H}_2\text{O}} = 0.345\text{ dm}^3\text{ mol}^{-1}$ $K_{a,\text{solvent}} = 0.106\text{ dm}^3\text{ mol}^{-1}$	With solvent (dimethyl sulfoxide). Solvent's adsorption is considered due to its strong polar nature.	[112]
Gly + acetaldehyde Catalyst: Amberlyst 47	$T = 283\text{--}313\text{ K}$ MR = 1:3–1:1 Cat _{load} = 2 wt% $\omega = 700\text{ rpm}$ $t_{\text{rxn}} \approx 1560\text{ min}$	$S_{\text{acetals}} = 100\%$	Power law (first order): $r = wk_{\text{Cacetaldehyde}}$	$E_a = 55.4\text{ kJ mol}^{-1}$ $\ln k_0 = 14.51$	Considered reaction is irreversible	[116]
Gly + Acetone Catalyst: Purolite CT275	$T = 298\text{--}323\text{ K}$ MR = 2:1–10:1 Cat _{load} = 1–5 wt% $\omega = 250\text{ rpm}$ $t_{\text{rxn}} = 320\text{ min}$	$X_{\text{Gly}} = 93\%$	Low range adsorption model (no adsorption occurs, n = 0): $r = k \frac{C_{\text{Gly}} C_{\text{acetone}} - C_{\text{Silk}} C_{\text{H}_2\text{O}}/K_{\text{eq}}}{(1 + K_{a,i} C_i)^n}$	$E_a = 39.78\text{ kJ mol}^{-1}$ $k_0 = 3.86 \times 10^3\text{ L}^2\text{ mol}^{-1}\text{ g}_{\text{cat}}^{-1}\text{ min}^{-1}$ $\Delta H_{\text{K}_{\text{eq}}} = -6.605\text{ kJ mol}^{-1}$ $\Delta S_{\text{K}_{\text{eq}}} = -$ $20.72\text{ J mol}^{-1}\text{ K}^{-1}$	Solventless system. Detailed thermodynamic study. Low range adsorption model (n = 0 for the adsorption terms); i.e. pseudo homogeneous; although ER and LHHW tested	[106]
Gly + Acetone Catalyst: Amberlyst-35	$T = 293\text{--}323\text{ K}$ MR = 1.48:1–2.46:1 Cat _{load} = 1% wt. of Gly $\omega = 700\text{ rpm}$ $t_{\text{rxn}} = 300\text{ min}$	$Y_{\text{Silk}} = 74\%$	LHHW: $r = k \frac{C_{\text{Gly}} C_{\text{acetone}} - C_{\text{Silk}} C_{\text{H}_2\text{O}}/K_{\text{eq}}}{(1 + K_{a,\text{H}_2\text{O}} C_{\text{H}_2\text{O}})^2}$	$E_a = 55.6\text{ kJ mol}^{-1}$ $k_0 = \text{not available}$ $\Delta H_{\text{K}_{\text{eq}}} = -30.1\text{ kJ mol}^{-1}$ $\Delta S_{\text{K}_{\text{eq}}} = -0.1\text{ kJ mol}^{-1}\text{ K}^{-1}$ $\Delta G_{\text{K}_{\text{eq}}} = -2.1\text{ kJ mol}^{-1}$ Adsorption constants $\Delta H_{a,\text{H}_2\text{O}} = -64.7\text{ kJ mol}^{-1}$ $k_0\text{--}K_{a,\text{H}_2\text{O}} = \text{not available}$	Includes thermodynamic study.	[108]
Gly + Acetone Catalyst: Amberlyst 35	$T = 303\text{--}323\text{ K}$ MR = 0.5:1–2:1 Cat _{load} = 0.25–0.5 wt % $\omega = 750\text{ rpm}$ $t_{\text{rxn}} = 480\text{ min}$	$X_{\text{Gly}} = 70\%$	LHHW: $r = k \frac{a_{\text{Gly}} a_{\text{acetone}} - a_{\text{Silk}} a_{\text{H}_2\text{O}}/K_{\text{eq}}}{(1 + K_{a,\text{H}_2\text{O}} a_{\text{H}_2\text{O}})^2}$	$E_a = 69.0\text{ kJ mol}^{-1}$ $k_0 = 492\text{ mol kg}_{\text{cat}}^{-1}\text{ s}^{-1}$ $\Delta H_{\text{K}_{\text{eq}}} = -20.1\text{ kJ mol}^{-1}$ $\Delta G_{\text{K}_{\text{eq}}} = 1.4\text{ kJ mol}^{-1}$ Adsorption constants $K_{a,\text{H}_2\text{O}} = 14.4$ (value given as constant with T)	With solvent. Thermodynamic study. LHHW most adequate, although PH and ER also tested. Adsorption constant for water only.	[109]
Gly + Acetone Catalyst: Lewatit GF101	$T = 303\text{--}313\text{ K}$ MR = 3–12 Cat _{load} = 0.5–1% wt. $\omega = 750\text{ rpm}$ $t_{\text{rxn}} = 240\text{ min}$	$Y_{\text{Silk}} = 96\%$	ER: $r = \frac{k_1 C_{\text{cat}} - k_{-1} C_{\text{cat}} C_{\text{Silk}} C_{\text{H}_2\text{O}}}{1 + K_{a,\text{H}_2\text{O}} C_{\text{H}_2\text{O}}}$	$E_{a1} = 124.0\text{ kJ mol}^{-1}$ $E_{a-1} = 127.3\text{ kJ mol}^{-1}$ $\ln k_{01} = 44.14$ $\ln k_{0-1} = 45.14$ Adsorption constants $\Delta H_{a,\text{H}_2\text{O}} = -128.0\text{ kJ mol}^{-1}$ $\ln k_0\text{--}K_{a,\text{H}_2\text{O}} = 51.17$	Best fit model is ER model with reverse reaction and zero order for reactants. Only adsorption constant for water.	[118]
Gly + Acetone Catalyst: zeolite H-BEA (SAR 19)	$T = 313\text{--}353\text{ K}$ MR = 4:1 Cat _{load} = 5 wt% of Gly $\omega = 700\text{ rpm}$ $t_{\text{rxn}} = 180\text{ min}$	$Y_{\text{Silk}} \approx 76\%$	Power law (Pseudo homogeneous): $r = k_1 C_{\text{Gly}} C_{\text{acetone}} - k_{-1} C_{\text{Silk}} C_{\text{H}_2\text{O}}$	$E_{a1} = 44.77\text{ kJ mol}^{-1}$ $E_{a-1} = 41.40\text{ kJ mol}^{-1}$ $\ln k_{01} = 11.34^*$ $\ln k_{0-1} = 10.74^*$	No LHHW or ER models contemplated.	[119]

(continued on next page)

Table 6 (continued)

Reactants and Catalyst	Reaction conditions ^a	(Best) X_{Gly} / Sel/Yield ^b	Kinetic rate type and equation ^c	Kinetic parameters ^d	Notes	Ref.
Gly + butyraldehyde Catalyst: Amberlyst 47	T = 338–353 K MR = 1:3–1:1 Cat _{load} = 0.5 wt% ω = 1000 rpm $t_{rxn} \approx 540$ min	$S_{acetals} = 100\%$	Power law (pseudo homogeneous): $r = wk_1 C_{Gly} C_{butyraldehyde} -$ $wk_{-1} C_{acetal} C_{H_2O}$	$E_{a1} = 55.6 \text{ kJ mol}^{-1}$ $E_{a-1} = 115 \text{ kJ mol}^{-1}$ $k_{01} = 5.33 \times$ $10^5 \text{ L}^2 \text{ mol}^{-1} \text{ g}_{cat}^{-1} \text{ min}^{-1}$ $k_{0-1} = 2.67 \times$ $10^{12} \text{ L}^2 \text{ mol}^{-1} \text{ g}_{cat}^{-1} \text{ min}^{-1}$	–	[117]

^a Reaction conditions used for kinetic studies. Temperature (T), aldehyde/ketone/ether to Gly molar ratio (MR), catalyst loading (Cat_{load}), stirring speed (ω), reaction time (t_{rxn}).

^b Best Gly conversion (X_{Gly}), selectivity (S) or yield (Y) with respect to solketal (Slk) or acetals, achieved at optimum operating conditions which are different than the reaction conditions^a for kinetic study presented in the table.

^c Rate of reaction (r_i), forward reaction rate constant (k_j), backward reaction rate constant (k_{-j}), concentration (C_i), overall equilibrium constant (K_{eq}), component adsorption equilibrium constant ($K_{a,i}$), component activity (a_i), catalyst loading (w), concentration of catalyst (C_{cat}). i : components, j =reactions. Subscripts: Slk = solketal.

^d Activation energy (E_{aj}), pre-exponential factor (k_{0j}/k_{0-j}), enthalpy of equilibrium constant ($\Delta H_{K_{eq}}$), entropy of equilibrium constant ($\Delta S_{K_{eq}}$), Gibbs free energy of equilibrium constant ($\Delta G_{K_{eq}}$), enthalpy of component adsorption constant ($\Delta H_{a,i}$), pre-exponential factor of component adsorption constant ($k_{0-K_{a,i}}$). Subscripts: i : components, j =reactions. $\ln k_{0j}$ obtained from Arrhenius plot provided, values taken as equal to the y-intercept of line equation.

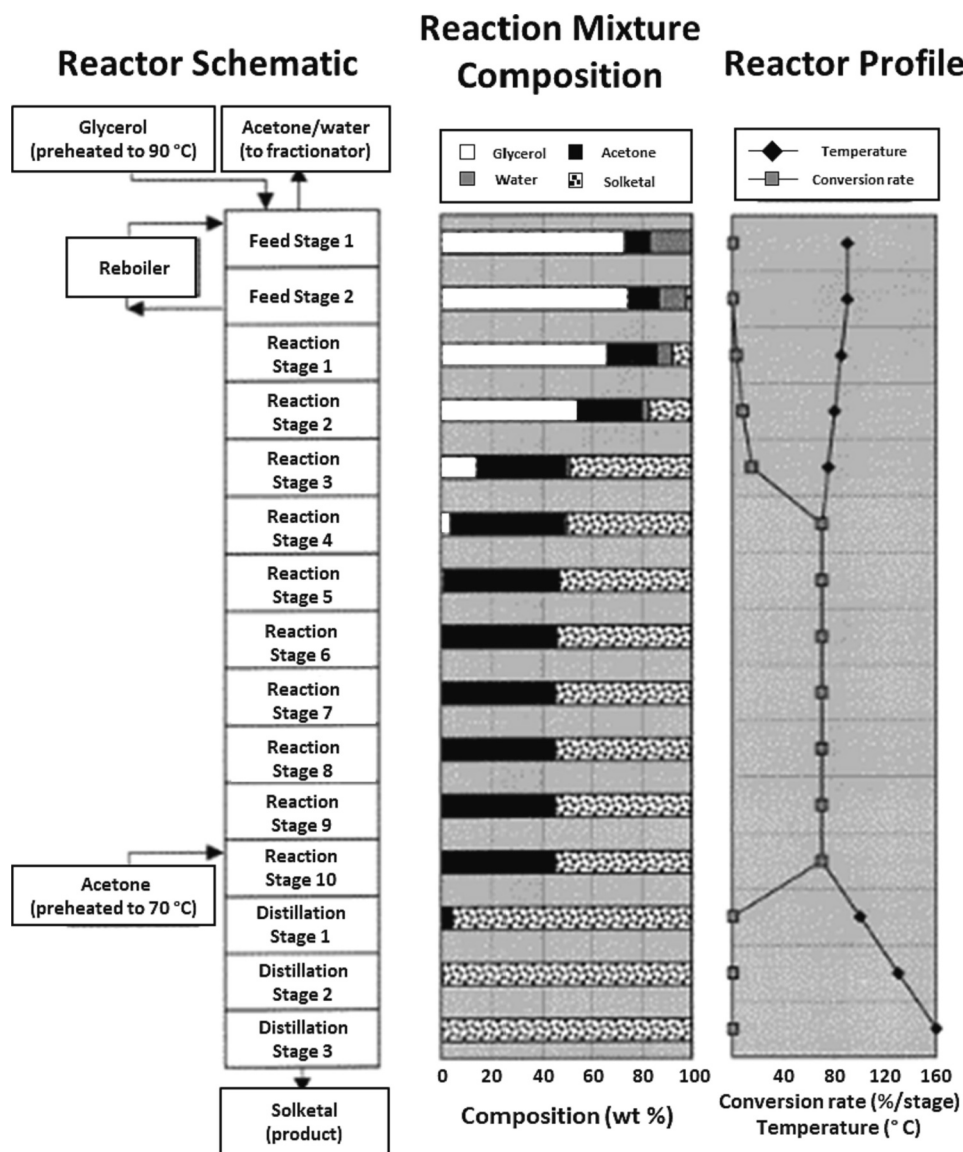


Fig. 8. Schematic diagram of a reactive distillation column for the production of Slk and the corresponding composition, conversion rate and temperature profiles in each stage. Edited figure for enhanced visibility reproduced with permission of ACS publishing [121].

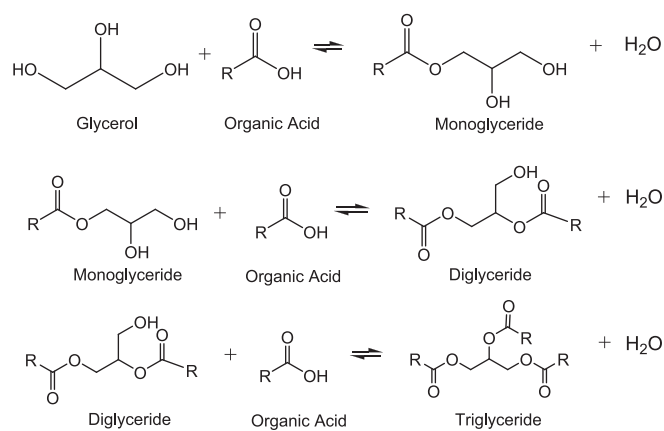


Fig. 9. Reaction scheme of the three in-series steps of the esterification of glycerol with organic acids.

better yields to monoesters were achieved [127]. Another study showed that in a two-phase system in which the reaction occurs in the organic phase, the Gly phase aids in shifting the equilibrium towards the forward reaction [128]. This is because of Gly molecules having high polarity attract water generated during the reaction [128]. Similarly, in the esterification with benzoic acid with CALB, the hydrophilic nature of Gly led water away from the catalytic active sites to the liquid bulk [129]. Water separation from active sites can also be achieved by designing hydrophobic catalysts [130]. These studies point in the direction of the opportunity to devise further strategies to separate water from the medium.

In addition to thermodynamic effects, the removal of water is also vital to avoid the deactivation of the catalyst due to poisoning. This is because the presence of water leads to leaching of the active sulphonic groups from the surface of the catalyst and encourages the accumulation of secondary products that are high in carbon content [68]. Such deactivation mechanisms are vital to consider in kinetic modelling as they can provide an outlook on catalyst stability [131] and thus can lead to the basis for designing deactivation resistant catalysts [68]. Okoye et al. [68] has provided several deactivation models that describe coking, sintering and poisoning.

Table 7 highlights kinetic studies for Gly esterification reactions with different organic acids with homogeneous, heterogeneous, and enzymatic catalysts featuring a wide array of models. In a study in which Gly reacts with acetic acid (ACA), LHHW based model was used but simplified to a pseudo-homogeneous first-order model to describe the reaction kinetics [125]. This is because resistance terms have been ignored due to the assumption that the reactants are weakly adsorbed on the catalyst surface. The concentration of the catalytic active sites are assumed constant due to large excess of ACA and, for the same reason, the backward reactions are ignored [125]. For the calculation of the rate constants, the effect of acid to Gly molar ratio (MR) along temperature was included [125]. The activation energies found for the production of MGs, DGs and TGs are 57.26 kJ mol⁻¹, 31.87 kJ mol⁻¹ and 13.90 kJ mol⁻¹, respectively [125].

Furthermore, a quasi-homogeneous first-order model was developed for the same reaction (Gly and ACA) using NKC-9 catalyst [132]. Both forward and backwards reactions were considered, and the E_a values found ranged between 19.33 and 65.58 kJ mol⁻¹. The model was validated and implemented to investigate reactive distillation as a process intensification approach for the reaction to attain high Gly conversion and TGs yield [132]. Moreover, pseudo-homogeneous first order kinetic equations were also found suitable for a reaction between Gly and hydrogenated rosin using subcritical CO₂-enriched high temperature compressed water (HTCW) as catalyst. This is due to the presence of excess Gly and thus its concentration can be assumed to be constant [133]. The E_a for the production of MGs, DGs and TGs are in the same

order as the studies mentioned before [133].

Ladero et al. [127,129] have made significant efforts in modelling the kinetics of enzyme catalysed Gly esterification. Using CALB to catalyse the esterification with ibuprofen in a system where water is eliminated (open system), the suitable kinetic model is an irreversible hyperbolic model with pseudo-zero order for Gly considering its excess [127]. Nevertheless, when considering that the water generated remains in the reaction mixture (closed system), a reversible Michaelis-Menten model with pseudo-first order for ibuprofen and monoester was found to be the most suitable [127]. The difference observed in the E_a for both systems went from 58 kJ mol⁻¹ to as little as 14–45 kJ mol⁻¹ [127]. In the study of the esterification with benzoic acid using the same enzyme, it was found that a Michaelis-Menten model with partial one-step deactivation took place, hence accounting for the dynamic decrease of activity, which was allocated to the presence of benzoic acid [129]. The E_a of the reaction is 45.4 kJ mol⁻¹, while the E_a for deactivation are 76.1–134 kJ mol⁻¹ [129]. A low E_a value (41.5 kJ mol⁻¹) was also obtained for the ultrasound assisted esterification of Gly and caprylic acid using the enzyme Lipase- *Candida antarctica* described by a second order power-law model [134].

Likewise, Ladero et al. [135] have also studied esterification with homogeneous catalysts, incorporating their deactivation in the models. When investigating the system in the presence of PTSA, the system can be described in two consecutive esterification reactions with partial first order with respect to the reactants and a first order reaction for the deactivation of the catalyst [135]. Similarly, this modelling approach was applied to the reaction of Gly and *p*-methoxycinnamic acid, with deactivation of the catalyst being ascribed to the acid molecules leaching the catalyst surface [130]. Based on this model, the E_a of the reactions are 87.33 kJ mol⁻¹ and 69.17 kJ mol⁻¹, while deactivation has an E_a of 104 kJ mol⁻¹.

In another study using HSO₃SBA-15 as catalyst, the esterification with lauric acid was modelled as parallel reactions where Gly underwent mono-, di- or tri- substitution, where such reactions were described as irreversible [126]. This unusual consideration was taken because the yield of MG did not decrease over time, indicating that the generation of DG and MG occurred due to Gly molecules taking part in the reaction instead of the glycerides (MG and DG). The kinetic model was concluded to be a second order model with respect to Gly and lauric acid [126]. The value of E_a for MGs formation is 42 kJ mol⁻¹, which is lower than the 51 kJ mol⁻¹ estimated when using zinc carboxylates as catalyst. The difference is expected to be due to the structural properties of the catalyst (high surface area and mesoporous structure), which led bulky lauric acid molecules to better access catalytic sites [126].

Furthermore, certain systems investigated are biphasic, as is the case of esterification with oleic acid, where Gly and oleic acid are only partially miscible. It was observed that the reaction takes place in the oleic acid phase and the presence of a separate Gly phase affects product distribution. The catalyst (ZnO/zeolite) has a greater affinity to the organic (i.e oleic) phase due to its hydrophobicity [128]. The kinetic model combines both series and parallel irreversible reactions, the latter due to the removal of water from the organic phase. To develop the model, it was assumed that the solubility of Gly in oleic phase is constant whilst neglecting the production of TG, reaching E_a ranging between 45.0 and 66.0 kJ mol⁻¹ [128]. The esterification of Gly with rosin also forms two phases [136]. It was found that for an uncatalyzed reaction, a hyperbolic model describes that the reaction behaves as a first order reaction initially but evolves to a second order at the end of the reaction [136]. Upon model discrimination with other alternatives, this model showed the best kinetics of the reaction, also accounting for the segregated phases and the limited solubility of Gly in rosin. This effect is particularly relevant at the start of the reaction, where the local concentration of Gly in the non-polar phase can be assumed constant. However, once the reaction proceeds, both reagents are in the same phase taking part in the reaction and thus a second order model becomes more fitted, similarly to the cases discussed for Gly carbonate in

Table 7
Summary of the most relevant aspects of kinetic studies for the production of glycerol esters.

Reactants and Catalyst	Reaction conditions ^a	(Best) X _{Gly} /Sel/ Yield ^b	Kinetic rate type and equations ^c	Kinetic parameters ^d	Notes	Ref.
Gly + ACA Catalyst: Amberlyst 15	T = 353–383 K MR = 3:1–9:1 Cat _{load} = 2.645 g ω = 1100 rpm t _{rxn} = 300 min	S _{DG} = 47.7% S _{TG} = 44.5%	LHHW (simplified to pseudo homogeneous first order): $r_{MG} = k_1 C_{Gly}$ $r_{DG} = k_2 C_{MG} - k_3 C_{DG}$	$E_{a1} = 57.26 \text{ kJ mol}^{-1}$ $E_{a2} = 31.87 \text{ kJ mol}^{-1}$ $E_{a3} = 13.90 \text{ kJ mol}^{-1}$ $k_{01} = 2.07 \times 10^6 \times MR^{0.274}$ $k_{02} = 18.66 \times MR^{1.82}$ $k_{03} = 1.16 \times MR^{-0.474}$ $E_{a1} = 50.656 \text{ kJ mol}^{-1}$ $E_{a-1} = 64.554 \text{ kJ mol}^{-1}$ $E_{a2} = 46.030 \text{ kJ mol}^{-1}$ $E_{a-2} = 19.333 \text{ kJ mol}^{-1}$ $E_{a3} = 65.575 \text{ kJ mol}^{-1}$ $E_{a-3} = 22.270 \text{ kJ mol}^{-1}$ $k_{01} = 753.61 \text{ L mol}^{-1} \text{ s}^{-1}$ $k_{0-1} = 216.53 \text{ L mol}^{-1} \text{ s}^{-1}$ $k_{02} = 136.22 \text{ L mol}^{-1} \text{ s}^{-1}$ $k_{0-2} = 14.88 \times 10^{-4} \text{ L mol}^{-1} \text{ s}^{-1}$ $k_{03} = 29.33 \times 10^5 \text{ L mol}^{-1} \text{ s}^{-1}$ $k_{0-3} = 19.31 \text{ L mol}^{-1} \text{ s}^{-1}$ $E_{a1}/R = 7650 \text{ K}$ $E_{a2}/R = 3198 \text{ K}$ $E_{a3}/R = 3030 \text{ K}$ $k_{01} = 0.0162 \text{ kmol (kg s)}^{-1}$ $k_{02} = 0.0118 \text{ kmol (kg s)}^{-1}$ $k_{03} = 0.003 \text{ kmol (kg s)}^{-1}$	It is assumed the components are weakly adsorbed and thus resistance term of LHHW is negligible. Model is based on pseudo homogeneous first order reactions occurring in series.	[125]
Gly + ACA Catalyst: NKC-9	T = 338–368 K MR = 3:1 Cat _{load} = 2.8 g ω = 1250 t _{rxn} = 460 min	Y _{DG} = 50% Y _{DG} = 35% Y _{TG} = 5%	Power-law (quasi-homogeneous first-order): $r_{MG} = k_1 C_{Gly} C_{acid} - k_{-1} C_{MG} C_{H_2O} - k_2 C_{MG} C_{acid} + k_{-2} C_{DG} C_{H_2O}$ $r_{DG} = k_2 C_{MG} C_{acid} - k_{-2} C_{DG} C_{H_2O} - k_3 C_{DG} C_{acid} + k_{-3} C_{TG} C_{H_2O}$ $r_{TG} = k_3 C_{DG} C_{acid} - k_{-3} C_{TG} C_{H_2O}$	$\Delta G_{-K_{eq1}} = -5.118 \text{ kJ mol}^{-1}$ $\Delta G_{-K_{eq2}} = -0.961 \text{ kJ mol}^{-1}$ $\Delta G_{-K_{eq3}} = -3.371 \text{ kJ mol}^{-1}$	Reactive distillation study.	[132]
Gly + ACA Catalyst: Purolite CT-275	T = 343–383 K MR = 4:1–9:1 Cat _{load} = 0.065 g/g _{Gly} ω = 1000 rpm t _{rxn} = 350 min	Y _{DG} = 56% Y _{TG} = 30%	LHHW: $r_{MG} = \frac{k_1 \left(a_{Gly} a_{acid} - \frac{a_{MG} a_{H_2O}}{K_{eq1}} \right)}{\left(1 + \sum_i K_{a,i} a_i \right)^2}$ $r_{DG} = \frac{k_2 \left(a_{MG} a_{acid} - \frac{a_{DG} a_{H_2O}}{K_{eq2}} \right)}{\left(1 + \sum_i K_{a,i} a_i \right)^2}$ $r_{TG} = \frac{k_3 \left(a_{DG} a_{acid} - \frac{a_{TG} a_{H_2O}}{K_{eq3}} \right)}{\left(1 + \sum_i K_{a,i} a_i \right)^2}$	Adsorption constants $K_{a,Gly} = 5.4$ $K_{a,acid} = 2.5$ $K_{a,H_2O} = 10.0$ $E_{a1}/R = 5550 \text{ K}$ $E_{a2}/R = 5838 \text{ K}$ $E_{a3}/R = 5893 \text{ K}$ $k_{01} = 9.31 \text{ ml}^2 \text{ mmol}^{-1} \text{ mol}^{-1} \text{ s}^{-1}$ $k_{02} = 3.07 \text{ ml}^2 \text{ mmol}^{-1} \text{ mol}^{-1} \text{ s}^{-1}$ $k_{03} = 0.24 \text{ ml}^2 \text{ mmol}^{-1} \text{ mol}^{-1} \text{ s}^{-1}$	Model considers non-ideal behaviour of the components. Uses liquid phase activities in rate equations (a_j).	[138]
Gly + ACA Catalyst: Dowex 650C	T = 353–393 K MR = 3:1–9:1 Cat _{load} = 4 and 8 wt% ω = 500 rpm t _{rxn} = 360 min	S _{MG} = 11% S _{DG} = 52% S _{TG} = 37%	ER model: $r_{MG} = k_x C_{Gly} K_{a,acid} C_{acid} C_{FS} - k_{-x} K_{a,MG} C_{MG} C_{H_2O} C_{FS}$ $r_{DG} = k_y C_{MG} K_{a,acid} C_{acid} C_{FS} - k_{-y} K_{a,DG} C_{DG} C_{H_2O} C_{FS}$ $r_{TG} = k_z C_{DG} K_{a,acid} C_{acid} C_{FS} - k_{-z} K_{a,TG} C_{TG} C_{H_2O} C_{FS}$	Adsorption constants $\Delta H_{a,Gly}/R = -5933 \text{ K}$ $\Delta H_{a,H_2O}/R = -1442 \text{ K}$ $k_{0,Gly} = 417 \text{ ml mol}^{-1}$ $k_{0,K_{a,H_2O}} = 570 \text{ ml mol}^{-1}$	Power law and LHHW models were also developed, but ER fits experimental data best.	[139]

(continued on next page)

Table 7 (continued)

Reactants and Catalyst	Reaction conditions ^a	(Best) X _{Gly} /Sel/ Yield ^b	Kinetic rate type and equations ^c	Kinetic parameters ^d	Notes	Ref.
Gly + ACA Catalyst: 3%Y/SBA-3	T = 373–393 K MR = 4:1 Cat _{load} = 0.40 g ω = 350 rpm t _{rxn} = 150 min	S _{DG} = 34% S _{TG} = 55%	$k_3 = k_2 K_{a,acid} C_{TS}$ $C_{FS} = \frac{C_{TS}}{1 + K_{a,Gly} C_{Gly} + K_{a,H_2O} C_{H_2O}}$ <p>Pseudo-first order (overall reaction):</p> $-r_{Gly} = k_1 C_{Gly} C_{acid}^{\theta} - k_{-1} C_{MG} C_{DG} C_{TG}$ <p>LHHW (for r.d.s):</p> $r_{r.d.s} = \frac{C_{FS}^2}{C_{TS}} \left(K_{a,Gly} K_{a,acid} C_{Gly} C_{acid} - \frac{k_{des} (C_{MG} + C_{DG} + C_{TG})}{K_{eq,surface\ rxn}} \right)$ <p>Michaelis-Menten model with partial deactivation:</p> $\frac{dC_{MG}}{dt} = -\frac{dC_{acid}}{dt} = \frac{k_2 C_{cat} a_{cat,R} C_{acid}}{K_{MMC} + C_{acid}}$ $a_{cat,R} = \frac{C_{cat} + C_{cat}^{\beta}}{C_{cat_0}}$ $\frac{dC_{cat}}{dt} = -\frac{dC_{cat}^{\beta}}{dt} = -k_{d1} C_{cat} - k_{d2} C_{cat} C_{acid}^m$ <p><i>a_{cat,R} is residual catalyst activity</i> <i>β describes the activity of partially deactivated catalyst relative to initial activity</i></p>	<p>Pseudo-first order (overall reaction):</p> $E_{a1} = 21.54 \text{ kJ mol}^{-1}$ $k_{01} = 0.883 \times 10^3 \text{ min}^{-1}$ $K_{eq,1} = 1.17$ <p>Parameters and equations are provided for surface reaction rate equation (<i>r_{r.d.s}</i>)</p> $m = 3.09$ $E_{a2} = 45.5 \text{ kJ mol}^{-1}$ $E_{ad1} = 76.1 \text{ kJ mol}^{-1}$ $E_{ad2} = 134 \text{ kJ mol}^{-1}$ $E_{a\beta} = -206 \text{ kJ mol}^{-1}$ $K_{MMC} = 0.427 \text{ mol L}^{-1}$ $\ln k_{02} = 5.46$ $\ln k_{0d1} = 24.3$ $\ln k_{0d2} = 49.2$ $\ln k_{0\beta} = -77.5$	In LHHW model, surface reaction is the r.d.s. Water concentration is ignored in model.	[140]
Gly + benzoic acid Catalyst: CALB	T = 323–343 K MR = not available C _{acid,feed} = 20–60 g L ⁻¹ Cat _{load} = 30 g L ⁻¹ ω = 450 rpm t _{rxn} ≈ 2880 min	X _{acid} ≈ 92%	<p>Power-law (second order):</p> $-r_{Gly} = k C_{Gly}^2$	$E_a = 41.5 \text{ kJ mol}^{-1}$ $k_0 = 1.17 \text{ L mol}^{-1} \text{ min}^{-1}$	Solventless system. Excess Gly used.	[129]
Gly + caprylic acid Catalyst: Lipase-Candida antarctica	T = 303–353 K MR = 4:1 Cat _{load} = not available ω = not available t _{rxn} = 480 min	Y _{ester} = 94.8%	<p>Power-law (second order):</p> $-r_{Gly} = k C_{Gly}^2$	$E_a = 41.5 \text{ kJ mol}^{-1}$ $k_0 = 1.17 \text{ L mol}^{-1} \text{ min}^{-1}$	Uses ultrasound assisted intensification (optimum frequency is 20 kHz).	[134]
Gly + cinnamic acid and Gly + p- Methoxy cinnamic acid Catalyst: PTSA	T = 413–433 K (cinnamic acid experiments) T = 423–443 K (p- Methoxy cinnamic acid experiments) MR = 1:3–1:9 Cat _{load} = not available ω: 250 rpm t _{rxn} = 300 min	S _{MG} = 91% S _{DG} = 9%	<p>Power law:</p> $r_{MG} = k_1 C_{cat} C_{Gly} C_{acid}$ $r_{DG} = k_2 C_{cat} C_{MG} C_{acid}$ $r_{cat,deactivation} = k_3 C_{cat}$	<p><i>Cinnamic acid</i></p> $E_{a1}/R = 4880 \text{ K}$ $E_{a2}/R = 5160 \text{ K}$ $E_{a3}/R = 4230 \text{ K}$ $\ln k_{01} = 5.3$ $\ln k_{02} = 5.4$ $\ln k_{03} = 6.2$ <p><i>p – Methoxy cinnamic acid</i></p> $E_{a1}/R = 7790 \text{ K}$ $E_{a2}/R = 5010 \text{ K}$ $E_{a3}/R = 11,900 \text{ K}$ $\ln k_{01} = 12.8$ $\ln k_{02} = 5.6$ $\ln k_{03} = 24.7$ <p><i>Cinnamic acid</i></p> $E_{a1}/R = 9623 \text{ K}$ $E_{a2}/R = 9739 \text{ K}$ $E_{a3}/R = 15,702 \text{ K}$ $E_{a4}/R = 26,154 \text{ K}$ $\ln k_{01} = 13.3$ $\ln k_{02} = 14.8$ $\ln k_{03} = 26.2$ $\ln k_{04} = 47.2$	Model discrimination. Model consists of two reactions in series with partial first order with respect to reactants and first-order deactivation of catalyst.	[135]
Gly + cinnamic acid and Gly + p- Methoxy cinnamic acid Catalyst: None	T = 423–473 K MR = 1:3–1:9 Cat _{load} = None ω = 250 rpm t _{rxn} ≈ 700–7500 min	S _{MG} = 80–90%	<p>Power law:</p> $r_{MG} = k_1 C_{Gly} C_{acid}$ $r_{DG} = k_2 C_{MG} C_{acid}$ $r_{MG} = k_3 C_{Gly} C_{DG}$ $r_{DG} = k_4 C_{MG}^2$	<p><i>p – Methoxy cinnamic acid</i></p> $E_{a1}/R = 11,139 \text{ K}$	Model considers esterification, reversible glycerolysis and disproportionation reactions.	[137]

(continued on next page)

Table 7 (continued)

Reactants and Catalyst	Reaction conditions ^a	(Best) $X_{Gly}/Sel/$ Yield ^b	Kinetic rate type and equations ^c	Kinetic parameters ^d	Notes	Ref.
Gly + <i>p</i> -methoxy cinnamic acid Catalyst: Mesopo- <i>S</i> -phenyl- endSO ₃ H (Ipr)	T = 423–443 K MR = 1:3–1:9 Cat _{load} = 1.2 mol% of acid ω = 250 rpm t _{rxn} = 60 min	$Y_{MG} \approx >80\%$ *	Power law: $r_{acid} = -k_1 C_{Cat} C_{Gly} C_{acid} - k_2 C_{Cat} C_{MG} C_{acid}$ $r_{MG} = -k_1 C_{Cat} C_{Gly} C_{acid} - k_2 C_{Cat} C_{MG} C_{acid}$ $r_{DG} = k_2 C_{Cat} C_{MG} C_{acid}$ $r_{Gly} = -k_1 C_{Cat} C_{Gly} C_{acid}$ $r_{cat} = -k_d C_{cat}$	$E_{a2}/R = 10,362\text{ K}$ $E_{a3}/R = 14,978\text{ K}$ $E_{a4}/R = 17,802\text{ K}$ $\ln k_{01} = 16.6$ $\ln k_{02} = 16.4$ $\ln k_{03} = 24.8$ $\ln k_{04} = 29.2$ $E_{a1} = 87.33\text{ kJ mol}^{-1}$ $E_{a2} = 69.17\text{ kJ mol}^{-1}$ $E_{ad} = 104.00\text{ kJ mol}^{-1}$ $\ln k_{01} = 17.80$ $\ln k_{02} = 11.80$ $\ln k_{0d} = 26.00$	Model discrimination. Model consists of two reactions in series and single-step first-order deactivation of the catalyst.	[130]
Gly + lauric acid Catalyst: HSO ₃ SBA-15	T = 413–433 K MR = 1:4 Cat _{load} = 5 wt% ω = 750 rpm t _{rxn} = 420 min T = 323–353 K	$S_{MG} \approx 70\%$	Power law (second order model): $-r_{acid} = k C_{Gly} C_{acid}$	$E_a = 42\text{ kJ mol}^{-1}$ $k_0 = 655\text{ mol (L g}_{cat}\text{ h)}^{-1}$	Model only considers the formation of MGs from Gly.	[126]
Gly + ibuprofen (Open system) Catalyst: CALB	MR = not available C _{acid,feed} = 20–100 g L ⁻¹ Cat _{load} = 2 g L ⁻¹ VR (Gly/Tol) = 20:5 ω = 720 rpm t _{rxn} = 480 min T = 323–353 K	$Y_{MG} \approx 96\%$	Irreversible hyperbolic model: $r_{MG} = \frac{k_1 C_{acid}}{1 + K_{eq,acid} C_{acid}}$	$E_{a1}/R = 6812\text{ K}$ $\ln k_{01} = 15.09$ $K_{eq,acid} = 0.68\text{ mol L}^{-1}$	Biphasic medium. Ping-pong bi-bi mechanisms. Open system means water is constantly removed using toluene. Model is pseudo-zero order for Gly.	[127]
Gly + ibuprofen (Closed system) Catalyst: CALB	MR = not available C _{acid,feed} = 20–100 g L ⁻¹ Cat _{load} = 2 g L ⁻¹ VR (Gly/Tol) = 20:5 ω = 720 rpm t _{rxn} = 1380 min	$Y_{MG} \approx 96\%$	Reversible Michaelis-Menten model: $r_{MG} = \frac{k_1 C_{acid} - k_2 C_{MG}}{1 + K_{eq,acid} C_{acid} + K_{eq,MG} C_{MG}}$	$E_{a1}/R = 5274\text{ K}$ $E_{a2}/R = 2468\text{ K}$ $\ln k_{01} = 11.42$ $\ln k_{02} = 2.30$ $K_{eq,acid} = 0.86\text{ mol L}^{-1}$ $K_{eq,MG} = 16.92\text{ mol L}^{-1}$	Biphasic medium. Ping-pong bi-bi mechanisms. Closed system means water stays in system. Model considers zero order for Gly and H ₂ O.	[127]
Gly + oleic acid Catalyst: ZnO/zeolite	T = 413–433 K MR = 1:2–1:6 Cat _{load} = 0.5 wt% ω = 700 rpm t _{rxn} = 360 min	$S_{MG} = 70\text{--}80\%$	Power law (using solubilities): $r_{MG} = k_1 x_{Gly} x_{acid} - k_2 x_{Gly} x_{MG}$ $r_{DG} = k_3 x_{Gly} x_{acid}^2 + k_2 x_{Gly} x_{MG}$ x_{Gly} is a constant describing solubility of Gly in acid. LHHW (catalytic reactions):	$E_{a1} = 45.0\text{ kJ mol}^{-1}$ $E_{a2} = 66.0\text{ kJ mol}^{-1}$ $E_{a3} = 52.9\text{ kJ mol}^{-1}$ $k_{01} = 240053.7\text{ kmol min}^{-1}\text{ L}^{-1}$ $k_{02} = 21285844\text{ kmol min}^{-1}\text{ L}^{-1}$ $k_{03} = 390003.1\text{ kmol min}^{-1}\text{ L}^{-1}$	Water removal investigated, but not considered in the model. Model consists of a combination of series and parallel irreversible reactions.	[128]
Gly + oleic acid Catalyst: Amberlyst 36 (USIRW reactor)	T = 333–353 K MR = 1:3–1:5 Cat _{load} = 0.004–0.006 g mL ⁻¹ ω = 700 rpm t _{rxn} = 30 min	$S_{MG} = 93\%$	$-r_{acid,LHHW} = \frac{k_1 (K_{a,acid} C_{acid} K_{a,Gly} C_{Gly})}{(1 + K_{a,acid} C_{acid} + K_{a,Gly} C_{Gly} + K_{a,MG} C_{MG})^2}$ Power-law (noncatalytic reactions): $-r_{acid,noncatalytic} = k_2 C_{acid}^m C_{Gly}^n$ Overall reaction rate equation: $-r_{acid,overall} = -r_{acid,LHHW} + -r_{acid,noncatalytic}$ Pseudo-homogeneous first-order kinetics:	$E_a = 8.520\text{ kJ mol}^{-1}$ Kinetic constant (k_j) and adsorption constants ($K_{a,i}$) are provided at different temperatures.	ER model also developed, but LHHW model fits best. Noncatalytic route improved data fitting thus considered in final model.	[141]
Gly + hydrogenated rosin (HR) Catalyst: Subcritical CO ₂ -enriched	T = 503–533 K P _{CO2} = 4 MPa MR = 1.5:1 Cat _{load} = not available	$Y_{MG} = 20.4\%$ * $Y_{DG} = 20.4\%$ * $Y_{TG} = 9.3\%$ *	$r_{HR} = -k_1 C_{HR} - k_2 C_{HR} C_{MG} - k_3 C_{HR} C_{DG}$ $r_{MG} = k_1 C_{HR} - k_2 C_{HR} C_{MG}$ $r_{DG} = k_2 C_{HR} C_{MG} - k_3 C_{HR} C_{DG}$ $r_{TG} = k_3 C_{HR} C_{TG}$	With CO ₂ $E_{a1} = 54.92\text{ kJ mol}^{-1}$ $E_{a2} = 53.05\text{ kJ mol}^{-1}$ $E_{a3} = 44.42\text{ kJ mol}^{-1}$	Concentration of Gly is assumed to be constant due to its excess.	[133]

(continued on next page)

Table 7 (continued)

Reactants and Catalyst	Reaction conditions ^a	(Best) $X_{Gly}/Sel/Yield^b$	Kinetic rate type and equations ^c	Kinetic parameters ^d	Notes	Ref.
high temperature compressed water (HTCW)	ω = not available t_{rxn} = 210 min			$k_{01} = 1.39 \times 10^3 \text{ min}^{-1}$ $k_{02} = 3.00 \times 10^3 \text{ min}^{-1}$ $k_{03} = 1.61 \times 10^2 \text{ min}^{-1}$ <i>Without CO₂</i> $E_{a1} = 63.67 \text{ kJ mol}^{-1}$ $E_{a2} = 60.90 \text{ kJ mol}^{-1}$ $E_{a3} = 49.66 \text{ kJ mol}^{-1}$ $k_{01} = 5.27 \times 10^3 \text{ min}^{-1}$ $k_{02} = 1.22 \times 10^4 \text{ min}^{-1}$ $k_{03} = 4.03 \times 10^2 \text{ min}^{-1}$		
Gly + rosin Catalyst: None	$T = 513\text{--}553 \text{ K}$ $MR = 2:1\text{--}4:1$ $Cat_{load} = \text{none}$ ω = not available $t_{rxn} = 720 \text{ min}$	$X_{rosin} = 99\%$	<p>Hyperbolic model:</p> $r = \frac{1}{3} \frac{dC_{rosin}}{dt} = \frac{k_1 C_{Gly} C_{rosin}}{1 + K_{eq,2} C_{Gly}}$ $\frac{dC_{Gly}}{dt} = \frac{1}{3} \frac{dC_{rosin}}{dt} = (1 + k_{st} C_{Gly})$	$E_a = 7.27 \text{ kJ mol}^{-1}$ $\ln k_{01} = 8.22$ $K_{eq,2} = 0.339 \text{ L mol}^{-1}$ $k_{st} = 0.281 \text{ (stripping of Gly)}$	Model discrimination. Model considers mass balance that accounts for stripping of Gly.	[136]

^a Reaction conditions used for kinetic studies. Temperature (T), acid to Gly molar ratio (MR), catalyst loading (Cat_{load}), stirring speed (ω), reaction time (t_{rxn}), acid concentration in the feed (C_{acid_feed}), volume ratio (VR), pressure (P_i).

^b Best Gly conversion (X_{Gly}) unless specified otherwise (X_i), selectivity (S) or yield (Y) with respect to esters, achieved at optimum operating conditions which are different than the reaction conditions^a for kinetic study presented in the table. *Calculated from concentration graphs provided by study.

^c Rate of reaction (r_i), forward reaction rate constant (k_j), backward reaction rate constant (k_{-j}), deactivation rate constant (k_{dj}), desorption step rate constant (k_{des}), equilibrium constant ($K_{eq,i/j}$), adsorption equilibrium constant ($K_{a,i}$), concentration (C_i), concentration of catalyst (C_{cat}), concentration of catalyst free active sites (C_{FS}), concentration of total active sites (C_{TS}), residual catalyst activity ($a_{cat,R}$), catalyst activity relative to initial activity (β), reaction order (m) and (n), component activity (a_i), component mole fraction (x_i), Michaelis-Menten constant (K_{MCC}). Subscripts: i = components, j = reactions. Subscript Tol = toluene, MG = monoglycerides, DG = diglycerides, TG = triglycerides, $r.d.s$ = rate determining step.

^d Activation energy (E_{aj}), pre-exponential factor (k_{0j}, k_{0-j}), equilibrium constant ($K_{eq,i/j}$), Gibbs free energy of equilibrium constant ($\Delta G_{K_{eq}}$), enthalpy of component adsorption constant ($\Delta H_{a,i}$), pre-exponential factor of component adsorption constant ($k_{0-K_{a,i}}$), reaction order (m) and (n), ideal gas constant (R), Michaelis-Menten constant (K_{MCC}). i : components, j =reactions.

previous sections [100–102]. The model also included terms for the stripping of Gly and terms that reflect mass transfer or solubilisation [136]. In further work in the absence of catalyst for the esterification of cinnamic acids, the reverse reaction of glycerolysis and disproportionation were considered at long reaction times [137].

Finally, studies with heterogeneous catalysts have used the LHHW and ER models. For the production of triacetin (Gly and ACA esterification) with Purolite CT-275 catalyst, the LHHW theory was used and activities instead of concentrations were assumed due to the non-ideality of the components [138]. The model considers internal mass transport limitation during the full reaction time, though the rate-determining step was taken as the reaction between the adsorbed molecules, while bulk liquid reactions are ignored. The model also calculated the equilibrium constants based on the concentrations of adsorbed molecules and activities in the bulk liquid [138]. In another study investigating the same system [139], it was demonstrated that the ER model best fit the experimental data when compared to the power law and LHHW models [139]. The activation energies based on the ER model are in the range 46–49 kJ mol⁻¹. Only the adsorption of Gly and water are associated with the concentration of the free active sites. This is due to the high polarity nature of Gly and water molecules and therefore their adsorption is stronger compared to the adsorption of ACA and the acetyl glycerides [139]. Moreover, for reaction of Gly and ACA using Y/SBA-3 catalyst, an overall rate equation was developed based on the assumption that the reaction occurs in one-step [140]. However, a further investigation of the system using the LHHW approach led to a rate equation of the rate determining step (i.e. surface reaction). Based on the model, the overall E_a is 21.54 kJ mol⁻¹ [140]. Furthermore, for the esterification of Gly with oleic acid using amberlyst 36 in an ultrasonic-infrared-wave (USIRW) reactor, a concurrent noncatalytic and heterogeneously catalysed mechanism has been considered. Here the heterogeneous reactions were described using the LHHW approach and the non-catalytic reaction is described by a power-law equation. The E_a was found to be 8.52 kJ mol⁻¹ which is much lower when compared to the E_a of the reaction in a conventional batch reactor (114.45 kJ mol⁻¹) [141].

Similar to the case of the conversion to acetals, strategies to remove water as product can intensify the process in terms of favouring the thermodynamics. For the production of triacetin, membrane pervaporation setups have proven effective, as shown in Fig. 10 [142]. Here the yield of TGs reached up to 76%, which is about 30% higher than values

attained under the same reaction conditions with conventional batch reactors [142]. Another process intensification approach investigated is the use of ultrasonic-infrared-wave (USIRW) reactor for the esterification of Gly with oleic acid using amberlyst 36. It was demonstrated that a 92.5% acid conversion and 93% MGs selectivity can be attained as opposed to a conversion of 36.39% and 77% MGs selectivity in a conventional batch reactor [141]. As explained above, other approaches may include hydrophobic catalyst design, which would also apply to the case of etherification, which would enhance the progress of the reaction to the triester or triether, thereby improving the selectivity.

4.4. Ethers

Gly etherification with alcohols (ROH) is an endothermic three-step acid catalysed reaction that produces water as a by-product as shown in Fig. 11. It generates alkyl ethers, monoethers (MEs), diethers (DEs) and triethers (TEs), that are utilised as oxygenated fuel additives [143]. The dimerization of alcohol also occurs as an independent undesired side reaction, which may limit the selectivity to the desired product on occasions [144].

Similar to esterification, the reaction is a thermodynamically limited equilibrium reaction where the production of water can limit the maximum conversion that can be attained [145]. Thus, implementing intensified reactors such as membrane pervaporation reactors can remove water which leads to shifting the equilibrium and increasing ethers' yields. Additionally, such a configuration can also resolve downstream separation problems such as the formation of azeotropes between water and the alcohol [146]. In terms of temperature, as it increases, the reaction rate and thus equilibrium conversion of the reactants also increases due to the reaction's endothermic nature [145]. However, the selectivity to MEs decreases due to the increased consecutive conversion of MEs to DEs [147]. Moreover, using excess Gly leads to the yields for MEs and DEs to increase and also lead the selectivity of alcohol dimers to decrease [147]. However, molar ratio needs to be optimised as excess Gly can lead to diffusional effects in the catalysts due to its high viscosity depending on operating temperature and degree of mixing, whilst an excess of alcohol can lead to the system favouring dimerization [69]. As an acid-initiated reaction, the acidity of the catalyst will directly affect their performance in terms of yield and selectivity, with reaction rate constants having been found to be nearly directly proportional to the density of catalytic acid sites [147].

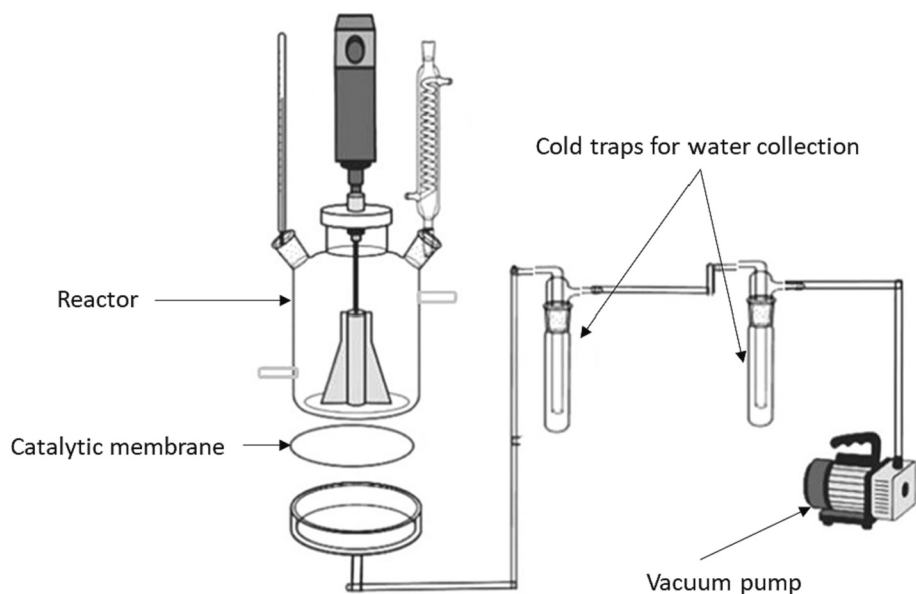


Fig. 10. Catalytic membrane pervaporation setup for the in-situ removal of water during the esterification of Gly to obtain triacetin. Edited figure for enhanced visibility reproduced with permission of ACS publishing [142].

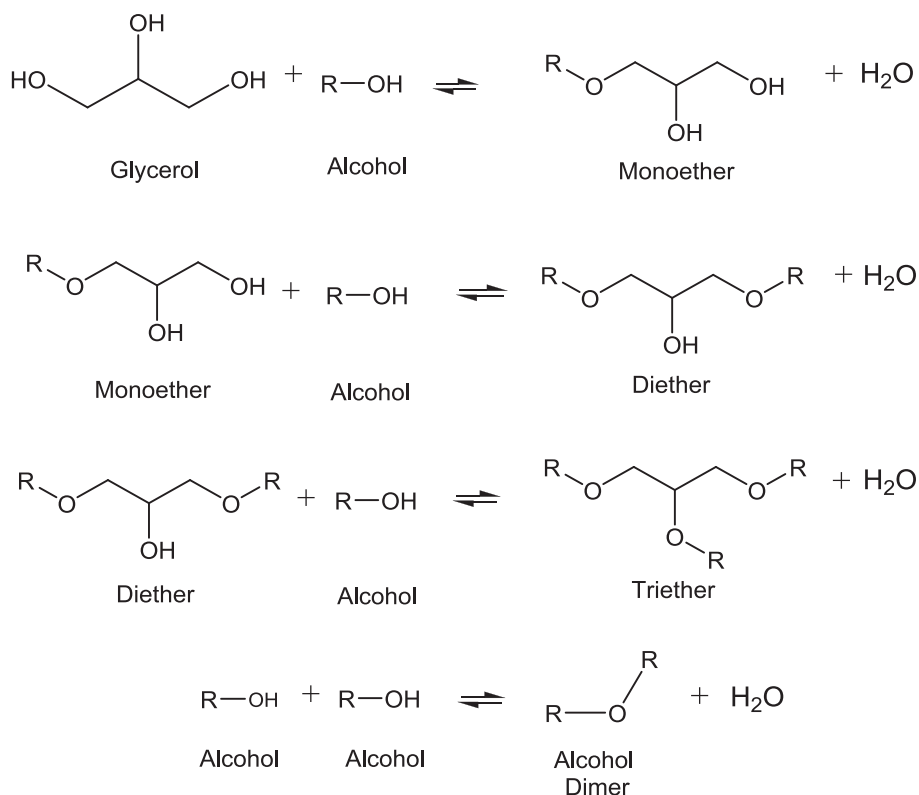


Fig. 11. General reaction scheme of the etherification of Gly with alcohols and their possible dimerization.

Several studies, shown in Table 8 below, investigated and developed kinetic models for etherification reactions of Gly with different alcohols. Two approaches were investigated by Santos et al. [145] in the etherification of Gly with *t*-butyl alcohol catalysed by Amberlyst 15, a lumping approach and an extended approach, where the former considers the isomers as a single product. In both approaches, the production of monoethers is the fastest. The models are described based on concentrations and not activities as the reaction mixture is assumed to behave ideally [145]. Based on the lumping approach, the E_a for MEs and DE are $75.93 \text{ kJ mol}^{-1}$ and $30.87 \text{ kJ mol}^{-1}$, respectively, while the extended approach, the values are around 46 kJ mol^{-1} for both compounds [145]. The lumping approach was also used by Al-Rabiah et al. [148] to develop a power-law kinetic model with second order rate equations using $\text{Sn}_{1.5}\text{PMo}_{12}\text{O}_{40}$ as catalyst. The E_a obtained showed higher values than with Amberlyst 15.

Furthermore, a kinetic model using dual site mechanism (LHHW) was developed for the etherification of Gly with 1-phenyl ethanol using 20%w/w DTP-HMS catalyst. It is assumed that the reactant species are weakly adsorbed on the catalytic sites and thus the surface reaction is taken as the rate determining step. Based on the model, it was found that an overall second order kinetic equation best describes the system and fits the experimental data [149]. The E_a obtained is $113.0 \text{ kJ mol}^{-1}$, concluding that the reaction is an intrinsic kinetically controlled reaction [149]. Another LHHW based model was developed for the etherification of Gly and *tert*-butyl alcohol using Amberlyst 15 [150]. The model was further verified and used to simulate a suitable reactive distillation column [150].

Moreover, a power-law and an ER model were developed for the etherification of Gly with benzyl alcohol using Amberlyst 15 catalyst [144]. In the latter, only Gly is assumed to be adsorbed due to its strong adsorption onto the surface of the catalyst, while benzyl alcohol reacts from bulk. The adsorption equilibrium constant $K_{a,i}$ is included in the model and was calculated using the Van't Hoff equation [144]. For both models, the reaction is assumed irreversible due to the constant removal

of water. The E_a based on the power-law model for the productions of MEs and DEs were close compared to the E_a obtained using the ER model for the same reaction ($96.18 \text{ kJ mol}^{-1}$ and $130.85 \text{ kJ mol}^{-1}$), which was finally deemed more appropriate [144]. Furthermore, the study by Jaworski et al. [147] developed a power-law and a hyperbolic kinetic model (only Gly is adsorbed onto the catalytic surface) for the same system ($2\text{S}/\text{ZrO}_2$ catalyst instead) using similar assumptions, this model also featured the self-condensation of benzyl alcohol to produce benzyl ether, which was concluded to be a second order reaction in contrast with the etherification reactions, both first order [147].

Multiphase reaction systems were also modelled, such as the etherification of Gly with isobutene [143]. The IER NKC-9 was used as catalyst, and due to its hydrophilicity, it shows higher wettability with Gly, which is assumed to be the phase where the reaction takes place and hence its concentration remaining constant and that of isobutene being equal to its solubility. An LHHW model was illustrated in which all components are assumed to be adsorbed onto the catalyst surface. Adsorption equilibrium terms for TE and isobutene dimers are ignored as they are much smaller compared to other components. The rate determining step is the surface reaction step. Initially, as the system is two-phased, the liquid-liquid-solid mass transfer occurs rapidly and therefore can be assumed to have negligible effect [143]. The reactant concentrations were taken to be equal to the concentration in the Gly phase in the event of phase separation, otherwise they are equal to the overall concentrations [143]. The study concluded with a model that described phase separation and the competitive adsorption nature of the system by using initial rates and kinetic data attained at high conversions [143].

It should be noted that for all the models presented in Table 8, it was assumed that no internal or external mass transfer limitations are present and therefore the reactions are kinetically controlled. All the studies also assumed catalytic activity remained constant, which neglects the possibility of deactivation.

Table 8
Summary of the most relevant aspects of kinetic studies for the production of glycerol ethers.

Reactants and Catalyst	Reaction conditions ^a	(Best) $X_{Gly}/$ Sel/Yield ^b	Kinetic rate type and equations ^c	Kinetic parameters ^d	Notes	Ref.							
Gly + isobutene Catalyst: NKC-9	T = 343–373 K MR = 0.6:1–4:1 Cat _{load} = 0.04% - 0.5% wt% of Gly ω = 1400 rpm t_{rxn} = 420 min	$Y_{ME} = 75\%*$ $Y_{DE} = 20\%*$	<p>LHHW:</p> $r_{ME} = \frac{k_1 K_{a,Gly} K_{a,ROH} C_{Gly} C_{ROH}}{\left(1 + \sum_i K_{a,i} C_i\right)^2}$ $r_{Gly} = \frac{k_2 K_{a,ME} C_{ME}}{1 + \sum_i K_{a,i} C_i}$ $r_{DE} = \frac{k_3 K_{a,ME} K_{a,ROH} C_{ME} C_{ROH}}{\left(1 + \sum_i K_{a,i} C_i\right)^2}$ $r_{ME} = \frac{k_4 K_{a,DE} C_{DE}}{1 + \sum_i K_{a,i} C_i}$ $r_{TE} = \frac{k_5 K_{a,DE} K_{a,ROH} C_{DE} C_{ROH}}{\left(1 + \sum_i K_{a,i} C_i\right)^2}$ $r_{DE} = \frac{k_6 K_{a,TE} C_{TE}}{1 + \sum_i K_{a,i} C_i} = \frac{k'_6 C_{TE}}{1 + \sum_i K_{a,i} C_i}$ $r_{di-ROH} = \frac{k_7 (K_{a,ROH} C_{ROH})^2}{\left(1 + \sum_i K_{a,i} C_i\right)^2}$ <p>Power-law:</p> $r_{ME1} = k_{1A} \left(C_{Gly} C_{ROH} - \frac{C_{ME1} C_{H_2O}}{K_{eq,1A}} \right)$ $r_{ME2} = k_{1B} \left(C_{Gly} C_{ROH} - \frac{C_{ME2} C_{H_2O}}{K_{eq,1B}} \right)$ $r_{DE1} = k_{2A} \left(C_{ME1} C_{ROH} - \frac{C_{DE1} C_{H_2O}}{K_{eq,2A}} \right)$ $r_{DE2} = k_{2B} \left(C_{ME1} C_{ROH} - \frac{C_{DE2} C_{H_2O}}{K_{eq,2B}} \right)$ $r_{DE2} = k_{3A} \left(C_{ME2} C_{ROH} - \frac{C_{DE2} C_{H_2O}}{K_{eq,3A}} \right)$ $r_{TE} = k_{4A} \left(C_{DE1} C_{ROH} - \frac{C_{TE} C_{H_2O}}{K_{eq,4A}} \right)$ $r_{TE} = k_5 \left(C_{DE2} C_{ROH} - \frac{C_{TE} C_{H_2O}}{K_{eq,5}} \right)$ $r_{di-ROH} = k_6 C_{ROH}$	$E_{a1} = 82.0 \text{ kJ mol}^{-1}$ $E_{a2} = 97.7 \text{ kJ mol}^{-1}$ $E_{a3} = 89.1 \text{ kJ mol}^{-1}$ $E_{a4} = 65.3 \text{ kJ mol}^{-1}$ $E_{a5} = 35.0 \text{ kJ mol}^{-1}$ $E'_{a6} = 39.3 \text{ kJ mol}^{-1}$ $E_{a7} = 20.0 \text{ kJ mol}^{-1}$	<p>Pre - exponential factors ($L(\text{molH}^+)^{-1} \text{ s}^{-1}$ or $L^2 \text{mol}^{-1} (\text{molH}^+)^{-1} \text{ s}^{-1}$):</p> $k_{01} = 7.36$ $k_{02} = 0.62$ $k_{03} = 2.43$ $k_{04} = 0.55$ $k_{05} = 0.49$ $k_{06} = 0.03$ $k_{07} = 0.01$	<p>Model considered adsorption and phase separation.</p> <p>For the calculation of k_i and $K_{a,i}$ the reference temperature was set to 357 K.</p>	[143]						
				Gly + <i>tert</i> -butyl alcohol Catalyst: Amberlyst 15				T = 323–353 K MR = 3:1–5:1 Cat _{load} = 8.5 wt% of gly ω = 1200 rpm t_{rxn} = 480 min	$X_{Gly} \approx 88\%$	<p>Power-law:</p> $r_{ME1} = k_{1A} \left(C_{Gly} C_{ROH} - \frac{C_{ME1} C_{H_2O}}{K_{eq,1A}} \right)$ $r_{ME2} = k_{1B} \left(C_{Gly} C_{ROH} - \frac{C_{ME2} C_{H_2O}}{K_{eq,1B}} \right)$ $r_{DE1} = k_{2A} \left(C_{ME1} C_{ROH} - \frac{C_{DE1} C_{H_2O}}{K_{eq,2A}} \right)$ $r_{DE2} = k_{2B} \left(C_{ME1} C_{ROH} - \frac{C_{DE2} C_{H_2O}}{K_{eq,2B}} \right)$ $r_{DE2} = k_{3A} \left(C_{ME2} C_{ROH} - \frac{C_{DE2} C_{H_2O}}{K_{eq,3A}} \right)$ $r_{TE} = k_{4A} \left(C_{DE1} C_{ROH} - \frac{C_{TE} C_{H_2O}}{K_{eq,4A}} \right)$ $r_{TE} = k_5 \left(C_{DE2} C_{ROH} - \frac{C_{TE} C_{H_2O}}{K_{eq,5}} \right)$ $r_{di-ROH} = k_6 C_{ROH}$	$E_{a1A} = 59.46 \text{ kJ mol}^{-1}$ $E_{a1B} = 33.69 \text{ kJ mol}^{-1}$ $E_{a2A} = 35.12 \text{ kJ mol}^{-1}$ $E_{a2B} = 59.32 \text{ kJ mol}^{-1}$ $E_{a3} = 43.77 \text{ kJ mol}^{-1}$ $E_{a4A} = \text{not available}$ $E_{a5} = \text{not available}$ $E_{a6} = 51.34 \text{ kJ mol}^{-1}$ $k_{01A} = 4.58 \times 10^7 \text{ kg mol}^{-1} \text{ min}^{-1}$ $k_{01B} = 2.50 \times 10^2 \text{ kg mol}^{-1} \text{ min}^{-1}$ $k_{02A} = 5.02 \times 10^2 \text{ kg mol}^{-1} \text{ min}^{-1}$ $k_{02B} = 1.79 \times 10^6 \text{ kg mol}^{-1} \text{ min}^{-1}$ $k_{03A} = 8.14 \times 10^4 \text{ kg mol}^{-1} \text{ min}^{-1}$ $k_{04A} = \text{not available}$ $k_{05} = \text{not available}$ $k_{06} = 3.29 \times 10^4 \text{ min}^{-1}$	<p>Heterogeneous model. Lumped and extended approach modelled. In extended, isomers of MEs (ME1 and ME2) and DEs (DE1 and DE2) are considered. K_{eq} values given as $f(T)$.</p>	[145]
											Gly + <i>tert</i> -butyl alcohol Catalyst: Sn _{1.5} PMo _{1.2} O ₄₀		

(continued on next page)

Table 8 (continued)

Reactants and Catalyst	Reaction conditions ^a	(Best) X_{Gly} /Sel./Yield ^b	Kinetic rate type and equations ^c	Kinetic parameters ^d	Notes	Ref.	
				$k_{03} = 0.7 \times 10^3 \text{ m}^3 \text{ mol}^{-1} \text{ s}^{-1}$ $k_{0-3} = 0.1 \times 10^3 \text{ m}^3 \text{ mol}^{-1} \text{ s}^{-1}$			
			LHHW:				
			$r_{ME} =$				
Gly + <i>tert</i> -butyl alcohol Catalyst: Amberlyst 15	T = 338–358 K MR = 4:1 Cat _{load} = 1.025 g ω = 600 rpm t_{rxn} = 480 min	$Y_{ME} = 11.7\%$ * $Y_{DE} = 3.5\%$ *	$\frac{k'_1 a_{Gly} a_{ROH} - k'_{-1} a_{ME} a_{H_2O}}{(1 + K_{a,H_2O} a_{H_2O})^2}$ $r_{DE} =$ $\frac{k'_2 a_{ME} a_{ROH} - k'_{-2} a_{DE} a_{H_2O}}{(1 + K_{a,H_2O} a_{H_2O})^2}$ $r_{TE} =$ $\frac{k'_3 a_{DE} a_{ROH} - k'_{-3} a_{TE} a_{H_2O}}{(1 + K_{a,H_2O} a_{H_2O})^2}$	$E_{a1} = 55.6 \text{ kJ mol}^{-1}$ $E_{a2} = 82.3 \text{ kJ mol}^{-1}$ $E_{a3} = 31.8 \text{ kJ mol}^{-1}$ $k'_1 = e^{(16.172 - 6689/T)}$ $k'_2 = e^{(25.506 - 9903/T)}$ $k'_3 = e^{(5.392 - 3830/T)}$	Reactive distillation study.	[150]	
			ER model:				
			$r_{ME} = \frac{k_1 C_{cat} C_{ROH} K_{a,Gly} C_{Gly}}{1 + K_{a,Gly} C_{Gly}}$ $r_{DE} = k_2 C_{cat} C_{ME} C_{ROH}$ $r_{TE} = k_3 C_{cat} C_{DE} C_{ROH}$ $r_{di-ROH} = k_4 C_{cat} C_{ROH}^2$ $r_{ME} =$ $\frac{k_5 C_{cat} C_{di-ROH} K_{a,Gly}^2 C_{Gly}^2}{(1 + K_{a,Gly} C_{Gly})^2}$	$E_{a1} = 96.18 \text{ kJ mol}^{-1}$ $E_{a2} = 130.85 \text{ kJ mol}^{-1}$ $E_{a3} = \text{not available}$ $E_{a4} = 159.68 \text{ kJ mol}^{-1}$ $E_{a5} = 197.63 \text{ kJ mol}^{-1}$	Reaction is considered irreversible due to constant removal of water.		
Gly + Benzyl alcohol Catalyst: Amberlyst 15	T = 353–373 K MR = 1:3–3:1 Cat _{load} = 3.45–14.4 wt% of reaction mass ω = 1200 rpm t_{rxn} = 480 min	$S_{ME} \approx 85\%$ $S_{DE} \approx 2\%$		$k_{01} = 1.33 \times 10^{11} \text{ kg}^2 (\text{g}_{cat} \text{ mol min})^{-1}$ $k_{02} = 1.08 \times 10^{13} \text{ kg}^2 (\text{g}_{cat} \text{ mol min})^{-1}$ $k_{03} = \text{not available}$ $k_{04} = 1.19 \times 10^{17} \text{ kg}^2 (\text{g}_{cat} \text{ mol min})^{-1}$ $k_{05} = 8.06 \times 10^{18} \text{ kg}^2 (\text{g}_{cat} \text{ mol min})^{-1}$	Power law also modelled. Catalyst concentration (C_{cat}) order is ≈ 1.0 .	[144]	
			Power-law model:				
			$r_{ME} = k_1 C_{ROH} C_{Gly}$ $r_{DE} = k_2 C_{ROH} C_{ME}$ $r_{di-ROH} = k_3 C_{ROH}^2$	$\Delta H_{a,Gly} = 3.25 \text{ kJ mol}^{-1}$ $k_{0-K_{a,Gly}} = 2.3 \times 10^{-2} \text{ kg mol}^{-1}$ Power-law model: $E_{a1}/R = 8.5 \times 10^3 \text{ K}$ $E_{a2}/R = 1.33 \times 10^4 \text{ K}$ $E_{a3}/R = 1.29 \times 10^4 \text{ K}$ $\ln k_{01} = 12.8$ $\ln k_{02} = 25.9$ $\ln k_{03} = 22.7$	Both models fit experimental data		
Gly + Benzyl alcohol Catalyst: 2S/ZrO ₂	T = 393–413 K MR = 1:2–1:1 Cat _{load} = 25 g/kg total initial mass of reactants ω = not available t_{rxn} = 360 min	$S_{ME} \approx 77\%$ $S_{DE} \approx 0\%$	Hyperbolic (ER) model:	Hyperbolic model: $r_{ME} = \frac{k_1 C_{ROH} C_{Gly}}{1 + K_{a,Gly} C_{Gly}}$ $r_{DE} = \frac{k_2 C_{ROH} C_{ME}}{1 + K_{a,Gly} C_{Gly}}$ $r_{di-ROH} = \frac{k_3 C_{ROH}^2}{1 + K_{a,Gly} C_{Gly}}$	$\ln k_{01} = 24.3$ $\ln k_{02} = 14.8$ $\ln k_{03} = 24.1$ $K_{a,Gly} = \text{not available}$	condensation of alcohol is a second order reaction -The production of ME and DE from alcohol are first order reactions.	[147]
			LHHW (simplified to overall second order equation)				
Gly + 1-phenyl ethanol Catalyst: 20% w/w DTP-HMS	T = 373–413 K MR = 1:3–1:5 Cat _{load} = 0.01–0.032 g cm ⁻³ ω = 1000 rpm t_{rxn} = 240 min	$S_{ME} = 75\%$	$-r_{ROH} = -\frac{dC_{ROH}}{dt} =$ $\frac{k_1 C_{ROH} C_{Gly}}{1 + K_{a,Gly} C_{Gly}}$	$E_{a1} = 113.0 \text{ kJ mol}^{-1}$ $\ln k_{01} = 28.91$	Dual Site reaction mechanism (LHHW model). Assumed reaction is far from equilibrium. and adsorption constants are very small	[149]	

^a Reaction conditions used for kinetic studies. Temperature (T), Alcohol to Gly molar ratio (MR), catalyst loading (Cat_{load}), stirring speed (ω), reaction time (t_{rxn}).

^b Best Gly conversion (X_{Gly}), selectivity (S) or yield (Y) with respect to MEs, achieved at optimum operating conditions which are different than the reaction conditions^a for kinetic study presented in the table. *value calculated using concentration/mol graphs provided by study.

^c Rate of reaction (r_i), forward reaction rate constant (k_j), backward reaction rate constant (k_{-j}), component adsorption equilibrium constant ($K_{a,i}$), overall equilibrium constant (K_{eq}), concentration (C_i), concentration of catalyst (C_{cat}), component activities (a_i). i : components, j =reactions. Subscript ROH = Alcohol, $di-ROH$ = alcohol dimer.

^d Activation energy (E_{aj}), pre-exponential factor (k_{0j}), enthalpy of component adsorption constant ($\Delta H_{a,i}$), entropy of component adsorption constant ($\Delta S_{a,i}$), pre-exponential factor of component adsorption constant ($k_{0-K_{a,i}}$), ideal gas constant (R). i : components, j =reactions.

4.5. Propanediols

Propylene glycol is also a very relevant product in the formulation of cosmetics and healthcare products that can be obtained from Gly as feedstock, there being the possibility of obtaining the isomers 1,2-

propanediol (1,2-PDO) and 1,3-propanediol (1,3-PDO) [76].

4.5.1. 1,2-Propanediol

Hydrogenolysis of Gly (Fig. 12) is an exothermic reaction ($\Delta H_{rxn} = -103 \text{ kJ mol}^{-1}$) that generates 1,2-PDO and other by-products,

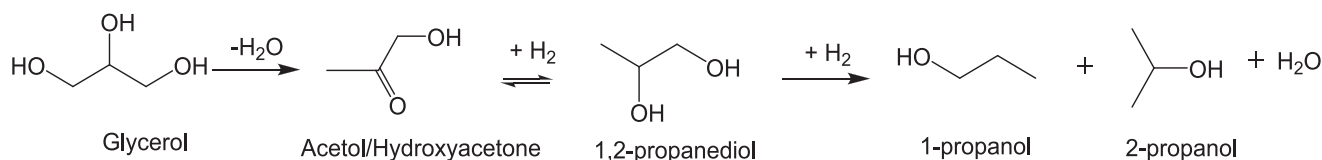
such as acetol, ethylene glycol (EG), propanal and methanol [151]. Depending on the nature of the catalyst utilised, the reaction can proceed via different reaction mechanisms. The dehydration-hydrogenation route typically occurs in the presence of an acid-metal catalyst. In this mechanism, Gly dehydrates to the intermediate acetol on Lewis acid sites which then further hydrogenates on metal sites to form 1,2 PDO. In addition to 1,2 PDO, propanol is also largely produced as a byproduct [70,76]. The second route is the dehydrogenation-dehydration-hydrogenation route which occurs in the presence of base-metal catalyst. The mechanism begins with the dehydrogenation of Gly to glyceraldehyde on metal sites. Glyceraldehyde then dehydrates to 2-hydroxyacrolein on the basic sites. Lastly, hydrogenation occurs on metal sites to convert 2-hydroxyacrolein to 1,2 PDO. In addition, C–C bond cleavage occurs in which ethylene glycol and C1 byproducts are also generated [70]. There is also the direct-hydrogenolysis route in the presence of a hydride, however this mechanism is more selective towards 1,3 PDO [70,76]. An extensive discussion of the reaction mechanism is presented by Vasiliadou et al. [76].

Furthermore, the reaction temperature must be optimised as it highly affects the conversion and selectivity achieved. Higher temperatures increase conversion and selectivity; however, overhydrogenolysis of 1,2-PDO can occur leading to degradation products [151,152]. Moreover, increasing pressure enhances Gly conversion and the reaction rate owing to a higher local availability of H₂ to the catalyst surface which is due to a higher solubility of H₂ as pressure increases. However, the selectivity to 1,2-PDO and EG were not affected much by change in pressure nor by a higher initial Gly concentration [151]. Additionally, the synthesis of effective bifunctional catalysts by combining metal and

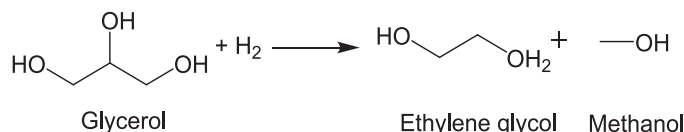
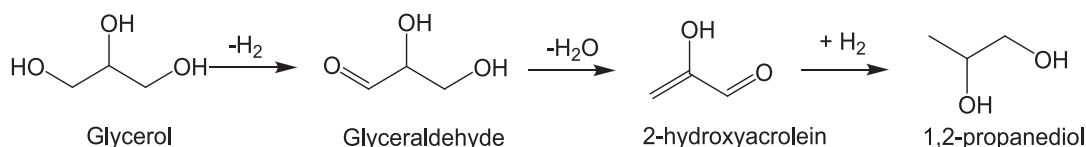
acid/basic sites determines the reaction mechanism and thus heavily influences product selectivity [70]. Therefore, factors that affect 1,2 PDO yield are the acidity/basicity of the catalyst, number of active sites, reducibility nature of the catalyst, ‘average crystallite size’ and catalyst loading [153]. Multiple reviews [70,71] have summarized studies regarding the preparation and performance of catalysts for Gly hydrogenolysis. Finally, it was suggested that the reaction can be carried out more efficiently by implementing in situ generation of H₂ using sources such as formic acid and methanol instead of externally supplying fossil based H₂ [154,155].

Table 9 summarizes studies investigating kinetic models for the reaction with a number of different catalysts. Using 35 wt% Cu/MgO as catalyst, the E_a is 84.9 kJ mol⁻¹ when considering a power-law model based on a one-step irreversible reaction where Gly is converted to products, with a reaction order for Gly of 1.2 [151]. A study with Cu–Ni–Al₂O₃ as catalyst, found an E_a of 67.7 kJ mol⁻¹ and a reaction order of 1.02, thus it can be considered a pseudo-first order. [152]. When considering the system as multiple reactions in which Gly is first converted to 1,2 PDO and ethylene glycol (EG) and then 1,2 PDO further reacts to form propanol (PO), a modified power-law model was developed. Based on this model, the E_a of the conversion of Gly to 1,2 PDO is 45.7 kJ mol⁻¹ [152].

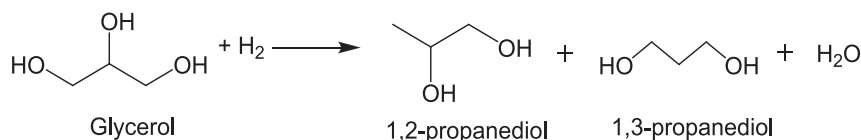
In addition to power-law models, kinetics based on the LHHW model were also derived when studying the reaction with a 35 wt% Cu/MgO catalyst [151]. The model was developed assuming the lack of any external or internal mass transfer limitations as well as heat transfer resistance as there were no significant changes in reaction temperature. In addition, low amounts of lower alcohols (<5%) were ignored in the



Route 1: Dehydration-hydrogenation (acid-metal catalyst)



Route 2: Dehydrogenation-dehydration-hydrogenation (base-metal catalyst)



Route 3: Direct-hydrogenolysis (hydride catalyst)

Fig. 12. Reaction network involved in the hydrogenolysis of glycerol.

Table 9
Summary of the most relevant aspects of kinetic studies for the production of 1,2-PDO.

Reactants and Catalyst	Reaction conditions ^a	(Best) $X_{Gly}/$ Sel./Yield ^b	Kinetic rate type and equation ^c	Kinetic parameters ^d	Notes	Ref.
Gly + H ₂ Catalyst: 35 wt% Cu/ MgO	T = 463–503 K P = 3–6 MPa C _{gly,feed} = 20–60 wt% Cat _{load} = 8 wt% of Gly ω = 700 rpm t _{rxn} = 720 min	S _{1,2} PDO ≈ 95%	<p>Power-law: $r = \frac{dC_{Gly}}{dt} = kC_{Gly}^n$</p> <p>LHHW: $(-r_{1,2-PDO}) = \frac{k_3 C_{Gly} P_{H2}}{\left(1 + K_{a,Gly} C_{Gly} + K_{a,H2} P_{H2} + \frac{C_{1,2PDO}}{K_{a,1,2PDO}} + \frac{C_{EG}}{K_{a,EG}}\right)^2}$ $(-r_{EG}) = \frac{k_4 C_{Gly} P_{H2}}{\left(1 + K_{a,Gly} C_{Gly} + K_{a,H2} P_{H2} + \frac{C_{1,2PDO}}{K_{a,1,2PDO}} + \frac{C_{EG}}{K_{a,EG}}\right)^2}$</p>	<p>Power-law: $E_a = 84.9 \text{ kJ mol}^{-1}$ $k_0 = 45.2 \times 10^7 \text{ mol g}_{cat}^{-1} \text{ h}^{-1}$ $n = 1.2$</p> <p>LHHW: $E_{a3} = 88.2 \text{ kJ mol}^{-1}$ $E_{a4} = 82.0 \text{ kJ mol}^{-1}$ $k_{03} = 1.1 \times 10^9 \text{ mol g}_{cat}^{-1} \text{ h}^{-1}$ $k_{04} = 1.7 \times 10^7 \text{ mol g}_{cat}^{-1} \text{ h}^{-1}$</p> <p>Adsorption constants $E_{a-K_{a,Gly}} = 71.3 \text{ kJ mol}^{-1}$ $E_{a-K_{a,H2}} = 53.2 \text{ kJ mol}^{-1}$ $E_{a-K_{a,1,2PDO}} = 66.7 \text{ kJ mol}^{-1}$ $E_{a-K_{a,EG}} = 50.3 \text{ kJ mol}^{-1}$ $k_{0-K_{a,Gly}} = 7.8 \times 10^{-9} \text{ L mol}^{-1}$ $k_{0-K_{a,H2}} = 8.9 \times 10^{-7} \text{ L mol}^{-1}$ $k_{0-K_{a,1,2PDO}} = 6.1 \times 10^{-8} \text{ L mol}^{-1}$ $k_{0-K_{a,EG}} = 5.5 \times 10^{-6} \text{ L mol}^{-1}$</p> <p>Power-law: $E_a = 67.7 \text{ kJ mol}^{-1}$ $k_0 = 2.39 \times 10^6 \text{ mol g}_{cat}^{-1} \text{ h}^{-1}$ $n = 1.02$</p>	LHHW model: two parallel reactions that forms 1,2-PDO and EG from gly	[151]
Gly + H ₂ Catalyst: Cu–Ni–Al ₂ O ₃	T = 453–493 K P = 4.5–6.0 MPa C _{gly,feed} = 20 wt% Cat _{load} = 10 wt% of gly ω = 700 rpm t _{rxn} = 720 min	S _{1,2} PDO ≈ 95%	<p>Power-law: $r = \frac{dC_{Gly}}{dt} = kC_{Gly}^n$</p> <p>Modified power-law: $r_{1,2-PDO} = k_1 C_{Gly} \frac{P_{H2}}{H_{H2}}$ $r_{EG} = k_2 C_{Gly} \frac{P_{H2}}{H_{H2}}$ $r_{PO} = k_3 C_{PO} \frac{P_{H2}}{H_{H2}}$</p> <p>Combined ER and LHHW: $(-r_{1,2-PDO}) = \frac{k_3 K_{a,Gly} C_{Gly} P_{H2}}{\left(1 + K_{a,Gly} C_{Gly} + (K_{a,H2} P_{H2})^{\frac{1}{2}} + \frac{C_{1,2PDO}}{K_{a,1,2PDO}} + \frac{C_{PO}}{K_{a,PO}}\right)^2}$ $(-r_{PO}) = \frac{k_4 K_{a,H2} C_{1,2PDO} P_{H2}}{K_5 \left(1 + K_{a,Gly} C_{Gly} + (K_{a,H2} P_{H2})^{\frac{1}{2}} + \frac{C_{1,2PDO}}{K_{a,1,2PDO}} + \frac{C_{PO}}{K_{a,PO}}\right)^3}$</p>	<p>Modified power-law: $E_{a1} = 45.7 \text{ kJ mol}^{-1}$ $E_{a2} = \text{not available}$ $E_{a3} = 141.3 \text{ kJ mol}^{-1}$ $k_{01} = 8.3 \times 10^3 \text{ mol g}_{cat}^{-1} \text{ h}^{-1}$ $k_{02} = \text{not available}$ $k_{03} = 1.21 \times 10^{15} \text{ mol g}_{cat}^{-1} \text{ h}^{-1}$</p> <p>Combined ER and LHHW: $E_{a3} = 70.5 \text{ kJ mol}^{-1}$ $E_{a4} = 79.5 \text{ kJ mol}^{-1}$ $k_{03} = 17.62 \times 10^8 \text{ mol g}_{cat}^{-1} \text{ h}^{-1}$ $k_{04} = 6.51 \times 10^8 \text{ mol g}_{cat}^{-1} \text{ h}^{-1}$</p> <p>Adsorption constants $E_{a-K_{a,Gly}} = 12.1 \text{ kJ mol}^{-1}$ $E_{a-K_{a,H2}} = 16.7 \text{ kJ mol}^{-1}$ $E_{a-K_{a,1,2PDO}} = 12.9 \text{ kJ mol}^{-1}$ $E_{a-K_{a,PO}} = 14.8 \text{ kJ mol}^{-1}$ $k_{0-K_{a,Gly}} = 2.12 \times 10^{-4} \text{ L mol}^{-1}$ $k_{0-K_{a,H2}} = 1.85 \times 10^{-7} \text{ L mol}^{-1}$ $k_{0-K_{a,1,2PDO}} = 2.07 \times 10^{-6} \text{ L mol}^{-1}$ $k_{0-K_{a,PO}} = 7.14 \times 10^{-6} \text{ L mol}^{-1}$</p>	Reactions considered are the conversion of Gly to 1,2-PDO and 1,2-PDO to propanol (PO).	[152]

(continued on next page)

Table 9 (continued)

Reactants and Catalyst	Reaction conditions ^a	(Best) X _{Gly} /Sel./Yield ^b	Kinetic rate type and equation ^c	Kinetic parameters ^d	Notes	Ref.	
Gly + H ₂ Catalyst: Cu–Ni/ γ-Al ₂ O ₃	T = 483–513 K P = 0.75 MPa C _{gly,feed} = 20 wt% W/F = 101–811 kg _{cat} h kmol ⁻¹ t _{rxn} = 840 min	S _{1,2} PDO ≈ 89.5%	ER model: $(-r_{Acetol}) = \frac{k'_2 K_{a,Gly} P_{Gly}}{\left(1 + K_{a,Gly} P_{Gly} + \frac{P_{Acetol}}{K_{a,acetol}} + \frac{P_{1,2 PDO}}{K_{a,1,2 PDO}}\right)}$ $(-r_{1,2-PDO}) = \frac{k'_3 P_{Acetol} P_{H2}}{K_{a,acetol} \left(1 + K_{a,Gly} P_{Gly} + \frac{P_{Acetol}}{K_{a,acetol}} + \frac{P_{1,2 PDO}}{K_{a,1,2 PDO}}\right)}$	E _{a2} = 55.14 kJ mol ⁻¹ E _{a3} = 50.87 kJ mol ⁻¹ k' ₀₂ = 2.49 × 10 ¹¹ mol g _{cat} ⁻¹ h ⁻¹ k' ₀₃ = 7.4 × 10 ¹¹ mol g _{cat} ⁻¹ h ⁻¹ Adsorption parameters : N/A	Vapor phase study. Model consists of two-step reaction (Gly dehydration to acetol which further reacts to 1,2 PDO).	[157]	
Gly + H ₂ Catalyst: Cu–Zn(4:1)/ MgO–La ₂ O ₃	T = 443–483 K P = 3–6 MPa C _{gly,feed} = 20 wt% Cat _{load} = 8 wt% of gly ω = 800 rpm t _{rxn} = 720 min	Y _{1,2} PDO ≈ 93.1%	LHHW (simplified to power law): $(-r_{1,2-PDO}) = k'_3 C_{Gly} P_{H2}$	E _{a3} = 69.6 kJ mol ⁻¹ k ₀₃ = 4.2 × 10 ⁷ mol g _{cat} ⁻¹ h ⁻¹	Ignored the inhibition term. One reaction in which Gly converts to 1,2 PDO.	[153]	
Gly + methanol Catalyst: Cu:Zn:Al	T = 473–543 K P = 3.0 MPa C _{gly,feed} = 1 wt% C _{ROH,feed} = 30 wt% Cat _{load} = 2.4 kg _{Gly} /kg _{cat} ω = 500 rpm t _{rxn} = 75 min	S _{1,2} PDO ≈ 79.4%	LHHW: $r_{H2} = \frac{k_1 K_{a,ROH} C_{ROH}}{\left[1 + K_{a,Gly} C_{Gly} + K_{a,ROH} C_{ROH} + K_{a,HA} C_{HA} + K_{a,1,2 PDO} C_{1,2 PDO} + (K_{a,H2} C_{H2})^{0.5} + K_{eq,HAH} K_{a,HA} C_{HA} (K_{a,H2} C_{H2})^{0.5}\right]^2}$ $r_{HA} = \frac{k_2 K_{a,Gly} C_{Gly}}{\left[1 + K_{a,Gly} C_{Gly} + K_{a,ROH} C_{ROH} + K_{a,HA} C_{HA} + K_{a,1,2 PDO} C_{1,2 PDO} + (K_{a,H2} C_{H2})^{0.5} + K_{eq,HAH} K_{a,HA} C_{HA} (K_{a,H2} C_{H2})^{0.5}\right]^2}$ $r_{1,2 PDO} = \frac{k_3 \left(\frac{1}{K_{eq,3}} K_{a,1,2 PDO} C_{1,2 PDO}\right)}{\left[1 + K_{a,Gly} C_{Gly} + K_{a,ROH} C_{ROH} + K_{a,HA} C_{HA} + K_{a,1,2 PDO} C_{1,2 PDO} + (K_{a,H2} C_{H2})^{0.5} + K_{eq,HAH} K_{a,HA} C_{HA} (K_{a,H2} C_{H2})^{0.5}\right]^2}$ $r_{EG} = \frac{k_4 K_{a,Gly} C_{Gly} (K_{a,H2} C_{H2})^{0.5}}{\left[1 + K_{a,Gly} C_{Gly} + K_{a,ROH} C_{ROH} + K_{a,HA} C_{HA} + K_{a,1,2 PDO} C_{1,2 PDO} + (K_{a,H2} C_{H2})^{0.5} + K_{eq,HAH} K_{a,HA} C_{HA} (K_{a,H2} C_{H2})^{0.5}\right]^2}$	E _{a1} = 115.0 kJ mol ⁻¹ E _{a2} = 87.0 kJ mol ⁻¹ E _{a3} = 68.4 kJ mol ⁻¹ E _{a4} = 82.2 kJ mol ⁻¹ k ₀₁ = 2.4 × 10 ¹⁶ min ⁻¹ k ₀₂ = 3.6 × 10 ¹⁴ min ⁻¹ k ₀₃ = 5.2 × 10 ¹³ min ⁻¹ k ₀₄ = 5.3 × 10 ¹³ min ⁻¹	Absorption parameters : ΔH _{a,ROH} = -98.7 ΔH _{a,Gly} = -65.1 ΔH _{a,1,2PDO} = -63.7 ΔH _{a,HA} = -91.5 ΔH _{a,H2} = -22.5 ΔS _{a,ROH} = -2.30 ΔS _{a,Gly} = -141.5 ΔS _{a,1,2PDO} = -121.9 ΔS _{a,HA} = -181 ΔS _{a,H2} = -52	H ₂ produced in situ via methanol aqueous phase reforming (APR)	[156]
Gly + H ₂ Catalyst: Ni catalyst supported on a silica-carbon composite	T = 493–533 K P _{H2} = 1.0–2.0 MPa C _{gly,feed} = 30–80 wt% Cat _{load} = 0.08–0.24 wt % ω = 1000 rpm t _{rxn} = 120 min	S _{1,2} PDO = 89.9%	Power law: r _{Gly} = k ₁ C _{Gly} ^{0.95} r _{1,2 PDO} = k ₂ C _{Gly} ^{0.38} C _{H2} ^{0.45} r _{EG} = k ₃ C _{Gly} ^{0.73} C _{H2} ^{-1.17} r _{acetol} = k ₄ C _{Gly} ^{1.21} C _{H2} ^{-0.97} r _{Ethanol} = k ₅ C _{Gly} ^{1.18} C _{H2} ^{0.22} r _{PO} = k ₆ C _{Gly} ^{0.80} C _{H2} ^{-0.49} r _{methanol} = k ₇ C _{Gly} ^{1.30} C _{H2} ^{-0.41} Activity factors (a _i) to describe the effect of impurities present in crude Gly: a _{NaOH} = 1 + 72.37 C _{NaOH} ² a _{NaCOOH} = 1 + 53.09 C _{NaCOOH} ² a _{NaCl} = 1 - $\frac{31.25 C_{NaCl}}{1 + 44.1 C_{NaCl}}$ a _{methanol} = 1 - $\frac{2.76 C_{MeOH}^2}{1 + 7.77 C_{MeOH}^2}$ a _{total} = 1 + ∑(a _i - 1) (-r' _{Gly}) = a _{total} * (-r _{Gly})	E _{a1} = 141.01 kJ mol ⁻¹ E _{a2} = 124.66 kJ mol ⁻¹ E _{a3} = 217.21 kJ mol ⁻¹ E _{a4} = 141.08 kJ mol ⁻¹ E _{a5} = 223.96 kJ mol ⁻¹ E _{a6} = 171.24 kJ mol ⁻¹ E _{a7} = 103.44 kJ mol ⁻¹ Ln k ₀₁ = 18.68 Ln k ₀₂ = 16.74 Ln k ₀₃ = 26.45 Ln k ₀₄ = 10.22 Ln k ₀₅ = 30.62 Ln k ₀₆ = 22.16 Ln k ₀₇ = 8.80	Uses crude Gly as feedstock. Activity factors (a _i) describe the effect of impurities on the rate of Gly consumption (-r' _{Gly}).	[158]	
Gly + H ₂ Catalyst: Cu catalyst	T = 483–513 K P = 6.5–8.0 MPa C _{gly,feed} = not available W/ F = 25–260 kg s mol ⁻¹ ω = not available t _{rxn} = 6000 min (100h)	S _{1,2 PDO} ≥90.0%	Deactivation model: Poison (p) adsorbs on catalytic site (*) to produce adsorbed poison (p*) p + * ⇌ p* r _p = k _p (C _p C* - $\frac{C_{p^*}}{K_{eq,p}}$)	Deactivation with thiophene: E _{ap} = 130.5 kJ mol ⁻¹ k _{op} = not available ΔH _{eq,p} = -77.8 kJ mol ⁻¹ Deactivation with glycerides: E _{ap} = 19.9 kJ mol ⁻¹ k _{op} = not available ΔH _{eq,p} = -41.1 kJ mol ⁻¹	Catalyst deactivation study. Model quantifies experimental data based on the use of contaminated crude glycerol feed with chlorine sulfur and	[159]	

(continued on next page)

Table 9 (continued)

Reactants and Catalyst	Reaction conditions ^a	(Best) $X_{Gly}/$ Sel./Yield ^b	Kinetic rate type and equation ^c	Kinetic parameters ^d	Notes	Ref.
					glycerides compounds.	

^a Reaction conditions used for kinetic studies. Temperature (T), pressure (P), Gly feed concentration ($C_{gly-feed}$), catalyst loading (Cat_{load}), stirring speed (ω), reaction time (t_{rxn}), contact time (W/F), alcohol feed concentration ($C_{ROH-feed}$).

^b Best Gly conversion (X_{Gly}), selectivity (S) or yield (Y) with respect to 1,2-PDO, achieved at optimum operating conditions which are different than the reaction conditions^a for kinetic study presented in the table.

^c Rate of reaction (r_i), reaction rate constant (k_j), concentration (C_i), component partial pressure (P_i), reaction order (n), overall equilibrium constant (K_{eq}), component adsorption equilibrium constant ($K_{a,i}$), Henry's constant (H_i), activity factor (a_i). i : components, j =reactions. Subscript EG = ethylene glycol, PO = propanol, HA = hydroxyacetone, HAH = partial hydrogenated hydroxyacetone, ROH = Alcohol.

^d Activation energy (E_{aj}), pre-exponential factor (K_{aj}), reaction order (n), overall equilibrium constant (K_{eq}), enthalpy of component adsorption constant ($\Delta H_{a,i}$), entropy of component adsorption constant ($\Delta S_{a,i}$). Subscripts: i : components, j =reactions.

model due to their low concentration. Likewise, the large excess of water generated as a by-product, (80 wt% of feed) was assumed to have no effect on conversion or selectivity. The reaction rate was set to be a function of Gly concentration at constant H_2 pressure, because of its excess making Gly the limiting reactant. The concentration of adsorbed components was calculated based on the assumption that adsorption and desorption steps are at equilibrium, with surface reaction being irreversible and the rate-determining step. The LHHW type model was found to fit the experimental data and describe the system as two parallel reactions producing 1,2-PDO and EG leading to a value of E_a of 88.2 kJ mol^{-1} for the conversion of Gly to 1,2-PDO [151].

Another LHHW model was developed in a study with the reaction being catalysed by Cu–Zn(4:1)/MgO–La₂O₃ [153]. This model included the adsorption of both Gly and H₂ on the catalytic surface with H₂ activity being described by partial pressure instead of concentration due to its presence in excess. In this case, it is also assumed that no mass transfer limitations occur and that the surface reaction is irreversible and the rate-determining step. The E_a for the conversion of Gly to 1,2-PDO is 69.6 kJ mol^{-1} [153].

Furthermore, a model combining assumptions of the LHHW and ER equations was illustrated by Mondal et al. for the reaction with Cu–Ni–Al₂O₃ [152]. They assumed that first Gly molecules are adsorbed, whilst H₂ molecules are only partially adsorbed on to the catalytic surface with the remaining excess H₂ being present in the bulk. The adsorbed Gly then reacts with H₂ in the bulk to generate 1,2-PDO and water, which are both adsorbed. The second step consists of the reaction of the adsorbed 1,2-PDO to generate adsorbed propanol. Lastly, both the adsorbed 1,2-PDO and propanol desorb from the catalytic surface. Here the rate-determining step is the irreversible surface reaction, with an E_a of 70.5 kJ mol^{-1} .

The study by Lemonidou et al. using Cu:Zn:Al catalyst [156] developed a LHHW based model for an intensified process in which H₂ is generated in situ via methanol aqueous phase reforming (APR). Similar to other studies, no mass or heat transfer limitations are assumed. This model ignores gaseous H₂ as it is produced close to the catalytic active sites and thus directly utilised by the adsorbed Gly molecules. Also, the presence of EG is ignored due to its low concentration in the products, hence simplifying the model and all adsorption steps are assumed to be quasi-equilibrated. The reaction kinetic parameters were calculated using the Arrhenius equation as usual, while adsorption enthalpies and entropies were calculated using Van't Hoff equation. Based on this model, the E_a for the formation of 1,2-PDO is 68.4 kJ mol^{-1} . It was found that the model developed best describes the system only when excess H₂ is present [156].

The reaction is usually investigated in liquid phase, though a study with Cu–Ni/γ-Al₂O₃ catalyst in a down flow tubular reactor explored the reaction in vapor phase [157]. An ER model was proposed assuming that organic molecules adsorbed on the catalytic surface, while H₂ remains in the bulk phase. Along water, adsorbed acetol is also generated and then

further reacts with H₂ to produce adsorbed 1,2-PDO. Finally, both 1,2-PDO and acetol desorb from the catalyst surface. The surface reaction step was assumed to be irreversible and set to be the rate-determining step. The E_a for the conversion of Gly to acetol is $55.14 \text{ kJ mol}^{-1}$ and for the conversion of acetol to 1,2-PDO is $50.87 \text{ kJ mol}^{-1}$. These values were found to be lower when compared to those of liquid phase reactions, where these values normally range between 83.7 and $104.6 \text{ kJ mol}^{-1}$ for Gly dehydration to acetol and is of 94.3 kJ mol^{-1} for the direct conversion of Gly to 1,2-PDO. The model fits experimental data and can describe the system as two reactions in series [157].

Currently, most of the kinetic models developed are based on the use of pure Gly as the reactant. However, Gatti et al. [158] utilised industrial crude glycerol as the starting material instead to develop a power law model of the reaction in the presence of a Ni catalyst supported on a silica–carbon composite. It was observed that the presence of impurities such as NaCl and methanol lowers the catalytic activity, while other impurities such as NaOH and NaCOOH positively affect the reaction by providing OH[−] molecules. To incorporate the effect of NaOH, NaCOOH, NaCl and methanol on the rate of consumption of Gly, activity factors were included in the model. The model successfully fits the experimental observations and can predict conversion with an average error of <8.0% [158]. Furthermore, Rajkhowa et al. [159] exclusively investigated the deactivation of a Cu based commercial catalyst by varying the concentration of impurities, such as glycerides, sulfur and chlorine compounds, present in the Gly feedstock. According to experimental observations, glycerides block the active sites due to their bulky nature. Sulfur compounds poison the active phase and chlorine compounds lead to sintering. Deactivation was modelled as an equation that describes the 'rate of production of poisoned sites' based on a reversible reaction where poison (p) adsorbs on the catalytic active sites. It was concluded that poisoning due to thiophene and glycerides has E_a values of $130.5 \text{ kJ mol}^{-1}$ and 19.9 kJ mol^{-1} , respectively [159].

4.5.2. 1,3-Propanediol

In addition to 1,2-PDO, Gly can be used to generate 1,3-PDO via microbial fermentation. The process offers various benefits such as low operating conditions, low costs and is more environmentally sustainable in comparison to the chemical route. On the other hand, fermentative processes require much longer reaction times. Microorganisms that are part of the *Klebsiella*, *Clostridium*, *Lactobacillus* and *Citrobacter* genera are typically used and could directly utilise crude Gly to generate 1,3-PDO [160]. Various studies have investigated the reaction and developed kinetic models based on the Monod equation [160–166]. The Monod equation describes the correlation between 'microbial specific growth rate and substrate concentrations.'

4.6. Acrolein and other glycerol dehydration products

Acr is a vital component typically used in the production of amino

acids, polymers, herbicides, and chemicals such as acrylic acid. Currently, Acr is generated by the oxidation of propylene [73]. However, Acr can also be produced by Gly dehydration, although other compounds like acetol and other by-products are generated in this acid-catalysed gas phase reaction, as shown in Fig. 13 [73,167,168].

The standard enthalpy ΔH_{rxn}^0 and entropy (ΔS°) of the reaction are $14.70 \text{ kJ mol}^{-1}$ and $0.09 \text{ kJ mol}^{-1} \text{ K}^{-1}$, respectively, hence making it an endothermic reaction, with a standard Gibbs free energy (ΔG°) of $-12.12 \text{ kJ mol}^{-1}$, proving that the reaction occurs spontaneously [168]. Using the Eyring equation based on transition state theory, it was concluded that the activation enthalpy (ΔH^\ddagger), entropy (ΔS^\ddagger), and Gibbs free energy (ΔG^\ddagger) are 40.6 kJ mol^{-1} , $0.1696 \text{ kJ mol}^{-1} \text{ K}^{-1}$ and $91.20 \text{ kJ mol}^{-1}$, respectively [169].

The reaction is affected by temperature, Gly concentration, catalyst loading and catalyst type. Temperature optimisation is important as high temperatures lead to a high Gly conversion but can also reduce Acr selectivity [169]. Furthermore, high Gly concentration affects catalyst activity negatively due to the condensation of Gly on the catalytic surface [168]. Additionally, Acr selectivity can decrease due to the presence of unconverted Gly, which promotes the consecutive consumption of Acr [168]. Similarly, catalyst loading requires optimisation as it can lead to an increase in Gly conversion and Acr selectivity [168]. Nevertheless, at higher temperatures and catalyst loading, coke formation becomes prominent and heavily reduces catalytic activity. Moreover, co-feeding oxygen aids in the maintenance of catalytic activity, reduces the production of by-products and increases Gly conversion and Acr selectivity [167]. Also, typically, fixed bed reactors are used for this reaction which can contain hot spots due to an uneven temperature distribution, thus further encourages the deactivation of the catalyst. However, alternatively, utilizing an intensified system such as microwave assisted fixed-bed reactors can lead to low coke formation and better catalyst stability due to even temperature distribution. Additionally, microwave heating can be an efficient system for in-situ catalytic regeneration [170,171]. These benefits led to 100% conversion of Gly and 70% Acr selectivity [171].

Furthermore, the reaction kinetics are heavily influenced by the catalyst structure and acidic properties [172]. Conversion of Gly to Acr occurs on Brønsted acid sites while the production of acetol occurs on Lewis acid sites. Using HZSM-5 catalyst containing $0.376 \text{ mmol g}^{-1}$ and

$0.099 \text{ mmol g}^{-1}$ of Brønsted and Lewis sites, respectively, causes the reaction rate of Gly to Acr to be 20 times faster than that of Gly to acetol [172], hence enhancing the selectivity by mitigating the progress of the side reaction. In addition, the rate constant for Gly to Acr is always higher than the rate constant for the conversion to acetol, indicating that Acr yield will always be higher than acetol's due to the presence of Brønsted acid sites, while the rate constants for other byproducts are much lower in comparison [169].

Although acidic catalysts are efficient, they tend to deactivate rapidly with time due to coking [167]. When using WO_3/TiO_2 , 2.2% of coke accumulated after 1 h increasing to as much as 4.4% after 6 h. As a result, catalytic surface area decreased from $30.5 \text{ m}^2 \text{ g}^{-1}$ to $25 \text{ m}^2 \text{ g}^{-1}$ [167], making catalyst regeneration crucial. A test with regenerated catalyst by partial coke oxidation leaving 44% of the coke on the catalytic surface allowed to improve Acr selectivity to 25% from the 10% shown when using the fresh catalyst.

Table 10 compiles studies on the kinetics of Acr production. The rate equation for carbon conversion developed by Dalil et al. [167] using WO_3/TiO_2 depends on temperature and mass of carbon. Partial pressure of oxygen was excluded from the equation as oxygen conversion is low ($<5\%$) and pressure was kept constant. The model included a degree of conversion term (α), which is calculated using the 'initial, instantaneous, and final mass' of deactivated catalyst [167]. The model successfully fits experimental data by 99.7%. It was shown that the overall E_a of the reaction is 100 kJ mol^{-1} , which is higher when compared to other models [167].

Further on considerations on the deactivation of the catalyst, Park et al. [172] developed a model for a fixed catalytic bed of HZSM-5 and ASPN-40 commercial catalysts. Catalytic activity was observed to decrease due to coking caused by the sequential reactions of primary product molecules. In the case of HZSM-5, its narrow pores constrain the diffusion of product molecules such as Acr and 3-HPA and, therefore, sequential reactions occur producing heavy components. Regarding ASPN-40, coking occurs due to the significant amount of acetol and acetaldehyde further undergoing condensation and oligomerization. Therefore, it was concluded that coking mechanism and thus catalyst deactivation are highly dependent on the catalyst properties. In the model, deactivation is described here as the decrease in mean integral activity ($\langle a \rangle$). This parameter is calculated by integrating the activity (a) with respect to the fixed catalytic bed's height (h). In addition, it was

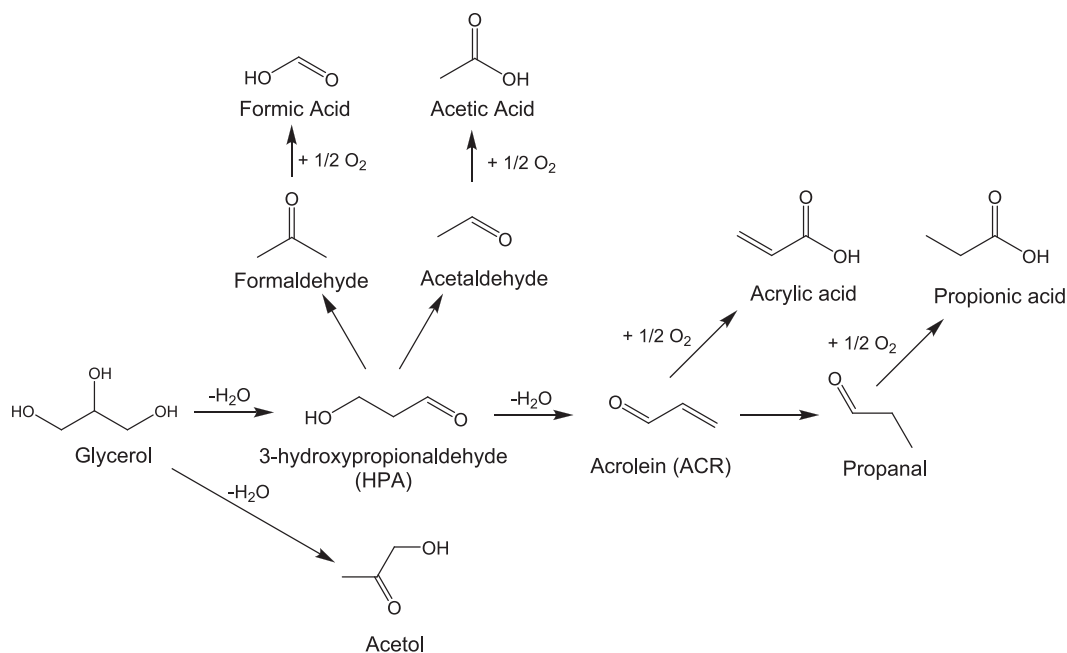


Fig. 13. Reaction network for the dehydration of glycerol.

Table 10

Summary of the most relevant aspects of kinetic studies in glycerol dehydration to yield Acr and other products.

Reaction and Catalyst	Reaction conditions ^a	(Best) X _{Gly} /Sel/Yield ^b	Kinetic rate type and equation ^c	Kinetic parameters ^d	Notes	Ref.
Gly dehydration to Acr Catalyst: WO ₃ /TiO ₂	T = 648–723 K P = 0.101 MPa C _{gly, feed} = 28 wt% Cat _{load} = 100 g t _{rxn} = 360 min	S _{Acr} ≥ 73%	Power-law (first order reaction): $\frac{d\alpha}{dt} = k(1 - \alpha)$ where $\alpha = \frac{m_0 - m_t}{m_0 - m_f}$ LHHW approach (expressed using power-law): $-r_{Gly} = \frac{k_2 K_{a,Gly} C_{Gly}^3}{[K_{a,Gly} C_{Gly} + 1]^3} = k_{Gly} C_{Gly}^n$ Substituting C _{Gly} , the logarithmic form of the equation: $\log r_{Gly} = \log k_{Gly} + n \log C_{Total} + n \log \left(\frac{1 - X_{Gly}}{1 + \delta_{Gly} X_{gly} + \kappa} \right)$	E _a = 100 kJ mol ⁻¹ k ₀ = 8.2 × 10 ⁻⁵ s ⁻¹	Pressure is excluded from model.	[167]
Gly dehydration to Acr Catalyst: 30HZ-20 A	T = 553–613 K P = 0.101 MPa C _{gly, feed} = 10 wt% V _{cat} /F = 0.05–0.26 m ³ s mol ⁻¹ t _{rxn} = 180 min	S _{Acr} = 88.8%	LHHW approach (expressed using power-law): $\frac{dC_{Gly}}{d\tau} = -k_1 C_{Gly} - k_2 C_{Gly} = -k_G C_{Gly}$ $\frac{dC_{Acr}}{d\tau} = k_1 C_{Gly} - k_3 C_{Acrolein} - k_4 C_{Acrolein} = k_1 C_{Gly} - k_A C_{Acrolein}$ $\frac{dC_{Acetol}}{d\tau} = k_2 C_{Gly} - k_5 C_{Acetol}$ $\frac{dC_{Acetaldehyde}}{d\tau} = k_3 C_{Acrolein}$ $\frac{dC_{minor-byproducts}}{d\tau} = k_4 C_{Acrolein}$ $\frac{dC_{Acetone}}{d\tau} = k_5 C_{Acetaldehyde}$ Power-law: $\frac{dC_{Gly}}{d\tau} = -(k_1 + k_2 + k_3 + k_4) C_{gly}$ $\frac{dC_{HPA}}{d\tau} = k_1 C_{Gly} - k'_1 C_{HPA}$ $\frac{dC_{Acr}}{d\tau} = k'_1 C_{HPA}$ $\frac{dC_{acetol}}{d\tau} = k_2 C_{Gly} - k'_2 C_{acetol}$ $\frac{dC_{acetaldehyde}}{d\tau} = k_3 C_{Gly} + k'_2 C_{acetol}$ $\frac{dC_{byproducts}}{d\tau} = k_4 C_{Gly}$ Model for catalyst deactivation (dependent on product concentration): $\frac{d(\alpha)}{dt} = -k_d C_{0,Gly} X_{Gly}(\alpha)$ $\frac{dX_{Gly}}{dt} = k_d C_{0,Gly} X_{Gly} (1 - X_{Gly}) \ln(1 - X_{Gly})$	n = ~ 1.0 E _a = 27.5 kJ mol ⁻¹ k ₀ = 5.35 × 10 ⁵ s ⁻¹ E _{aG} = 46.9 kJ mol ⁻¹ E _{a1} = 46.0 kJ mol ⁻¹ E _{a2} = 53.3 kJ mol ⁻¹ E _{aA} = 5.7 kJ mol ⁻¹ E _{a3} = 5.0 kJ mol ⁻¹ E _{a4} = 6.1 kJ mol ⁻¹ E _{a5} = 46.6 kJ mol ⁻¹ k _{0G} = 27.7 m ³ kg _{cat} ⁻¹ s ⁻¹ k ₀₁ = 20.7 m ³ kg _{cat} ⁻¹ s ⁻¹ k ₀₂ = 12.1 m ³ kg _{cat} ⁻¹ s ⁻¹ k _{0A} = 2.5 × 10 ⁻⁴ m ³ kg _{cat} ⁻¹ s ⁻¹ k ₀₃ = 6.3 × 10 ⁻⁵ m ³ kg _{cat} ⁻¹ s ⁻¹ k ₀₄ = 1.8 × 10 ⁻⁴ m ³ kg _{cat} ⁻¹ s ⁻¹ k ₀₅ = 2.6 m ³ kg _{cat} ⁻¹ s ⁻¹ E _{a1} = 40.4 kJ mol ⁻¹ E _{a1} = not available E _{a2} = 44.8 kJ mol ⁻¹ E _{a2} = 70.5 kJ mol ⁻¹ E _{a3} = 69.1 kJ mol ⁻¹ E _{a4} = 33.9 kJ mol ⁻¹ k _{0j} = not available	For gas phase reaction K ₁ C _{Gly} ≪ 1.	[168]
Gly dehydration to Acr Catalyst: SiW ₂₀ -Al/Zr ₁₀	T = 553–613 K P = 0.101 MPa C _{gly, feed} = 10 wt% W/F = 0–3 (10 ³ kg _{cat} s m ⁻³) t _{rxn} = 180 min	S _{Acr} = 87.6%	Power-law: $\frac{dC_{Gly}}{d\tau} = -(k_1 + k_2 + k_3 + k_4) C_{gly}$ $\frac{dC_{HPA}}{d\tau} = k_1 C_{Gly} - k'_1 C_{HPA}$ $\frac{dC_{Acr}}{d\tau} = k'_1 C_{HPA}$ $\frac{dC_{acetol}}{d\tau} = k_2 C_{Gly} - k'_2 C_{acetol}$ $\frac{dC_{acetaldehyde}}{d\tau} = k_3 C_{Gly} + k'_2 C_{acetol}$ $\frac{dC_{byproducts}}{d\tau} = k_4 C_{Gly}$ Model for catalyst deactivation (dependent on product concentration): $\frac{d(\alpha)}{dt} = -k_d C_{0,Gly} X_{Gly}(\alpha)$ $\frac{dX_{Gly}}{dt} = k_d C_{0,Gly} X_{Gly} (1 - X_{Gly}) \ln(1 - X_{Gly})$	E _{a1} = 40.4 kJ mol ⁻¹ E _{a1} = not available E _{a2} = 44.8 kJ mol ⁻¹ E _{a2} = 70.5 kJ mol ⁻¹ E _{a3} = 69.1 kJ mol ⁻¹ E _{a4} = 33.9 kJ mol ⁻¹ k _{0j} = not available	Study also includes thermodynamic parameters (ΔH [‡] , ΔS [‡] , ΔG [‡]) obtained using the Eyring equation.	[169]
Gly dehydration to Acr Catalyst: HZSM-5	T = 523–573 K P = 0.101 MPa C _{gly, feed} = 10.8 wt% W/F = 2.08–104.17 g _{cat} h mol ⁻¹ t _{rxn} = 4200 min (70 h)	Y _{Acr} ≈ 70%	Model for catalyst deactivation (dependent on product concentration): $\frac{d(\alpha)}{dt} = -k_d C_{0,Gly} X_{Gly}(\alpha)$ $\frac{dX_{Gly}}{dt} = k_d C_{0,Gly} X_{Gly} (1 - X_{Gly}) \ln(1 - X_{Gly})$	Deactivation terms At W/F = 50 g _{cat} h mol ⁻¹ , k _d = 2.98 h ⁻¹ At W/F = 83.33 g _{cat} h mol ⁻¹ , k _d = 2.55 h ⁻¹ At W/F = 104.17 g _{cat} h mol ⁻¹ , k _d = 1.35 h ⁻¹	Heterogeneous kinetic modelling assuming first order with respect to reactant. A kinetic model for the deactivation behaviour based on mean integral activity ((a))	[172]
Gly dehydration to Acr Catalyst: ASPN-40	T = 523–573 K P = 0.101 MPa C _{gly, feed} = 10.8 wt% W/F = 2.08–104.17 g _{cat} h mol ⁻¹ t _{rxn} = 6900 min (115 h)	Y _{Acr} ≈ 50%	Power-law: $\frac{dC_{Gly}}{d\tau} = -(k_1 + k_2 + k_3 + k_4) C_{gly}$ $\frac{dC_{HPA}}{d\tau} = k_1 C_{Gly} - k'_1 C_{HPA}$ $\frac{dC_{Acr}}{d\tau} = k'_1 C_{HPA}$ $\frac{dC_{acetol}}{d\tau} = k_2 C_{Gly} - k'_2 C_{acetol}$ $\frac{dC_{acetaldehyde}}{d\tau} = k_3 C_{Gly} + k'_2 C_{acetol}$ $\frac{dC_{byproducts}}{d\tau} = k_4 C_{Gly}$ Model for catalyst deactivation (dependent on product concentration): $\frac{d(\alpha)}{dt} = -k_d C_{0,Gly} X_{Gly}(\alpha)$ $\frac{dX_{Gly}}{dt} = k_d C_{0,Gly} X_{Gly} (1 - X_{Gly}) \ln(1 - X_{Gly})$	E _{a1} = 44.6 kJ mol ⁻¹ E _{a1} = not available E _{a2} = 66.6 kJ mol ⁻¹ E _{a2} = 74.7 kJ mol ⁻¹ E _{a3} = 36.2 kJ mol ⁻¹ E _{a4} = 48.0 kJ mol ⁻¹ k _{0j} = not available	Heterogeneous kinetic modelling assuming first order with respect to reactant. A kinetic model for the deactivation behaviour based on mean integral activity ((a))	[172]

(continued on next page)

Table 10 (continued)

Reaction and Catalyst	Reaction conditions ^a	(Best) $X_{Gly}/$ Sel./Yield ^b	Kinetic rate type and equation ^c	Kinetic parameters ^d	Notes	Ref.
Gly dehydration to Acr Catalyst: heteropolyacid ZR24	T = 543–583 K P = 0.27 MPa $C_{gly,feed} = 2-4$ vol% Cat _{load} = 0.966 g $\tau = 0.098-0.20$ s $t_{rxn} = 480$ min	$S_{Acr} = 75\%$	$\frac{d(a)}{dt} = -k_d C_{0,Gly} X_{Gly}(a)$ $\frac{dX_{Gly}}{dt} =$ $k_d C_{0,Gly} X_{Gly} (1 - X_{Gly}) \ln(1 - X_{Gly})$ Deactivation model (based on Gly conversion): $-\frac{dX_{Gly}}{dt} =$ $k_d \tau^{-1.4} P_{Gly}^{1.7} P_{H_2O}^{-0.6} P_{O_2}^{-0.77} X_{Gly}^2$	At $W/F =$ $104.17 \text{ g}_{cat} \text{ h mol}^{-1}$, $k_d = 0.71 \text{ h}^{-1}$	Catalyst deactivation study. Model is based on observations made when varying temperature, concentrations, and residence time.	[173]
Gly Oxydehydration to acrylic acid (Gly + H ₂ O ₂) Catalyst: V6-SiW/HZSM-5	T = 333–363 K P = 0.101 MPa $C_{gly,feed} = 1.37-5.50 \text{ mol L}^{-1}$ $C_{H_2O_2,feed} = 1.37-6.85 \text{ mol L}^{-1}$ Cat _{load} = SiW loading of 30 wt % $t_{rxn} = 240$ min	$Y_{acrylic acid} = 36.23\%$	ER model $-r_{Gly} = \frac{k_2 K_a^2 C_{H_2O_2}^2 C_{Gly}}{(1 + K_a C_{H_2O_2} C_{H_2O_2})^2}$ $-r_{Gly} = \frac{k_2 K_a^2 C_{H_2O_2}^2 C_{Gly}}{(1 + K_a C_{H_2O_2} C_{H_2O_2})^2}$	$E_{ad} = -157 \text{ kJ mol}^{-1}$ $k_{0d} = 4.96 \times 10^{-22} \text{ s}^{-2.4} \text{ Pa}^{-0.33}$ $E_{a2} = 28.57 \text{ kJ mol}^{-1}$ $k_{02} = 9.95 \times 10^{-2}$ Adsorption parameter $\Delta H_{a,H_2O_2} =$ $18.45 \text{ kJ mol}^{-1}$ $k_{0-K_a,H_2O_2} = 4.25 \times 10^4$	Power-law and LHHW models were also developed. ER fits experimental results the best.	[174]

^a Reaction conditions used for kinetic studies. Temperature (T), pressure (P), Gly feed concentration ($C_{gly,feed}$), catalyst loading (Cat_{load}), reaction time (t_{rxn}), contact time (V_{cat}/F) and (W/F), H₂O₂ feed concentration ($C_{H_2O_2,feed}$), residence time (τ).

^b Best Gly conversion (X_{Gly}), selectivity (S) or yield (Y) with respect to acrolein (Acr) or acrylic acid, achieved at optimum operating conditions which are different than the reaction conditions^a for kinetic study presented in the table.

^c Rate of reaction (r_i), reaction rate constant (k_j), deactivation rate constant (k_d), reaction order (n), component adsorption equilibrium constant ($K_{a,i}$), concentration (C_i), total molar concentration (C_{Total}), concentration of total active sites (C_{TS}), initial concentration ($C_{0,i}$), degree of conversion (α), initial mass of coked catalyst (m_0), instantaneous mass of coked catalyst (m_i), final mass of coked catalyst (m_f), material ratio (κ), expansion factor (δ_{Gly}), conversion (X_i), mean integral activity ($\langle a \rangle$), residence time (τ), Partial pressure (P_i). i : components, j =reactions. Subscript HPA = 3-hydroxypropionaldehyde.

^d Activation energy (E_{aj}), pre-exponential factor (k_{0j}), reaction order (n), deactivation rate constant (k_d), enthalpy of component adsorption constant ($\Delta H_{a,i}$), pre-exponential factor of component adsorption constant ($k_{0-K_{a,i}}$). i : components, j =reactions.

concluded that deactivation rate is dependent on product concentrations only [172]. In their model, external mass transfer is ignored as there were no changes to conversion when varying flowrates. Based on the model developed, the E_a of the main reaction when using HZSM-5 and ASPN-40 is 40.4 kJ mol^{-1} and 44.6 kJ mol^{-1} , respectively.

Furthermore, Talebian-Kiakalaieh et al. [168] used the LHHW approach to model the reaction in a packed-bed reactor of 30HZ-20 A. Based on this approach, Gly molecules are adsorbed to react, and then Acr and water desorb of the catalytic surface. The model included two parameters, a material ratio (κ) due to the presence of a solvent (water) and an expansion factor (δ_{Gly}) due to the generation of 3 mol of product from 1 mol of Gly. The model was concluded suitable as it predicted Acr selectivity (88.3%) with an error of 0.57% compared to the experimental value (88.8%). The E_a is 27.5 kJ mol^{-1} when using 30HZ-20 A catalyst [168]. The LHHW approach was also used by the same authors [169] to develop a model using SiW₂₀-Al/Zr₁₀ catalyst. In both studies, the concentrations of the adsorbed species were calculated by assuming adsorption and desorption occur in equilibrium [168,169]. The E_a obtained by Talebian-Kiakalaieh et al. [169], in which SiW₂₀-Al/Zr₁₀ is used, is comparable to those of commercial catalysts HZSM-5 and ASPN-40 [172]. All the studies assumed the reactions are first order with respect to the reactant [167–169,172]. The dehydration reaction was assumed to be pseudo-first order as the water concentration is large compared to that of Gly and thus the quantity of water is assumed to be constant [169,172]. In addition, the rate-determining step is the dehydration of Gly to Acr [168,169,172].

Moreover, Martinuzzi et al. [173] focused on modelling catalyst deactivation only. The authors investigated the effect of reaction parameters such as temperature, residence time and concentrations on the deactivation of a commercial heteropolyacid catalyst ZR24. It was observed that deactivation rate constant is influenced by the formation of cyclic compounds. Based on experimental data, a kinetic model describing deactivation in terms of the decrease of glycerol conversion as a function of time was developed. The E_a value for deactivation was

concluded to be 157 kJ mol^{-1} [173].

Acr is typically used as intermediate to produce acrylic acid [82], however Thanasilp et al. [174] investigated an oxydehydration reaction in which Gly is directly converted to acrylic acid in a single reactor using V6-SiW/HZSM-5 catalyst. Based on a power-law model, the E_a of the reaction is $26.63 \text{ kJ mol}^{-1}$ and the orders of Gly, and the oxidant (H₂O₂) are 1.2 and 0.3, respectively. Thus, the reaction rate is pseudo-first order with respect to Gly, and zero order with respect to H₂O₂. In addition, two models using the LHHW approach and one using the ER approach were also developed. The ER model, which best fits the experimental data, assumes that the reaction occurs between Gly molecules and adsorbed oxygen molecules, with an E_a of $28.57 \text{ kJ mol}^{-1}$.

4.7. Halogenated products (Chlorohydrins)

Chlorination of Gly produces dichlorohydrins (DCH, with isomers α,γ -DCH and α,β -DCH), which are intermediates for epichlorohydrin production [175]. Epichlorohydrin is a vital feedstock for the manufacturing of epoxide resins and plasticisers [176]. Conventionally, DCHs are produced by reacting allyl chloride and hypochlorous acid. However, the DCH mixture produced only contains 30% of the desired isomer α,γ -DCH [175]. High selectivity towards α,γ -DCH can be attained via the glycerol-based route (Fig. 14), which is an exothermic reaction [77]. Gly reacts with HCl to produce monochlorohydrins (MCH, with isomers α -MCH and β -MCH) and water as by-product. The isomer α -MCH further reacts to produce DCH [175], although intermediates like epoxides and esters are also formed due to the presence of carboxylic acid catalysts [176].

Temperature wise, it was observed that Gly conversion increases up to 105°C but stays constant at higher temperatures, which is due to the decrease of HCl solubility despite the reaction rate increasing [177]. Moreover, increasing HCl pressure significantly increases Gly conversion and DCH selectivity [178], because at higher pressures, the solubility and mass transfer of HCl increases [175,177]. Furthermore,

increasing catalyst loading also causes α,γ -DCH selectivity to increase [175]. The reaction is typically catalysed using ACA, however it is volatile under the usual reaction conditions. Therefore, more stable catalysts with comparable performance to ACA have been evaluated [175,178]. According to Tesser et al. [178], a catalyst requires to have a pK_a value of 4–5 to be suitable for attaining high activity and α,γ -DCH selectivity [178].

Table 11 presents studies that have investigated the reaction kinetics. At the beginning of the reaction, HCl rate of consumption is high due to its movement from the gas to the liquid phase and the ‘reaction rate effect’. This indicates the need of describing the gas-liquid mass transfer phenomenon using HCl solubility data [178]. For instance, HCl solubility data were determined experimentally [178], and a solubility corrective factor was included to match the model results with the experimental data [178]. Similarly, HCl solubility data were calculated using the UNIFAC model by Vitiello et al. [175]. The model by De Araujo Filho et al. [177] assumed HCl solubility to be constant, while Medina et al. [176] obtained HCl concentration real values by using titration.

The two-film theory was also used to describe the gas-liquid HCl mass transfer in [175,177,178]. The mass transfer coefficient attained by Tesser et al. [178] is 3 min^{-1} which is higher compared to 0.0542 min^{-1} obtained by Vitiello et al. [175], which could be due to the nature of the catalysts as the higher the activity, the lower the coefficient [175].

Moreover, Tesser et al. [178] investigated a gas-liquid biphasic kinetic model for multiple catalysts (ACA, monochloroacetic acid, dichloroacetic acid and trichloroacetic acid) at a constant operating temperature (373 K). The model included a HCl gas-liquid partition parameter to describe the reaction in a fed-batch reactor. Additionally, catalyst activity was related to its chemical structure using the Taft equation accounting for the electronic nature of the substituents (F^*) and the steric effect (δ). To develop the model, it was assumed the reactions to yield β -MCH and α,β -DCH are irreversible. It is also recommended using Taft equation along pK_a values to improve predictions related to the catalyst behaviour [178].

Furthermore, the same authors modified the previous model to describe an isothermal semi-batch system at different pressures and catalysts (glycolic, thioglycolic, diglycolic, aspartic, glutamic acids and cysteine) at temperature of 373 K. [175]. In this study, they considered the reverse reactions to β -MCH and α,β -DCH to have an equal kinetic constant. It was determined that the fitting did not improve significantly when varying the values of the reverse kinetic constants and thus this assumption was verified [175].

A comprehensive model was developed by De Araujo Filho et al. [177] for the reaction catalysed by ACA in a back mixed semi-batch reactor. According to the authors [177], using gaseous HCl led to a significant increase in the liquid volume during the reaction. Therefore, unlike the case of using aqueous HCl, the volume of the reaction mixture cannot be assumed constant. In addition, it was observed that at temperatures between 105 °C and 120 °C, high Gly conversion to α -MCH

occurs in the absence of catalyst. Therefore, the parameters κ and α_w , were included in the model to describe the effect of the non-catalytic pathway. The quasi-steady state hypothesis was assumed for all the intermediates due to their low concentrations and therefore were excluded [177]. To confirm the validity of the model, catalyst modulus (\mathcal{P}) was introduced, which is based on the formation rate of α,γ -DCH and is defined as the ratio between the real reaction rate to the theoretical maximum when the catalyst concentration is infinite [177]. The E_a obtained were comparable to results in literature. However, it was noted that the activation energy for the conversion α,γ -MCH to α,γ -DCH (47.8 kJ mol^{-1}) is higher compared to other cases (40.9 kJ mol^{-1} [179]), due to the consideration of the non-catalytic reaction [177].

Using ACA as catalyst, Medina et al. [176] extended the model by De Araujo Filho et al. [177]. The chlorination steps were assumed irreversible, while the other steps are reversible. Unlike De Araujo Filho et al. [177], quasi-steady state hypothesis is not valid for esters, which is due to the high stability and high concentration of esters. However, the quasi-equilibrium approximation is applied as their formation is much faster compared to the hydrochlorination steps. Therefore, equilibrium constants for the formation of esters were calculated assuming independence of temperature due to the reactions having low enthalpies. In addition, mean activity coefficients for HCl and water were incorporated into the model. Furthermore, the model describes a non-isothermal system, this is because the dissolution of HCl gas to the liquid phase is exothermic and causes the reactor’s temperature to vary considerably. Finally, it was illustrated that the reaction is of zero order with respect to Gly, while for HCl, the reaction order is close to first at the beginning of the reaction but then it increases to second order as water is produced. The model fits experimental data successfully, however in certain conditions, deviations occur as reaction mixture deviates from ideal behaviour due to HCl being a strong electrolyte [176].

Moreover, quasi-stationary-state assumption was made for the reaction system to develop a simple power-law kinetic model when using ACA as a catalyst [180]. It was also assumed that the concentrations of ACA, HCl and H_2O are constant. The model was used to design and investigate several large-scale configurations such as continuous stirred tank reactors (CSTRs) and reactive distillation columns. Additionally, intensified systems which combines reactive distillation with thermally coupled distillation and divided-wall distillation were explored [180]. Lastly, a further detailed overview of the reaction kinetics for Gly chlorination is also presented in the review by Santacesaria et al. [77].

4.8. Glycerol reforming: production of H_2

In a context where H_2 production from renewable resources is being spurred by the implementation of renewable energy policies, its generation from bioresource waste streams is an increasing field of research. Glycerol steam reforming (GSR) is an overall endothermic ($\Delta H_{rxn}^0 = +128.0 \text{ kJ mol}^{-1}$) reaction that generates H_2 and/or syngas as end products [81]. However, the reaction network can become quite

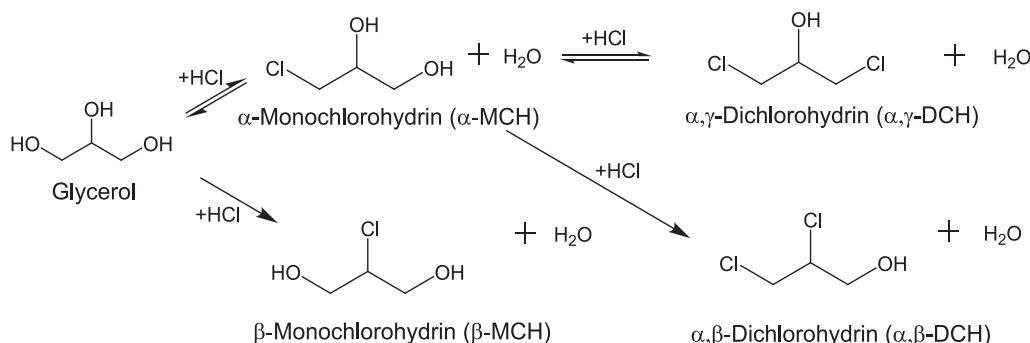


Fig. 14. Reaction scheme for the halogenation of glycerol.

Table 11
Summary of the most relevant aspects of kinetic studies in glycerol halogenation reactions.

Reactants and Catalyst	Reaction conditions ^a	(Best) X _{Gly} /Sel/ Yield ^b	Kinetic rate type and equation ^c	Kinetic parameters ^d	Notes	Ref.
Gly + gaseous HCl Catalyst: Glycolic acid Thioglycolic acid Diglycolic acid Cysteine Aspartic acid Glutamic acid	T = 373 K P _{HCl} = 0.1–0.8 MPa m _{Gly,feed} = 150 g Cat _{load} = 4.80–19.13 g ω = 1000 rpm t _{rxn} = 240 min	S _{DCH} = 84 mol%	Power-law: $r_{\alpha-MCH} = C_{cat}(k_1 C_{Gly} C_{HCl} - k_{-1} C_{H_2O} C_{\alpha-MCH})$ $r_{\beta-MCH} = C_{cat}(k_2 C_{Gly} C_{HCl})$ $r_{\alpha,\gamma-DCH} = C_{cat}(k_3 C_{\alpha-MCH} C_{HCl} - k_{-3} C_{H_2O} C_{\alpha,\gamma-DCH})$ $r_{\alpha,\beta-DCH} = C_{cat}(k_4 C_{\alpha-MCH} C_{HCl})$	Not available Kinetic constants (k _j) values given at various operating conditions at constant temperature (373 K).	None	[175]
			Power-law based model: $r_{\alpha-MCH} = \frac{k_3 C_{Gly} C_{HCl}^2 \left(\frac{C_{cat}}{C_{H_2O} + K_{eq1} C_{Gly} + K_{eq2} C_{\alpha-MCH}} + \theta \right)}{C_{cat} C_{H_2O} + K_{eq1} C_{Gly} + K_{eq2} C_{\alpha-MCH}} + \theta_{3HCl} C_{HCl} + \theta_{H_2O} C_{H_2O}$ $r_{\beta-MCH} = \frac{k_4 C_{Gly} C_{HCl}^2 \left(\frac{C_{cat}}{C_{H_2O} + K_{eq1} C_{Gly} + K_{eq2} C_{\alpha-MCH}} + \theta \right)}{C_{cat} C_{H_2O} + K_{eq1} C_{Gly} + K_{eq2} C_{\alpha-MCH}} + \theta_{3HCl} C_{HCl} + \theta_{H_2O} C_{H_2O}$ $r_{\alpha,\gamma-DCH} = \frac{k_7 C_{\alpha-MCH} C_{HCl}^2 \left(\frac{C_{cat}}{C_{H_2O} + K_{eq1} C_{Gly} + K_{eq2} C_{\alpha-MCH}} \right)}{C_{cat} C_{H_2O} + K_{eq1} C_{Gly} + K_{eq2} C_{\alpha-MCH}} + \theta_{7HCl} C_{HCl}$ $r_{\alpha,\beta-DCH} = \frac{k_8 C_{\alpha-MCH} C_{HCl}^2 \left(\frac{C_{cat}}{C_{H_2O} + K_{eq1} C_{Gly} + K_{eq2} C_{\alpha-MCH}} \right)}{C_{cat} C_{H_2O} + K_{eq1} C_{Gly} + K_{eq2} C_{\alpha-MCH}} + \theta_{7HCl} C_{HCl}$	$E_{a3} = 71.4363 \text{ kJ mol}^{-1}$ $E_{a4} = 85.3036 \text{ kJ mol}^{-1}$ $E_{a7} = 40.2159 \text{ kJ mol}^{-1}$ $E_{a8} = 57.1005 \text{ kJ mol}^{-1}$ $E_{a\theta} = 12.0728 \text{ kJ mol}^{-1}$ $k_{03} = 1.31574$ $k_{04} = 0.06005$ $k_{07} = 0.16391$ $k_{08} = 0.00340$ $k_{0\theta} = 0.00048$		
Gly + gaseous HCl Catalyst: ACA	T = 343–388 K P _{HCl} = 0.0253–0.101 MPa m _{Gly,feed} = not available Cat _{load} = 0–15 mol% ω = not available t _{rxn} = 180 min	Y _{DCH} = 65%*	Power-law (combined catalysed and non-catalysed reactions) $r_{\alpha-MCH} = \frac{k_3 C_{Gly} C_{HCl}^2 (C_{cat} + \theta)}{C_{cat} C_{H_2O} + \theta_{HCl} C_{HCl} + \theta_{H_2O} C_{H_2O}}$ $r_{\beta-MCH} = \frac{k_4 C_{Gly} C_{HCl}^2 (C_{cat} + \theta)}{C_{cat} C_{H_2O} + \theta_{HCl} C_{HCl} + \theta_{H_2O} C_{H_2O}}$ $r_{\alpha,\gamma-DCH} = \frac{k_7 C_{cat} C_{\alpha-MCH} C_{HCl}^2}{C_{cat} C_{H_2O} + (\gamma C_{H_2O} + \delta) C_{HCl}}$	Merged parameters $\theta_{3HCl} = 934.772$ $\theta_{H_2O} = 747.316$ $\theta_{7HCl} = 3984.59$	Estimated parameters for three model sets are provided. Model set 2 is presented here as it has the highest degree of explanation value (R ² = 0.9878).	[176]
			Equilibrium coefficients $K_{eq1} = 4.2522$ $K_{eq2} = 2.2390$			
			Power law: combined catalysed and non-catalysed reactions $r_{\alpha-MCH} = \frac{k_3 C_{Gly} C_{HCl}^2 (C_{cat} + \theta)}{C_{cat} C_{H_2O} + \theta_{HCl} C_{HCl} + \theta_{H_2O} C_{H_2O}}$ $r_{\beta-MCH} = \frac{k_4 C_{Gly} C_{HCl}^2 (C_{cat} + \theta)}{C_{cat} C_{H_2O} + \theta_{HCl} C_{HCl} + \theta_{H_2O} C_{H_2O}}$ $r_{\alpha,\gamma-DCH} = \frac{k_7 C_{cat} C_{\alpha-MCH} C_{HCl}^2}{C_{cat} C_{H_2O} + (\gamma C_{H_2O} + \delta) C_{HCl}}$	$E_{a3}' = 47.8 \text{ kJ mol}^{-1}$ $E_{a4}' = 56.1 \text{ kJ mol}^{-1}$ $E_{a7}' = 35.0 \text{ kJ mol}^{-1}$ $\ln k_{03}' = 2.55$ $\ln k_{04}' = 2.37$ $\ln k_{07}' = -3.06$		
Gly + gaseous HCl Catalyst: ACA	T = 343–393 K P _{HCl} = 0.0253–0.101 MPa m _{Gly,feed} = 220 g Cat _{load} = 0–50 mol% ω = 1000 rpm t _{rxn} = 180 min	Y _{DCH} = 64%*	Power law (non-catalysed reactions): $r_{\alpha-MCH} = \frac{k_3 C_{Gly} C_{HCl}^2}{\theta_{HCl} C_{HCl} + \theta_{H_2O} C_{H_2O}}$ $r_{\beta-MCH} = \frac{k_4 C_{Gly} C_{HCl}^2}{\theta_{HCl} C_{HCl} + \theta_{H_2O} C_{H_2O}}$	Power-law: non-catalysed reactions $E_{a3}'' = 74.0 \text{ kJ mol}^{-1}$ $E_{a4}'' = 82.3 \text{ kJ mol}^{-1}$ $\ln k_{03}'' = 13.37$	Very comprehensive kinetic model (proposed Catalyst modulus). Non-catalytic hydrochlorination reaction is considered. Volume increase of the liquid phase is considered.	[177]

(continued on next page)

Table 11 (continued)

Reactants and Catalyst	Reaction conditions ^a	(Best) X_{Gly} /Sel/ Yield ^b	Kinetic rate type and equation ^c	Kinetic parameters ^d	Notes	Ref.
				$\ln k'_{04} = 13.19$		
				<i>Merged parameters:</i> $\theta_{HCl} = 990.97$ $\delta' = 3992.66$ $\theta_{H_2O} = 1240.39$ $\gamma' = 1.05$		
				θ' values are provided at different T		
Gly + gaseous HCl Catalyst: ACA monochloroacetic acid (MCA) dichloroacetic acid (DCA) trichloroacetic acid (TCA)	T = 373 K $P_{HCl} = 0.2\text{--}0.9$ MPa $m_{Gly,feed} = 150$ g $Cat_{load} = 8.0$ mol% $\omega = 1200$ rpm $t_{rxn} = 240$ min	$Y_{DCH} = 89.37\%$ (cat = ACA)	Power-law: $r_{\alpha-MCH} = k_1 C_{cat} C_{Gly} C_{HCl} - k_{-1} C_{cat} C_{H_2O} C_{\alpha-MCH}$ $r_{\beta-MCH} = k_2 C_{cat} C_{Gly} C_{HCl}$ $r_{\alpha,\gamma-DCH} = k_3 C_{cat} C_{Gly} C_{\alpha-MCH} - k_{-3} C_{cat} C_{H_2O} C_{\alpha,\gamma-DCH}$ $r_{\alpha,\beta-DCH} = k_4 C_{cat} C_{Gly} C_{\alpha-MCH}$	Not available Kinetic constants (k_j) values given at various operating conditions at constant temperature (373 K).	Includes HCl gas-liquid partition. Solubility correction factor calculated and included in the model. Taft equation is used.	[178]
Gly + HCl Catalyst: ACA	T = 363–393 K P_{HCl} = not available $m_{Gly,feed}$ = not available Cat_{load} = not available ω = not available t_{rxn} = not available	$Y_{DCH} = 33.3\%$	Power-law: $r_{Gly} = k_1 C_{Gly}$ $r_{\alpha-MCH} = k_2 C_{Gly} - k_3 C_{\alpha-MCH}$ $r_{\beta-MCH} = k_4 C_{Gly} - k_5 C_{\beta-MCH}$ $r_{\alpha,\gamma-DCH} = k_3 C_{\alpha-MCH}$ $r_{\alpha,\beta-DCH} = k_5 C_{\beta-MCH}$	$k_1 = - (k_2 + k_4)$ $k_2 = 491.6e^{-5380.8/T}$ $k_3 = 55.41e^{-5469.2/T}$ $k_4 = 0.3789e^{-4221.2/T}$ $k_5 = 33.7e^{-6294.6/T}$	Model is based on optimising model developed by Luo et al. [179]. Study of several intensified systems that include CSTRs and reactive distillations	[180]

^a Reaction conditions used for kinetic studies. Temperature (T), HCl partial pressure (P_{HCl}), Gly feed mass ($m_{gly,feed}$), catalyst loading (Cat_{load}), stirring speed (ω), reaction time (t_{rxn}).

^b Best Gly conversion (X_{Gly}), selectivity (S) or yield (Y) with respect to α , γ - DCH achieved at optimum operating conditions which are different than the reaction conditions for kinetic study presented in the table.

*Calculated using data from concentration graphs presented in study.

^c Rate of reaction (r_i), forward reaction rate constant (k_j), backward reaction rate constant (k_{-j}), concentration (C_i), concentration of catalyst (C_{cat}), overall equilibrium constant (K_{eq}), merged parameters in which definition differs between articles ($\theta', \theta_{ji}, \theta_i, \gamma', \delta'$). i : components, j =reactions.

^d Activation energy (E_{aj}), pre-exponential factor (k_{0j}), overall equilibrium constant (K_{eq}), merged parameters in which definition differs between articles ($\theta', \theta_{ji}, \theta_i, \gamma', \delta'$). i : components, j =reactions.

Table 12

Summary of the most relevant aspects of kinetic studies in glycerol reforming for the production of H₂.

Reaction/ reactants and Catalyst	Reaction conditions ^a	(Best) X _{Gly} / Sel./Yield ^b	Kinetic rate type and equation ^c	Kinetic parameters ^d	Notes	Ref.
Supercritical water gasification (SCWG) of Gly Catalyst: None	T = 760–873 K P = 25 MPa C _{gly,feed} = 10 wt% τ = 3.9–9.0 s Cat _{load} = none t _{rxn} = not available	Y _{H2} = 3.4 mol mol _{Gly} ⁻¹	Power-law: r _{Gly-pyrolysis1} = k ₁ C _{Gly} r _{Gly-pyrolysis2} = k ₂ C _{Gly} r _{Int-SR1} = k ₃ C _{int} C _{H2O} r _{Int-SR2} = k ₄ C _{int} C _{H2O} r _{Int-pyrolysis} = k ₅ C _{int} r _{WGSR} = k ₆ C _{CO} C _{H2O} r _{Methanation} = k ₇ C _{CO} C _{H2}	E _{a1} = 53.3 kJ mol ⁻¹ E _{a2} = 59.8 kJ mol ⁻¹ E _{a3} = 114.1 kJ mol ⁻¹ E _{a4} = 109.6 kJ mol ⁻¹ E _{a5} = 66.7 kJ mol ⁻¹ E _{a6} = 76.5 kJ mol ⁻¹ E _{a7} = 74.3 kJ mol ⁻¹ ln k ₀₁ = 6.00 ln k ₀₂ = 6.37 ln k ₀₃ = 15.28 ln k ₀₄ = 14.18 ln k ₀₅ = 9.51 ln k ₀₆ = 4.86 ln k ₀₇ = 10.19 Power law m = 0.253 n = 0.358 E _a = 63.3 kJ mol ⁻¹ k ₀ = 0.0360 mol m ⁻² s ⁻¹ kPa ^{-(m+n)}	All reaction rate equations are assumed to be 1st order with respect to the reactants.	[181]
Gly SR (Gly + Steam) Catalyst: Co-Ni/Al ₂ O ₃	T = 773–823 K P = 0.101 MPa MR: 3:1–12:1 C _{gly,feed} = 30–60 wt% Cat _{load} = not available t _{rxn} = not available	S _{H2} = 65.5%	Power-law: - r _{Gly} = kP _{Gly} ^m P _{steam} ⁿ LHHW r = $\frac{kP_{Gly}P_{steam}}{(1 + K_{a,Gly}P_{Gly})(1 + K_{a,steam}P_{steam})}$	LHHW E _a = 69.36 kJ mol ⁻¹ Ln k ₀ = -7 × 10 ^{-7*} Adsorption constants ΔH _{a,Gly} = -28.70 kJ mol ⁻¹ ΔS _{a,Gly} = -39.93 J mol ⁻¹ K ⁻¹ ΔH _{a,steam} = 15.81 kJ mol ⁻¹ ΔS _{a,steam} = -8.11 J mol ⁻¹ K ⁻¹ Power law n ₁ = 0.63 n ₂ = 0.66 n ₃ = 0.38 n ₄ = 1.12 n ₅ = 1.61 E _{a1} = 66.1 kJ mol ⁻¹ E _{a2} = 71.4 kJ mol ⁻¹ E _{a3} = 67.0 kJ mol ⁻¹ E _{a4} = 66.5 kJ mol ⁻¹ E _{a5} = 90.7 kJ mol ⁻¹ k ₀₁ = 49.0 mol min ⁻¹ g _{cat} ⁻¹ atm ⁻ⁿ k ₀₂ = 660.3 mol min ⁻¹ g _{cat} ⁻¹ atm ⁻ⁿ k ₀₃ = 45.2 mol min ⁻¹ g _{cat} ⁻¹ atm ⁻ⁿ k ₀₄ = 9.1 mol min ⁻¹ g _{cat} ⁻¹ atm ⁻ⁿ k ₀₅ = 1827.7 mol min ⁻¹ g _{cat} ⁻¹ atm ⁻ⁿ	ER model also developed but it did not fit experimental data	[182]
Gly SR (Gly + Steam) Catalyst: 5% Ni-UGSO	T = 753–853 K P = 0.101 MPa MR = 9:1 W/ F = 17.886–39.305 g h mol ⁻¹ Cat _{load} = 0.5 g t _{rxn} = 150 min	Y _{H2} = 77.07%	Power-law: r _{Gly} = k ₁ P _{Gly} ⁿ¹ r _{H2} = k ₂ P _{Gly} ⁿ² r _{CO2} = k ₃ P _{Gly} ⁿ³ r _{CO} = k ₄ P _{Gly} ⁿ⁴ r _{CH4} = k ₅ P _{Gly} ⁿ⁵ LHHW: r = $\frac{2}{(1 + K_{a,Gly}P_{Gly}^3 + K_{des,CO2}P_{CO2})^2}$	E _a = 62.8 kJ mol ⁻¹ k ₀ = 53.4 mol min ⁻¹ g _{cat} ⁻¹ atm ^{-2/3}	To develop power law, zero order with respect to water is assumed. LHHW model describes single site dissociative adsorption of Gly and molecular adsorption of steam.	[183]

(continued on next page)

Table 12 (continued)

Reaction/ reactants and Catalyst	Reaction conditions ^a	(Best) $X_{Gly}/$ Sel/Yield ^b	Kinetic rate type and equation ^c	Kinetic parameters ^d	Notes	Ref.
				<p><i>Adsorption and desorption constants</i></p> $\Delta H_{a,Gly} = -34.1 \text{ kJ mol}^{-1}$ $\Delta S_{a,Gly} = -39.3 \text{ kJ mol}^{-1}$ $\Delta H_{des,CO_2} = 41.1 \text{ J mol}^{-1} \text{ K}^{-1}$ $\Delta S_{des,CO_2} = 12.4 \text{ J mol}^{-1} \text{ K}^{-1}$ <p><i>For :</i></p> $r_{Gly}, E_a = 70.82 \text{ kJ mol}^{-1}, m = 0.31, n = 0.52$ $r_{H_2}, E_a = 55.79 \text{ kJ mol}^{-1}, m = 0.31, n = 0.34$ $r_{CO_2}, E_a = 73.18 \text{ kJ mol}^{-1}, m = 0.28, n = 0.40$ $r_{CO}, E_a = 90.42 \text{ kJ mol}^{-1}, m = 0.50, n = 0.03$ $r_{CH_4}, E_a = 109.53 \text{ kJ mol}^{-1}, m = 0.21, n = 0.15$ <p><i>Power law</i></p> $E_a = 29.0 \text{ kJ mol}^{-1}$ $k_0 = 65.08 \text{ kmol atm}^{-0.93} \text{ kg}_{cat}^{-1} \text{ h}^{-1}$ <p><i>LHHW</i></p> $E_a = 30.0 \text{ kJ mol}^{-1}$ $k_0 = 37.0 \text{ kmol kg}_{cat}^{-1} \text{ h}^{-1} \text{ atm}^{-1}$ <p><i>Adsorption parameters</i></p> $K_{a,Gly}, K_{a,H_2O} \text{ and } K_{eq,surface rxn} \text{ values are provided at 723 K, 773 K and 823 K.}$		
Gly SR (Gly + Steam) Catalyst: 10Ni-1Ru/Al ₂ O ₃ /5CeO ₂	T = 823–1073 K P = 0.101 MPa MR = 12:1 WHSV = 10 h ⁻¹ t _{rxn} = not available	S _{H₂} = 88.6%	Power law: $-r_i = k C_{Gly}^m C_{H_2O}^n$			[184]
Gly SR (Gly + Steam) Catalyst: Ni/Fly ash	T = 723–823 K P = 0.101 MPa MR = 12:1 W/F = 7.94–19.27 kg cat h kmol ⁻¹ t _{rxn} = 180 min	Y _{H₂} = 5.8 mol mol _{Gly} ⁻¹	Power-law model: $-r = k P_{Gly}^{0.54} P_{H_2O}^{0.39}$ LHHW: $-r = \frac{kK_{a,Gly}K_{a,H_2O}K_{eq,surface rxn}P_{Gly}P_{H_2O}}{(1 + K_{a,Gly}K_{a,H_2O}K_{eq,surface rxn}P_{Gly}P_{H_2O} + K_{a,Gly}P_{Gly} + K_{a,H_2O}P_{H_2O})}$		For LHHW model, dual site mechanism and pseudo-steady state hypothesis is used. The r.d.s is assumed to be the desorption step.	[185]
Gly SR (Gly + Steam) Catalyst: Ni–Cu–Al	T = 773–873 K P = 0.101 MPa MR = 9:1 W/F = not available t _{rxn} = 180 min	S _{H₂} = 78.6%	Power-law with first order: $-r = k\alpha(t)X$ Where $\alpha(t) = \frac{1}{1 + k't}$ $X_{Gly} = \frac{1}{(1 + k't) \frac{k m_{cat}}{F_0}}$	$E_a' = 96.8 \text{ kJ mol}^{-1}$ $k_0' = 9.76 \times 10^4 \text{ min}^{-1}$ $E_a = 55.3 \text{ kJ mol}^{-1}$ $k_0 = 2.21 \times 10^2 \text{ min}^{-1}$	Model developed by separable kinetics that includes catalyst decay and reaction kinetics. $\alpha(t)$ is activity of the catalyst at time t. k' is a constant for carbon deposition.	[186]
Gly SR (Gly + Steam) Catalyst: Ni/Nb ₂ O ₅ /Al ₂ O ₃	T = 723–923 K P = 0.101 MPa VR = 30–50 (%v/v Gly in feed) GHSV = (2–5) × 10 ⁶ h ⁻¹ t _{rxn} = not available	Y _{H₂} = 50%	Power law: $r = kC_{Gly}^m C_{steam}^n$	<i>First approach</i> $m = 0.4$ $n = 0.0$ $E_a = 32.9 \text{ kJ mol}^{-1}$ $k_0 = 33.6 \text{ mol}^{0.6} \text{ L}^{0.4} \text{ g}^{-1} \text{ h}^{-1}$ <i>Second approach</i> $m = 0.9$ $n = 2.0$	Pseudo-steady state hypothesis.	[187]
				For VR = 50%v/v gly in feed $E_a = 31.2 \text{ kJ mol}^{-1}$ $k_0 = 2.7 \times 10^7 \text{ L}^{-0.1} \text{ mol}^{0.1} \text{ h}^{-1}$ For VR = 30%v/v gly in feed		

(continued on next page)

Table 12 (continued)

Reaction/ reactants and Catalyst	Reaction conditions ^a	(Best) $X_{Gly}/$ Sel./Yield ^b	Kinetic rate type and equation ^c	Kinetic parameters ^d	Notes	Ref.
Gly autothermal reforming Catalyst: dual layer monolith of Pt in the partial oxidation layer and Rh/Pt for SR layer supported on γ -Al ₂ O ₃	T = 823–923 K P = 0.1 MPa MR (steam:carbon) = 0.4–1.2 Cat _{load} = 0.012 g t _{rxn} = not available	Y _{H2} = 15%	LHHW (single site mechanism): $r = \frac{kP_{Gly}\sqrt{P_{H_2O}}}{(1 + K_{a,Gly}P_{Gly} + \sqrt{K_{a,H_2O}P_{H_2O}})^2}$	$E_a = 120.1 \text{ kJ mol}^{-1}$ $k_0 = 3.9 \times 10^{19} \text{ L}^{1.9} \text{ mol}^{-1.9} \text{ h}^{-1}$ $E_a = 130.73 \text{ kJ mol}^{-1}$ $\ln k_0 = -5.2056^*$ k values given at 823–923 K. Adsorption parameters ($K_{a,Gly}$) and (K_{a,H_2O}) given at 923 K.	Model describes non-dissociative adsorption of Gly and dissociative adsorption of steam	[188]
			Power law (overall crude Gly autothermal reforming): $r = k_1 p_{Gly}^{1.04} p_{H_2O}^{0.54} p_{O_2}^{1.78}$	Power law (overall crude Gly autothermal reforming) $E_{a1} = 87.8 \text{ kJ mol}^{-1}$ $k_{01} = 4.3 \times 10^{10} \text{ mol (g}_{cat} \text{ min)}^{-1}$		
			ER (SR of Gly): $r = \frac{k_2 \left(C_{Gly}^{0.8} C_{H_2O}^{2.4} C_{CO_2}^{-1.5} C_{H_2}^{-4.2} - \frac{C_{CO_2}^{0.5} C_{H_2}}{K_{eq,2}} \right)}{\left[1 + K_{a,1} C_{Gly}^{0.8} + K_{a,W} C_{Gly}^{0.8} C_{CO_2}^{2.2} C_{H_2}^{-1.5} C_{H_2O}^{-4.2} + K_{a,C} C_{CO_2}^{1.5} C_{H_2}^{4.2} C_{H_2O}^{-2.2} \right]}$	ER (SR of Gly): $E_{a2} = 93.2 \text{ kJ mol}^{-1}$ $k_{02} = 1.17 \times 10^5 \text{ mol (g}_{cat} \text{ min)}^{-1}$ $K_{eq,2} = 1.13 \times 10^9$ Adsorption parameters $K_{a,1} = 1.56 \times 10^{-2}$ $K_{a,C} = 2.74 \times 10^{11}$ $K_{a,W} = 1.35 \times 10^6$	Uses Crude Gly as feedstock.	
Crude Gly autothermal reforming Catalyst: 5% Ni/CeZrCa	T = 773–923 K P = 0.1 MPa MR (steam:carbon) = 2.6 MR (oxygen:carbon) = 0.125 Cat _{load} = not available t _{rxn} = not available	not available	LHHW (total oxidative reforming): $r = \frac{k_3 \left(C_{Gly}^{0.2} - \frac{C_{CO_2}^{0.5} C_{H_2O}^{0.7}}{C_{O_2}^{0.65} K_{eq,3}} \right)}{\left[1 + K_{a,3} C_{O_2}^{0.65} + K_{a,6} C_{CO_2}^{0.5} + K_{a,H_2O} C_{H_2O}^{0.7} + K_{a,W} C_{CO_2}^{0.5} C_{H_2O}^{0.7} C_{O_2}^{-0.65} \right]}$	LHHW (total oxidative reforming) $E_{a3} = 72.6 \text{ kJ mol}^{-1}$ $k_{03} = 2.96 \times 10^5 \text{ mol (g}_{cat} \text{ min)}^{-1}$ $K_{eq,3} = 1.08 \times 10^{-10}$ Adsorption parameters $K_{a,H_2O} = 4.56 \times 10^{-1}$ $K_{a,W} = 5.383 \times 10^2$ $K_{a,3} = 1.7 \times 10^{-2}$ $K_{a,6} = 3.62 \times 10^3$	Several comprehensive models based on LHHW and ER approaches presented for GSR, total oxidative reforming and methanation reactions. The most suitable models were further tested for thermodynamic scrutiny. Study also explored reactor simulation.	[189]
			ER (CO₂ methanation): $r = \frac{k_4 \left(C_{CO_2}^{0.5} - \frac{C_{CH_4}^{0.5} C_{H_2O}}{C_{H_2} K_{eq,4}} \right)}{\left[1 + K_{a,3} C_{CH_4}^{0.5} C_{H_2O} + K_{a,1} C_{CH_4}^{0.5} C_{H_2O} C_{H_2}^2 \right]}$	ER (CO₂ methanation) $E_{a4} = 81.2 \text{ kJ mol}^{-1}$ $k_{04} = 8.84 \times 10^6 \text{ mol (g}_{cat} \text{ min)}^{-1}$ $K_{eq,4} = 6.79 \times 10^{-5}$ Adsorption parameters $K_{a,1} = 7.435 \times 10^2$ $K_{a,3} = 7.6 \times 10^4$		

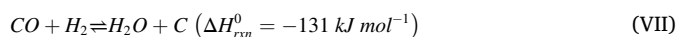
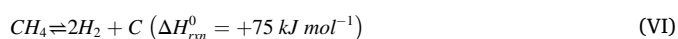
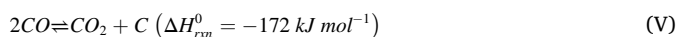
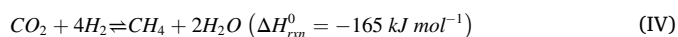
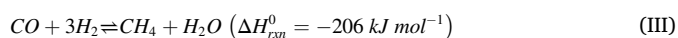
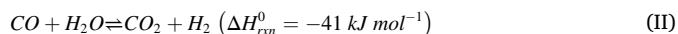
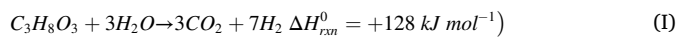
^a Reaction conditions used for kinetic studies. Temperature (T), Pressure (P), steam to Gly molar ratio (MR), Gly feed concentration ($C_{gly-feed}$), catalyst loading (Cat_{load}), reaction time (t_{rxn}), residence time (τ), contact-time (W/F), weight hourly space velocity ($WHSV$), volume ratio (VR).

^b Best Gly conversion (X_{Gly}), selectivity (S) or yield (Y) with respect to H₂, achieved at optimum operating conditions which are different than the reaction conditions^a for kinetic study presented in the table.

^c Rate of reaction (r_i), reaction rate constant (k_j), partial pressure (P_i), concentration (C_i), component reaction order (m) and (n), component adsorption equilibrium constant ($K_{a,i}$), component desorption equilibrium constant ($K_{des,i}$), equilibrium constant (K_{eq}), activity of catalyst at time t ($\alpha(t)$), mass of catalyst (m_{cat}), molar flow rate (F_0), Gly conversion (X_{Gly}). i : components, j =reactions. Subscripts: Int = intermediates.

^d Activation energy (E_{aj}), pre-exponential factor (k_{0j}), reaction order (m) and (n), enthalpy of component adsorption/desorption constant ($\Delta H_{a,i}/\Delta H_{des,i}$), entropy of component adsorption/desorption constant ($\Delta S_{a,i}/\Delta S_{des,i}$), component adsorption equilibrium constant ($K_{a,i}$), equilibrium constant (K_{eq}). i : components, j =reactions. *Calculated from data provided by study.

complex since, together with GSR (eq. I), water–gas shift (WGS) reaction (eq. II) and methanation (eq. III and IV) can also occur [81]. In addition, coke typically forms (eq. V, VI and VII) on the catalyst surface causing deactivation [81]. Other side reactions that have been observed to also occur are Gly pyrolysis as well as the SR and pyrolysis of intermediates (aldehydes, Acr, acetol, organic acids) [181].



Operating conditions and type of catalyst used highly affect the reaction and the presence of intermediates. Usually, liquid components, mainly Acr, are produced at low temperatures, high pressures, and high Gly feed concentration in the presence of an acidic catalyst. For H₂ generation, the reaction requires an alkali catalyst, high temperatures, low pressures, and low Gly concentration in the feed [72]. These conditions increase the yield of H₂ and CO₂ substantially as it promotes WGS reaction [72]. However, similar to other cases, the catalyst tends to deactivate due to carbon deposition, which reduces catalytic surface area and pore volume [182]. Under the usual reaction conditions (>1023–1073 K and 1.0 atm), coking is mainly dependent on the partial pressure of Gly only, although it can be reversed [182]. In addition, including basic promoters to the catalyst reduces the concentration of acidic sites and this is beneficial as coking usually occurs in acidic sites while molecular adsorption of Gly occurs in basic sites [183]. Furthermore, high temperatures, short residence time and diluted Gly feed also reduce the formation of carbon deposits [72].

Several studies presented in Table 12 have investigated the kinetics of the reaction. Most studies [181–187] use power-law models to describe the progress of the reactions. Using a bimetallic Co-Ni/Al₂O₃ catalyst, the overall E_a of the reaction is 63.3 kJ mol⁻¹ and the reaction order for Gly and steam are 0.253 and 0.358, respectively [182]. Product wise, the rate of formation of methane is the slowest, requiring the highest E_a (101 kJ mol⁻¹), whilst the formation of other products (H₂, CO₂ and CO) has E_a in the range of 60–67 kJ mol⁻¹, indicating that the reactions have a similar rate-controlling step [182].

Moreover, when using a Ni-based catalyst (5% Ni-UGSO), another model was developed assuming a zero order with respect to water due to its presence in excess with the same reaction network to the previous case [183]. The overall E_a is 66.1 kJ mol⁻¹ with an order of Gly of 0.63. Similarly, it was observed that the E_a of methane formation (90.7 kJ mol⁻¹) is much higher in comparison to the E_a of other products which had close values to 66.1 kJ mol⁻¹, which indicates that other products mainly come from Gly consumption [183]. With a Ru-doped Ni/Al₂O₃/5CeO₂, Densash et al. [184] found different reaction orders for Gly (0.31) and H₂O (0.52), thus the excess of the latter not playing a constant role on the kinetics as in the previous case. The overall E_a has a similar value to the ones in the previous two references, but that of the formation of the by-products were somewhat higher. In addition, Bepari et al. [185] tested a Ni/Fly ash catalyst. In their study, the overall E_a was remarkably low (29.0 kJ mol⁻¹) and the order of reaction for Gly (0.54) and H₂O (0.39) were relatively similar to other studies. It is noteworthy that upon consideration of the by-products, the production of CO in the WGS reaction showed a negative order of reaction with respect to steam (-0.03), which entails that increasing water concentration can lead to

the inhibition of CO production [184].

Furthermore, using Ni–Cu–Al as catalyst, a study developed the only model that considered deactivation as a relevant assumption using separable kinetic method to enable the investigation of kinetics independently from catalytic deactivation [186]. A parameter $a(t)$ was implemented representing the activity of the catalyst at time (t) and it is defined as the reaction rate on used catalyst for time (t) divided by reaction rate on fresh catalyst [186]. As simplifications for the model, several assumptions were made such as no mass or heat transfer effects, no gas expansion due to constant flow rate, no CO and CH₄ due to their presence in small amounts and the reactor is considered to be plug-flow. The reaction is fit well to a first order power-law model [186]. The E_a of the main reaction is 55.3 kJ mol⁻¹ and that of the catalyst decay was calculated to be 96.8 kJ mol⁻¹ [186].

The kinetics of the reaction has also been reported in the absence of a catalyst at 760–873 K and 25 MPa as opposed to atmospheric pressure operation (0.101 MPa). In this case, WGS and methanation reactions were assumed irreversible and the formation of char and tar were also ignored as the quantity observed was minimal. Further simplifications include the lumping of all intermediates owing to experimental quantification constraints and all the reactions were assumed to be first order with respect to each of the reactants. Based on these assumptions, the activation energies ranged from 53.3 to 114.1 kJ mol⁻¹ [181].

While using Ni/Nb₂O₅/Al₂O₃, Menezes et al. [187] developed two models based on power-law equations. When assuming that steam is in excess (steam's reaction order = 0), the reaction order with respect to Gly is 0.4 and E_a is 32.9 kJ mol⁻¹. This model is based on H₂ formation rate and thus describes GSR only [187]. The second model used differential method for a tubular reactor assuming steady state conditions. In this case, the orders were 0.9 and 2.0 for Gly and H₂O, respectively. Interestingly, the E_a values changed significantly from 31.2 kJ mol⁻¹ (50% v/v Gly in feed) to 120.1 kJ mol⁻¹ (30% v/v Gly in feed). The difference is due to different rate determining steps. As opposed to the first model, the second model is based on Gly consumption and therefore, also describes parallel reactions occurring along GSR [187].

As the system is usually heterogeneously catalysed, some studies developed LHHW based models [182,183,185,188], for which single and dual site mechanisms have been investigated. In single-site mechanisms, it is assumed that Gly and steam adsorb on identical sites, as opposed to dual site mechanism, in which they adsorb on different active sites. According to Cheng et al. [182], it was concluded that the system is described by a LHHW-based model using dual site mechanism which associative adsorption of Gly and steam occurs and surface reaction is the rate determining step [182]. The E_a attained is 69.36 kJ mol⁻¹, which is close in comparison to the value attained by power-law in the same study [182]. Additionally, a LHHW based model using dual-site mechanism was also developed; however, in this case the desorption step was assumed to be rate-determining [185]. The activation energy is 30.0 kJ mol⁻¹, which is close compared to that of the power-law model [185]. Several ER-based models were also developed assuming that only one reactant (either Gly or steam) is adsorbed due to steric and geometric constraints, while the other remains in the bulk (in gas phase) [182]. It was concluded that the ER based models did not fit experimental data [182].

Moreover, Liu et al. [188] investigated autothermal reforming using a dual layer monolith catalyst of Pt in the partial oxidation layer and Rh/Pt for steam reforming layer supported on γ -Al₂O₃. In addition to neglecting heat and mass transfer limitations under the operating conditions, the model considered steam reforming, partial oxidation and WGS as the three reactions taking place. The study illustrated that the model suitable for the system is a LHHW model using single-site mechanism where Gly adsorption is non-dissociative while steam adsorption is dissociative. It is assumed that the rate determining step is the surface reaction [188]. Furthermore, Desgagnés et al. [183] used single site mechanism when utilizing a 5% Ni-UGSO catalyst. It was assumed that all the elementary steps are partial first order with respect

to each reactant. The best fitting model consists of a two-step rate determining step, where the first step is dehydrogenation of adsorbed intermediate (dissociative adsorption of Gly), which generates adsorbed CO molecules. Then, CO reacts with adsorbed steam to generate H₂ and CO₂ [183]. This model led to an E_a of 62.8 kJ mol⁻¹, is close to the one using power-law [183].

The kinetics for autothermal reforming of crude Gly using 5% Ni/CeZrCa catalyst was developed by Odoom et al. [189]. The reaction system was considered to consist of four reactions. A power law model was developed for the overall autothermal reforming reaction which had an E_a value of 87.8 kJ mol⁻¹. The GSR considered was found to be best described by the ER approach in which the surface reaction between an adsorbed intermediate and steam, was the rate determining step. The E_a value for GSR is 93.2 kJ mol⁻¹. Total oxidative reforming of Gly was also considered and was best described by a LHHW model in which molecular adsorption of crude Gly occurs. This model showed that the E_a value for the reaction is 72.6 kJ mol⁻¹. Finally, an ER based model was developed for CO₂ methanation in which CO₂ is adsorbed and has an E_a of 81.2 kJ mol⁻¹ [189].

Furthermore, several reviews [79–81] further discussed in detail the effect of operating conditions, catalyst being developed and some kinetic studies for the reaction. Along the investigation of appropriate catalysts and reaction kinetics, intensified reactor types have also been explored such as sorption enhanced reactors, membrane reactors, and hybrid reactors. The aim of these systems is to overcome any thermodynamic limitations present and generate high purity H₂ at potentially milder operating conditions leading to economic benefits [79,190,191]. Moreover, considering the high temperatures demanded for the process, efforts have been made for the supply of energy by alternative technologies like microwave plasma, although challenges concerning fuel retention time in the setup are yet to be overcome. A schematic diagram of the device is shown in Fig. 15 [192]. Finally, it is worth noting that several works [193–195] have coupled kinetic models with multi-fluid models to simulate various reactor configurations via computational fluid dynamics (CFD).

4.9. Organic acids

Organic acids can be produced from Gly (Fig. 16) by selective

oxidation and hydrothermal conversion [196,197]. The oxidation of Gly first occurs on Brønsted and Lewis acid sites in which the intermediates, glyceraldehyde (GLCD) and dihydroxyacetone (DHA) are generated [198]. The intermediates then further undergo selective oxidation and C—C bond cleavage to generate various organic acids like glyceric (GCA), glycolic (GLCA), formic (FA), tartronic (TA), oxalic (OA) and mesoxalic acid (MA) [198,199]. Furthermore, hydrothermal conversion is the route in which lactic acid (LA) is produced. After the generation of GLCD and DHA, the dehydration of these intermediates to produce pyruvaldehyde then occurs on Lewis acids. Lastly, pyruvaldehyde transforms to LA on Brønsted acid sites either by internal Cannizzaro or by benzylic acid rearrangement. Due to the instability of LA, over-oxidation to other organic acid can occur [198]. A detailed description of the reaction pathway for the production of LA has been demonstrated by Abdullah et al. [198]. Several other reactions can also occur simultaneously in the system such as dehydrogenation, hydrogenolysis, dehydration, and C—C bond cleavage [197].

The reactions usually occur in alkaline conditions, typically in presence of NaOH, and use mixed metal oxides and bimetallic catalysts [74,196,197]. Parameters such as temperature, pressure, concentration of NaOH and Gly, catalyst loading and type, all affect the Gly conversion and product selectivity [200,201]. Additionally, due to the complexity of the system, various variables influence the overall reaction selectivity such as the type and number of the oxidation sites, the degree of oxidation, the presence of other chemical reactions like dehydration and isomerisation and the nature of the cleavage site within the C—C bonds [199]. Therefore, to improve product selectivity and reduce separation costs downstream, effective catalyst design is vital [202] as well as approaches such as electrooxidation, photooxidation and photo-electrooxidation and systems such as co-electrolysis and fuel cells can be considered for Gly oxidation [199]. Furthermore, deactivation of catalyst should be further explored as it can occur [198]. For example, the adsorption of acids like TA and OA formed during the reaction can inhibit catalytic activity [201]. When considering process intensification of the system, in situ generation of oxygen for oxidation and hydrogen simultaneously via water splitting of the basic aqueous Gly solution has been investigated [203]. This was done by using a photo catalyst such as titanium disilicide (TiSi₂) in the presence of solar light. The results show that at long reaction times (12h), high Gly conversion (97.6%) and 100%

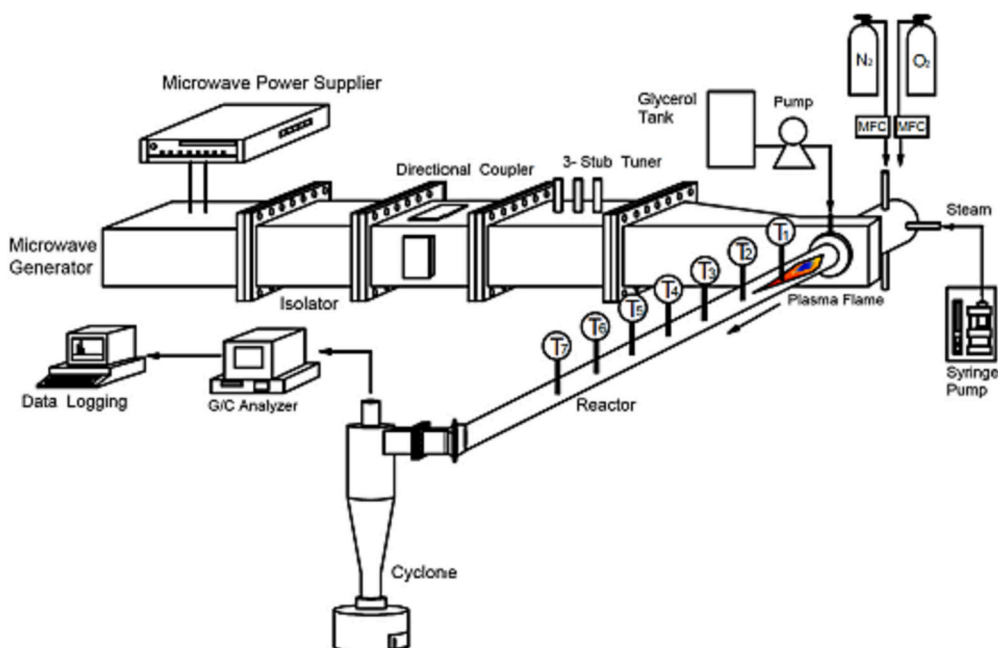


Fig. 15. Setup used for the gasification of Gly with microwave induced plasma. Figure reproduced with permission of Elsevier [192].

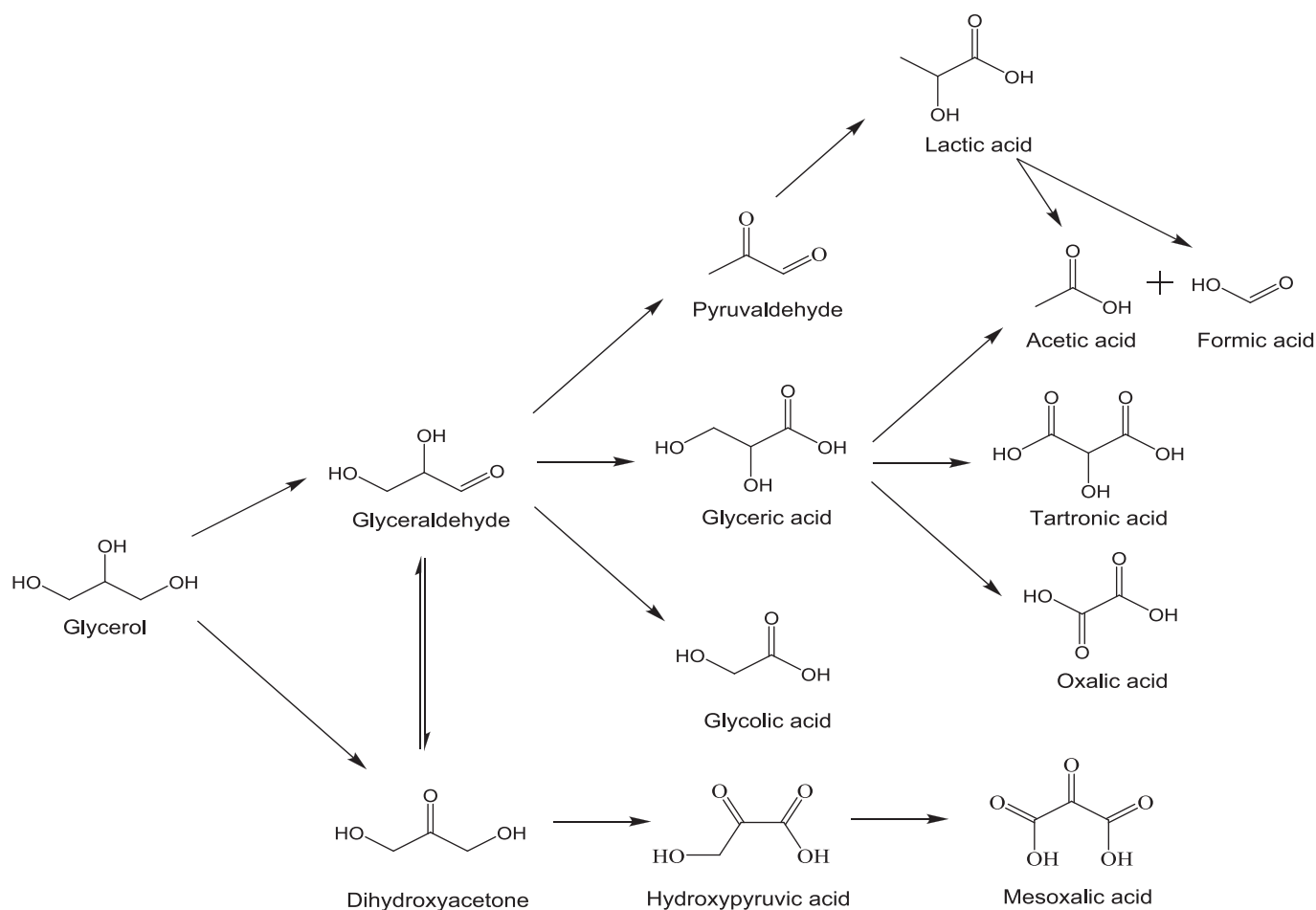


Fig. 16. General reaction network involved in glycerol oxidation.

selectivity of glyceric acid (GCA) can be obtained [203].

Moreover, several studies presented in Table 13, have investigated the kinetics of the conversion of Gly to organic acids, all of which neglected mass or heat transfer limitations. The oxidation of Gly using Pt/Al₂O₃, Au/Al₂O₃ and Ag/Al₂O₃ catalysts in the presence of NaOH has been explored by Diaz et al. [196]. A power-law model was used with partial first reaction order for all the components involved. In addition, Khang–Levenspiel model was used to include the deactivation of the catalyst described by activity. Based on the model, the activation energies of the reactions using Pt/Al₂O₃, Au/Al₂O₃ and Ag/Al₂O₃ are 46–76 kJ mol⁻¹, 15–103 kJ mol⁻¹ and 48–97 kJ mol⁻¹, respectively. Additionally, it was demonstrated that Pt/Al₂O₃ and Au/Al₂O₃ had the highest kinetic constants for the formation of GCA, whilst Ag/Al₂O₃ had the highest constants for the production of glycolic acid. Regarding deactivation, only Pt/Al₂O₃ had considerable deactivation parameters (E_{ad} equal to 8.4 kJ mol⁻¹) indicating that it is the least stable in comparison to the other catalysts [196].

Furthermore, Ma et al. [204] explored the reaction mechanism of base-free oxidation of Gly using Pt supported by carbon nanotubes (Pt/CNTs) catalyst. Using a LHHW based model, two routes were modelled, namely the oxidation of Gly to GLCD and DHA in parallel. It was illustrated that the rate-determining step of both parallel reactions are the C–H bond cleavage with the assistance of an adsorbed intermediate (OH*). The E_a values for the formation of GLCD and DHA are 33.3 kJ mol⁻¹ and 44.9 kJ mol⁻¹, respectively. These values show that the formation of GLCD is favoured at lower temperatures [204]. In addition, Namdeo et al. [201] also extensively investigated the reaction mechanism and developed a LHHW based model assuming first-order reactions using a Pd catalyst supported on activated carbon. Deactivation of the catalyst

was also considered in the model, although the authors recommended that the model be further validated [201].

Regarding the catalytic conversion of Gly to lactic acid, a power-law model described the reaction in the presence of NaOH and a Ni_{0.3}/graphite catalyst [200]. Based on the model, the reaction order with respect to Gly and NaOH is 0.41 and 0.91, respectively, thus indicating that the concentration of NaOH has more effect on the reaction rate compared to Gly. Finally, the E_a of the overall reaction is 69.2 kJ mol⁻¹ [200]. Moreover, Wang et al. investigated the reaction in a Ca(OH)₂ aqueous solution in the presence of CuO(16)/CaO and Cu(16)/CaO catalysts. A power law model was developed in which the E_a on CuO(16)/CaO is higher (102.8 kJ mol⁻¹) compared to Cu(16)/CaO (22.2 kJ mol⁻¹). These values indicate that the active component Cu is much more efficient in catalysing the reaction [205]. In base-free conditions, Kano et al. explored the reaction mechanism in a continuous flow reactor in the presence of 0.5 wt% Pt/L-Nb₂O₅ which is a bifunctional (metal-acid) catalyst. A power law model was provided showing the E_a for rate of Gly consumption is 68.5 kJ mol⁻¹ [206]. Furthermore, through a combined power-law-ER-LHHW based model, the reaction mechanism of the same reaction was extensively explored in the presence of NaOH using copper nanoparticles (Cu NPs). The E_a value observed (81.4 kJ mol⁻¹) was lower than the 104.0 kJ mol⁻¹ obtained in the absence of catalyst [197].

In addition to catalytic reactions, Gly is commonly used as substrate in fermentation processes to produce organic acids. Coelho et al. [207] developed a kinetic model for the anaerobic fermentation of crude Gly to carboxylic acids. It was found that the formation of propionic, butyric, isovaleric, valeric and caproic acids can be described by exponential models (Cone and Fitzhugh models), while a sigmoidal model (Logistic

Table 13
Summary of the most relevant aspects of kinetic studies to obtain organic acids from glycerol.

Reaction and Catalyst	Reaction conditions ^a	(Best) X _{Gly} / Sel/ Yield ^b	Kinetic rate type and equation ^c	Kinetic parameters ^d	Notes	Ref.
Gly oxidation Catalyst: Pt/Al ₂ O ₃	T = 301–353 K P _{O2} = 0.5 MPa MR = 4:1 C _{gly,feed} = 0.3 mol L ⁻¹ Cat _{load} = 0.5 g t _{rxn} = 120 min ω = 1500 rpm	S _{GCA} = 77.4%	Power-law model: $r_{GCA} = k_1 C_{Gly} C_{NaOH} a$ $r_{TA} = k_2 C_{GCA} C_{NaOH} a$ $r_{GLCA+FA} = k_3 C_{Gly} C_{NaOH} a$ $r_{FA} = k_4 C_{Gly} C_{NaOH} a$ $r_{OA+FA} = k_5 C_{GCA} C_{NaOH} a$ Catalyst deactivation: $\frac{da}{dt} = -k_d a C_{NaOH}$	$E_{a1} = 72.0 \text{ kJ mol}^{-1}$ $E_{a2} = 52.0 \text{ kJ mol}^{-1}$ $E_{a3} = 75.2 \text{ kJ mol}^{-1}$ $E_{a4} = 46.0 \text{ kJ mol}^{-1}$ $E_{a5} = 54.0 \text{ kJ mol}^{-1}$ $E_{ad} = 8.4 \text{ kJ mol}^{-1}$ $\ln k_{01} = -1.87$ $\ln k_{02} = -3.35$ $\ln k_{03} = -3.71$ $\ln k_{04} = -5.98$ $\ln k_{05} = -4.31$ $\ln k_{0d} = -3.72$	Partial first order is assumed with respect to each reactant. Khang–Levenspiel model used to describe deactivation.	[196]
Gly oxidation Catalyst: Au/Al ₂ O ₃	T = 301–353 K P _{O2} = 0.5 MPa MR = 4:1 C _{gly,feed} = 0.3 mol L ⁻¹ Cat _{load} = 0.33 g t _{rxn} = 120 min ω = 1500 rpm	S _{GCA} = 65.7%	Power-law model: $r_{GCA} = k_1 C_{Gly} C_{NaOH} a$ $r_{TA} = k_2 C_{GCA} C_{NaOH} a$ $r_{GLCA+FA} = k_3 C_{Gly} C_{NaOH} a$ $r_{FA} = k_4 C_{Gly} C_{NaOH} a$ $r_{OA+FA} = k_5 C_{GCA} C_{NaOH} a$ Catalyst deactivation: $\frac{da}{dt} = -k_d a C_{NaOH}$	$E_{a1} = 34.0 \text{ kJ mol}^{-1}$ $E_{a2} = 103.0 \text{ kJ mol}^{-1}$ $E_{a3} = 15.3 \text{ kJ mol}^{-1}$ $E_{a4} = 44.0 \text{ kJ mol}^{-1}$ $E_{a5} = 40.8 \text{ kJ mol}^{-1}$ $E_{ad} = \text{not available}$ $\ln k_{01} = -2.59$ $\ln k_{02} = -5.75$ $\ln k_{03} = -3.22$ $\ln k_{04} = -6.32$ $\ln k_{05} = -6.19$ $\ln k_{0d} = \text{not available}$	Partial first order is assumed with respect to each reactant. Khang–Levenspiel model used to describe deactivation.	[196]
Gly oxidation Catalyst: Ag/Al ₂ O ₃	T = 301–353 K P _{O2} = 0.5 MPa MR = 4:1 C _{gly,feed} = 0.3 mol L ⁻¹ Cat _{load} = 0.35 g t _{rxn} = 120 min ω = 1500 rpm	S _{GCA} = 25.0%	Power-law model: $r_{GCA} = k_1 C_{Gly} C_{NaOH} a$ $r_{TA} = k_2 C_{GCA} C_{NaOH} a$ $r_{GLCA+FA} = k_3 C_{Gly} C_{NaOH} a$ $r_{FA} = k_4 C_{Gly} C_{NaOH} a$ $r_{OA+FA} = k_5 C_{GCA} C_{NaOH} a$ Catalyst deactivation: $\frac{da}{dt} = -k_d a C_{NaOH}$	$E_{a1} = 48.0 \text{ kJ mol}^{-1}$ $E_{a2} = \text{not available}$ $E_{a3} = 66.0 \text{ kJ mol}^{-1}$ $E_{a4} = 97.0 \text{ kJ mol}^{-1}$ $E_{a5} = \text{not available}$ $E_{ad} = \text{not available}$ $\ln k_{01} = -6.20$ $\ln k_{02} = \text{not available}$ $\ln k_{03} = -5.29$ $\ln k_{04} = -7.48$ $\ln k_{05} = \text{not available}$ $\ln k_{0d} = -5.07$	Partial first order is assumed with respect to each reactant. Khang–Levenspiel model used to describe deactivation.	[196]
Gly conversion to Lactic acid Catalyst: Cu NPs	T = 483–518 K MR = 0.25:1–3:1 C _{gly,feed} = 0.27–2.06 mol L ⁻¹ Cat _{load} = 0.26–160.0 mol _{Gly} ⁻¹ mol _{Cu} ⁻¹ t _{rxn} = 480 min ω = 1000 rpm	S _{LA} = 83.5%	Combined power-law-ER-LH: $r_{LA} = k_1 C_{Gly} C_{HO}^- + \frac{m_{cat} k_{s1} K_{a,Gly} C_{Gly} C_{HO}^-}{1 + K_{a,Gly} C_{Gly} + K_{a,1.2 PDO} C_{1.2 PDO}}$ $r_{diglycerol} = k_2 C_{Gly}^2 C_{HO}^-$ $r_{Gly} = k_3 C_{diglycerol} C_{HO}^-$ $r_{ACA} = k_4 C_{LA}^n C_{HO}^-$ $r_{1.2-PDO} = k_5 C_{Gly} C_{HO}^- + \frac{m_{cat} k_{s2} K_{a,Gly} C_{Gly} C_{HO}^-}{1 + K_{a,Gly} C_{Gly} + K_{a,1.2 PDO} C_{1.2 PDO}}$ $r_{LA} = \frac{m_{cat} k_{s3} K_{a,1.2 PDO} C_{1.2 PDO} C_{HO}^-}{1 + K_{a,Gly} C_{Gly} + K_{a,1.2 PDO} C_{1.2 PDO}}$	Without Cu NPs (NaOH only) $E_{a1} = 104 \text{ kJ mol}^{-1}$ $E_{a2} = 122 \text{ kJ mol}^{-1}$ $E_{a3} = 95.4 \text{ kJ mol}^{-1}$ $E_{a4} = 123 \text{ kJ mol}^{-1}$ $E_{a5} = 109 \text{ kJ mol}^{-1}$ $E_{a6} = 94.6 \text{ kJ mol}^{-1}$ $E_{a7} = 100 \text{ kJ mol}^{-1}$ $k_{01} = 2.13 \times 10^7 \text{ mol min}^{-1}$ $k_{02} = 1.86 \times 10^8 \text{ mol min}^{-1}$ $k_{03} = 2.53 \times 10^5 \text{ mol min}^{-1}$ $k_{04} = 2.16 \times 10^9 \text{ mol min}^{-1}$	Comprehensive reaction mechanism and model.	[197]

(continued on next page)

Table 13 (continued)

Reaction and Catalyst	Reaction conditions ^a	(Best) X _{Gly} / Sel/ Yield ^b	Kinetic rate type and equation ^c	Kinetic parameters ^d	Notes	Ref.
			$r_{\text{byproducts}} = k_6 C_{1,2 \text{ PDO}} C_{\text{HO}}$ $r_{\text{byproducts}} = k_7 C_{\text{Gly}} C_{\text{HO}}$	$k_{05} = 7.04 \times 10^6 \text{ mol min}^{-1}$ $k_{06} = 1.33 \times 10^5 \text{ mol min}^{-1}$ $k_{07} = 7.42 \times 10^6 \text{ mol min}^{-1}$		
				<p><i>Cu NPs with NaOH</i></p> $E_{as1} = 81.4 \text{ kJ mol}^{-1}$ $E_{as2} = 102 \text{ kJ mol}^{-1}$ $E_{as3} = 89.9 \text{ kJ mol}^{-1}$ $k_{0s1} = 5.05 \times 10^8 \text{ mol g}_{\text{cat}}^{-1} \text{ min}^{-1}$ $k_{0s2} = 6.21 \times 10^9 \text{ mol g}_{\text{cat}}^{-1} \text{ min}^{-1}$ $k_{0s3} = 2.77 \times 10^2 \text{ mol g}_{\text{cat}}^{-1} \text{ min}^{-1}$		
				<p><i>Adsorption constants</i></p> $E_{a-K_{a,Gly}} = 65.4 \text{ kJ mol}^{-1}$ $E_{a-K_{a,1,2 \text{ PDO}}} = 52.6 \text{ kJ mol}^{-1}$ $k_{0-K_{a,Gly}} = 1.33 \times 10^{-9} \text{ L mol}^{-1}$ $k_{0-K_{a,1,2 \text{ PDO}}} = 7.67 \times 10^{-9} \text{ L mol}^{-1}$		
Gly conversion to Lactic acid Catalyst: Ni _{0.3} /graphite	T = 413–443 K C _{gly,feed} = 1 mol L ⁻¹ C _{NaOH} = 1.1 mol L ⁻¹ Cat _{load} = 0.552 g t _{rxn} = 60 min ω = 500 rpm	S _{LA} = 92.2%	<p>Power law:</p> $-r_{\text{Gly}} = k C_{\text{Gly}}^m C_{\text{NaOH}}^n$	$m = 0.41$ $n = 0.91$ $E_a = 69.2 \text{ kJ mol}^{-1}$ $k_0 = 4.5 \times 10^6 \text{ mol}^{1-(a+b)} \text{ g}_{\text{cat}}^{(a+b)-1} \text{ h}^{-1}$	none	[200]
				$E_1/R = -8632$ $E_2/R = -4210$ $E_3/R = -9551$ $E_4/R = -3274$ $E_5/R = -8532$ $\ln k_{01} = 24.34$ $\ln k_{02} = 11.17$ $\ln k_{03} = 25.79$ $\ln k_{04} = 8.79$ $\ln k_{05} = 24.14$	First-order kinetics is assumed for all reaction steps.	[201]
Gly oxidation Catalyst: Pd/Activated carbon	T = 318–348 K P _{O2} = 0.3–1.0 MPa MR = 1:1–4:1 C _{gly,feed} = 0.6 mol L ⁻¹ Cat _{load} = 1000 mol% Gly/mol% metal t _{rxn} = 240 min ω = 800 rpm	S _{GCA} ≈ 45.0%	<p>LHHW:</p> $r_{\text{GCA}} = \frac{k_1 C_{\text{Gly}} - k_2 C_{\text{GCA}}}{1 + K_{a,\text{gly}} C_{\text{GLY}} + K_{a,\text{TA}} C_{\text{TA}} + K_{a,\text{OA}} C_{\text{OA}}}$ $r_{\text{TA}} = \frac{k_2 C_{\text{GCA}}}{1 + K_{a,\text{gly}} C_{\text{GLY}} + K_{a,\text{TA}} C_{\text{TA}} + K_{a,\text{OA}} C_{\text{OA}}}$ $r_{\text{GLCA}} = \frac{k_3 C_{\text{Gly}} - k_4 C_{\text{GLCA}}}{1 + K_{a,\text{gly}} C_{\text{GLY}} + K_{a,\text{TA}} C_{\text{TA}} + K_{a,\text{OA}} C_{\text{OA}}}$ $r_{\text{FA}} = \frac{k_3 C_{\text{Gly}}}{1 + K_{a,\text{gly}} C_{\text{GLY}} + K_{a,\text{TA}} C_{\text{TA}} + K_{a,\text{OA}} C_{\text{OA}}}$ $r_{\text{OA}} = \frac{k_4 C_{\text{GLCA}}}{1 + K_{a,\text{gly}} C_{\text{GLY}} + K_{a,\text{TA}} C_{\text{TA}} + K_{a,\text{OA}} C_{\text{OA}}}$ $r_{\text{CO}_2} = \frac{3k_5 C_{\text{Gly}}}{1 + K_{a,\text{gly}} C_{\text{GLY}} + K_{a,\text{TA}} C_{\text{TA}} + K_{a,\text{OA}} C_{\text{OA}}}$ $r_{\text{Gly}} = \frac{-(k_1 + k_3 + k_5) C_{\text{Gly}}}{1 + K_{a,\text{gly}} C_{\text{GLY}} + K_{a,\text{TA}} C_{\text{TA}} + K_{a,\text{OA}} C_{\text{OA}}}$	<p>Adsorption parameters</p> $\Delta H_{a,\text{gly}}/R = 3037$ $\Delta H_{a,\text{TA}}/R = 12452$ $\Delta H_{a,\text{OA}}/R = \text{not available}$ $\ln k_{0-K_{a,\text{gly}}} = -5.6$ $\ln k_{0-K_{a,\text{TA}}} = -30.44$ $\ln k_{0-K_{a,\text{OA}}} = \text{not available}$		
Gly oxidation Catalyst: Pt/CNTs	T = 313–343 K P _{O2} * = 0.008–0.01 MPa MR = not available C _{gly,feed} * = 2.46–13.5% Cat _{load} = 4000 mol% Gly/mol% metal t _{rxn} = 120 min ω = 700 rpm	Y _{GLCD} = 11%*	<p>LHHW:</p> $r_{\text{GLCD}+\text{GCA}} = \frac{\theta_7 C_{\text{Gly}} P_{\text{O}_2}^{0.5}}{\left(\theta_4 C_{\text{GLY}} + \theta_1 + \theta_2 P_{\text{O}_2} + \theta_3 P_{\text{O}_2}^{0.25} + \theta_5 C_{\text{Gly}} P_{\text{O}_2}^{0.25} + 1\right)^2}$ $r_{\text{DHA}} = \frac{\theta_8 C_{\text{Gly}} P_{\text{O}_2}^{0.5}}{\left(\theta_4 C_{\text{GLY}} + \theta_1 + \theta_2 P_{\text{O}_2} + \theta_3 P_{\text{O}_2}^{0.25} + \theta_5 C_{\text{Gly}} P_{\text{O}_2}^{0.25} + 1\right)^2}$	$E_{a7} = 33.3 \text{ kJ mol}^{-1}$ $E_{a8} = 44.9 \text{ kJ mol}^{-1}$	Base-free oxidation. Tested two models that considered different r.d.s.	[204]
				<p>Values of merged kinetic parameters ($\theta_1, \theta_2, \theta_3, \theta_4, \theta_5, \theta_7, \theta_8$) provided at different temperatures (313–343 K).</p>		

(continued on next page)

Table 13 (continued)

Reaction and Catalyst	Reaction conditions ^a	(Best) X _{Gly} / Sel/ Yield ^b	Kinetic rate type and equation ^c	Kinetic parameters ^d	Notes	Ref.
Gly conversion to Lactic acid Catalyst: Cu(16)/CaO	T = 473–503 K C _{gly_feed} = 0.5–2.0 mol L ⁻¹ C _{Ca(OH)2} = 0.8–2.0 mol L ⁻¹ Cat _{load} = 0.46–3.68 g t _{rxn} = 30 min ω = 500 rpm T = 473–503 K	S _{LA} = 97%	Power law: – r _{Gly} = km _{cat} ^{0.22} C _{Gly} ^{0.86} C _{Ca(OH)2} ^{0.85}	E _a = 22.2 kJ mol ⁻¹ k ₀ = 197.7 mol ^{-0.71} L ^{0.71} g _{cat} ^{-0.22}	Reaction proceeds in a Ca(OH) ₂ aqueous solution.	[205]
Gly conversion to Lactic acid Catalyst: CuO (16)/CaO	T = 473–503 K C _{gly_feed} = 0.5–2.0 mol L ⁻¹ C _{Ca(OH)2} = 0.8–2.0 mol L ⁻¹ Cat _{load} = 0.46–3.68 g t _{rxn} = 30 min ω = 500 rpm T = 473–503 K	S _{LA} = 94.4%	Power law: – r _{Gly} = km _{cat} ^{0.26} C _{Gly} ^{0.72} C _{Ca(OH)2} ^{1.38}	E _a = 102.8 kJ mol ⁻¹ k ₀ = 2.17 × 10 ¹⁰ mol ^{-1.1} L ^{1.1} g _{cat} ^{-0.26}	Reaction proceeds in a Ca(OH) ₂ aqueous solution.	[205]
Gly conversion to Lactic acid Catalyst: 0.5 wt% Pt/L-Nb ₂ O ₅	T = 393–423 K P _{O2} = 0.025–0.5 MPa C _{gly_feed} = 0.1–0.4 mol L ⁻¹ Cat _{load} = 200 mg t _{rxn} = 300 min ω = not available	S _{LA} = 80%	Power law: – r _{Gly} = kC _{Gly} ^{0.62} P _{O2} ^{0.73}	E _a = 68.5 kJ mol ⁻¹ k ₀ = not available	Base-free conditions.	[206]

^a Reaction conditions used for kinetic studies. Temperature (*T*), oxygen partial pressure (*P*_{O₂}), NaOH to Gly molar ratio (MR), Gly feed concentration (*C*_{gly_feed}), NaOH concentration (*C*_{NaOH}), catalyst loading (*Cat*_{load}), stirring speed (*ω*), reaction time (*t*_{rxn}). *calculated from data provided by study.

^b Best Gly conversion (*X*_{Gly}), selectivity (*S*) or yield (*Y*) with respect to glyceric acid (*GCA*) or lactic acid (*LA*) or glyceraldehyde (*GLCD*), achieved at optimum operating conditions which are different than the reaction conditions^a for kinetic study presented in the table. *calculated from concentration graphs presented by study.

^c Rate of reaction (*r*_{*i*}), reaction rate constant (*k*_{*j*}), deactivation rate constant (*k*_{*d*}), component adsorption equilibrium constant (*K*_{*a,i*}), concentration (*C*_{*i*}), mass of catalyst (*m*_{cat}), catalyst activity (*a*), component reaction order (*m*) and (*n*), merged kinetic parameters defined in referenced article (*θ*_{*j*}). *i*: components, *j*=reactions. Subscript *GCA* = glyceric acid, *TA* = tartronic acid, *GLCA*=glycolic acid, *FA*= formic acid, *OA* = oxalic acid, *LA* = Lactic acid, *GLCD* = glyceraldehyde, *AcA* = acetic acid, 1, 2 – *PDO* = 1,2-propanediol, *DHA* = dihydroxyacetone.

^d Activation energy (*E*_{*a,j*}), pre-exponential factor (*k*_{*0,j*}), enthalpy of component adsorption constant (*ΔH*_{*a,i*}), pre-exponential factor of component adsorption constant (*k*₀·*K*_{*a,i*}), activation energy of component adsorption constant (*E*_{*a*}·*K*_{*a,i*}), ideal gas constant (*R*), component reaction order (*m*) and (*n*), merged kinetic parameters defined in referenced article (*θ*_{*j*}). *i*: components, *j*=reactions.

model) better describes ACA formation. Another work focused on illustrating the cell growth in the fermentation of Gly to succinic acid using the *Yarrowia lipolytica* yeast, which can be explained with a Monod model, while the Luedeking–Piret model was implemented to describe the generation of products [208].

5. Conclusions and perspective

As years have gone by and biodiesel production has become an established process in industry, the concomitant generation of massive amounts of glycerol as by-product has affected its prices. The subsequent supply shock has exceeded the volume of this commodity required by its traditional applications. As a consequence, industrial and academic researchers have paid increasing attention to its conversion to value-added products attempting to enhance the overall profitability of the process.

At this stage, hundreds of works have focused on the synthesis of different products, the predominant being glycerol carbonate, glycerol acetals, esters, ethers, propanediols, Acr, halogenated products, organic acids and hydrogen. With the exception of the halogenated products, these compounds are considered green chemicals, showing high biodegradability and low toxicity [209]. For this reason, they have found applications as (bio)fuel additives or as part of the formulation of foods, cosmetics, and other consumer goods similarly to glycerol in itself.

Although many review articles have been published especially in the last decade, many of them have compiled and described thoroughly the reaction conditions and catalysts used in the transformation of glycerol, sometimes with some specific products as target, as presented in the supplementary information of this work. In comparison, the insights into reaction kinetic models and the thermodynamics of the reactions have been paid little attention to in previous reviews. Here, in the sections dedicated to each product, we present the thermodynamic information of the reactions, when available, concluding on their *endo*- or *exothermicity* and spontaneity. In addition, a very comprehensive survey of reaction conditions, catalysts used and their performance for glycerol conversion. In addition, the models developed by different authors to describe the evolution of the corresponding reactions are explained in detailed, including the equations on which they are based with explanations on their assumptions as well as the parameters. All of this information is of great value for prospective process design and subsequent techno-economic analyses [210] to be followed up with sustainability and life cycle assessments to evaluate industrial implementation [211].

For all of the reactions described here, the development of catalytic materials is of paramount importance, not only to improve their activity, but also their recyclability. However, aside from the ever-growing study of catalysts, some of the cases studied here point in the direction of the relevance of devise strategies to enhance the productivity of the reactions with an eye on process intensification. Examples have been provided throughout this work, mainly regarding alternative ways of mixing (mainly ultrasound), hybrid operations (e.g. reactive pervaporation, reactive distillation) and the use of microwave to provide energy. Concerning the latter, the development of microwave responsive catalysts [212] could help reduce the energy inputs and appears as an interesting path to explore, particularly for high-temperature demanding reactions like glycerol reforming.

One last aspect that is worthwhile mentioning is that, only with a few exceptions, in the vast majority the studies analysed in this review, the substrate used was high purity glycerol as a model system. The purification of glycerol from biodiesel production processes can be cumbersome and features a series of steps that can make the process economically challenging, but the use of such substrate is industrially very relevant. For this reason, it is of great importance that kinetic studies starting from crude glycerol or partly purified glycerol follow the studies already covered in this work. This opens the door to studies on the deactivation of catalysts to be included in kinetic models that make more realistic assumptions for potential implementation. In these

regards, *operando* measurements using different types of spectroscopic techniques are key to reach a more thorough understanding not only of reaction mechanisms, but also of the deactivation of molecular [213] and heterogeneous catalysts [214]. The studies covered here monitor the chemical evolution of the corresponding reaction systems with-drawing samples and mostly analysing by means of chromatographic techniques and the analysis of the deactivation of the catalyst is mostly ignored. In some cases, assumptions on the deactivation have been implemented in kinetic models, but these have been mostly as a resort to obtain good fittings of the model to the data than based on observations of catalytic deactivation mechanisms.

Nomenclature

Abbreviations

APR	Aqueous phase reforming
CALB	<i>Candida antarctica</i> lipase B
CFD	Computational fluid dynamics
CSTRs	Continuous stirred tank reactors
DES	Deep eutectic solvents
ER	Eley-Rideal
GSR	Glycerol steam reforming
HTCW	High temperature compressed water
IER	Ion exchange resin
LHHW	Langmuir-Hinshelwood-Hougen-Watson model
LLE	Liquid-liquid equilibria
MR	Molar ratio of reactants (–)
PH	Pseudo homogeneous
PL	Power-law
r.d.s	Rate determining step/rate controlling step
UCST	Upper critical solution temperature
USIRW	Ultrasonic-infrared-wave reactor
WGS	Water-gas shift reaction

Chemicals

1,2-PDO	1,2-propanediol
1,3-PDO	1,3-propanediol
Ac	Acetone
ACA	Acetic acid
Acr	Acrolein
BC	1,2-butylene carbonate
DCA	Dichloroacetic acid
DCH	Dichlorohydrin
DE	Diether
DEC	diethyl carbonate
DG	Diglyceride
DHA	Dihydroxyacetone
DMC	Dimethyl carbonate
EC	Ethylene carbonate
EG	Ethylene glycol
FA	Formic acid
FAME	Fatty acid methyl ester
GC	Glycerol carbonate
GCA	Glyceric acid
GLCA	Glycolic acid
GLCD	Glyceraldehyde
Gly	Glycerol
HA	Hydroxyacetone
HAH	Partial hydrogenated hydroxyacetone
HPA	3-hydroxypropionaldehyde
INT	Intermediates
LA	Lactic acid
MA	Mesoxalic acid
MCH	Monochlorohydrins

ME	Monoether
MEA	monoethanolamine
MG	Monoglyceride
NaOH	Sodium Hydroxide
OA	Oxalic acid
OC	Organic carbonate
PC	1,2-propylene carbonate
PO	Propanol
PTSA	<i>p</i> -toluene sulfonic acid
ROH	Alcohols
Slk	Solketal
TA	Tartonic acid
TCA	Trichloroacetic acid
TE	Triether
TG	Triglyceride
Tol	Toluene
U	Urea

Symbols

Latin

<i>a</i>	activity (–)
C_{acid_feed}	Acid concentration in the feed (mol L ⁻¹)
C_{cat}	Concentration of catalyst (mol L ⁻¹)
C_{FS}	Concentration of catalyst free active sites (mol L ⁻¹)
C_{gly_feed}	Gly feed concentration (mol L ⁻¹)
$C_{H_2O_2_feed}$	H ₂ O ₂ feed concentration
C_i	Concentration of component <i>i</i> (mol L ⁻¹)
$C_{i,0}$	Initial concentration of component <i>i</i> (mol L ⁻¹)
C_{NaOH}	NaOH concentration
C_{ROH_feed}	Alcohol feed concentration (mol L ⁻¹)
C_{TS}	Concentration of total active sites (mol L ⁻¹)
C_{Total}	Total molar concentration (mol L ⁻¹)
Ca_{load}	Catalyst loading (variable units)
E_a	Activation energy (kJ mol ⁻¹)
F_0	Molar flow rate (mol h ⁻¹)
<i>h</i>	height (m)
H_i	Henry's constant (–)
k_0	Pre-exponential factor (variable units)
k_d	Deactivation rate constant (variable units)
k_j	Forward reaction rate constant for reaction <i>j</i> (variable units)
k_{-j}	Backward reaction rate constant for reaction <i>j</i> (variable units)
$K_{a,i}$	Component adsorption equilibrium constant (variable units)
$K_{des,i}$	Component desorption equilibrium constant (variable units)
K_{eq}	Overall reaction equilibrium constant (–)
<i>m</i>	Component reaction order (–)
m_{cat}	Mass of catalyst (g)
<i>MR</i>	Molar ratio of reactants (–)
MR_0	Initial molar ratio (–)
<i>n</i>	Component reaction order (–)
<i>P</i>	Pressure (bar)
P_i	Partial pressure of component <i>i</i>
<i>r</i>	Rate of reaction (variable units)
<i>R</i>	Ideal gas constant (J mol ⁻¹ K ⁻¹)
<i>S</i>	Selectivity (%)
<i>t</i>	Time (variable units)
t_{rxn}	Reaction time (min)
<i>T</i>	Temperature (K)
<i>V</i>	Volume (m ³)
V_{cat}/F	Contact time (varied units)
<i>VR</i>	Volume ratio
<i>w</i>	Catalyst loading unless state otherwise (variable units)
W/F	Contact time (variable units)
<i>WHSV</i>	Weight hourly space velocity (h ⁻¹)
x_i	Molar fraction of component <i>i</i> (–)

<i>X</i>	Conversion (%)
<i>Y</i>	Yield (%)

Greek

ΔG	Gibb's free energy (kJ mol ⁻¹)
ΔH	Enthalpy (kJ mol ⁻¹)
$\Delta H_{a,i}/\Delta H_{des,i}$	Enthalpy of component <i>i</i> adsorption/desorption constant (kJ mol ⁻¹)
ΔS	Entropy (J K ⁻¹ mol ⁻¹)
$\Delta S_{a,i}/\Delta S_{des,i}$	Entropy of component <i>i</i> adsorption/desorption constant (J K ⁻¹ mol ⁻¹)
κ	Material ratio
δ_{Gly}	Expansion factor
τ	Residence time (s)
ψ	Catalyst modulus
ω	Stirring speed (rpm)
$\theta', \theta_{ji}, \theta_i, \theta_j, \gamma', \delta'$	Merged parameters in which definition differs between articles

Subscripts

<i>a</i>	Refers to adsorption
<i>Cat</i>	Catalyst
<i>des</i>	Refers to desorption
<i>f</i>	Refers to formation
<i>FS</i>	Related to the free active sites concentration
<i>i</i>	Refers to a component <i>i</i>
<i>j</i>	Refers to a reaction <i>j</i>
<i>TS</i>	Related to the total active sites concentration
<i>rxn</i>	Refers to reaction

Superscripts

°	Refers to standard conditions
‡	Refers to activation

CRedit authorship contribution statement

Aya Sandid: Conceptualization, Data curation, Formal analysis, Investigation, Methodology, Visualization, Writing – original draft, Writing – review & editing. **Vincenzo Spallina:** Funding acquisition, Project administration, Resources, Supervision, Validation, Writing – review & editing. **Jesús Esteban:** Conceptualization, Data curation, Formal analysis, Funding acquisition, Investigation, Methodology, Project administration, Resources, Supervision, Validation, Visualization, Writing – original draft, Writing – review & editing.

Declaration of Competing Interest

The authors declare that they have no known competing financial interests or personal relationships that could have appeared to influence the work reported in this paper.

Data availability

This is a review article. All the information consulted for this work is available in the open literature.

Acknowledgments

The University of Manchester is acknowledged for funding of a PhD scholarship for AS. VS would like to acknowledge the financial support from the UKRI-EPSC SPACING project, EP/V026089/1 and the European Union's Horizon 2020 research and innovation programme for finding GLAMOUR project under grant agreement No 884197.

This work is dedicated to the memory of Carmelo Esteban, with whom the corresponding author had many discussions throughout the

years about the use of glycerol and modelling of its reactions as the topic of his PhD thesis.

Appendix A. Supplementary data

Supplementary data to this article can be found online at <https://doi.org/10.1016/j.fuproc.2023.108008>.

References

- [1] BP, BP Energy Outlook, 2023 edition, 2023.
- [2] International Energy Agency, Global Energy Review: CO2 Emissions in 2021 Global Emissions Rebound Sharply to Highest Ever Level, 2022.
- [3] International Energy Agency, World Energy Investment 2023, 2023.
- [4] A.P. Saravanan, T. Mathimani, G. Deviram, K. Rajendran, A. Pugazhendhi, Biofuel policy in India: a review of policy barriers in sustainable marketing of biofuel, *J. Clean. Prod.* 193 (2018) 734–747, <https://doi.org/10.1016/j.jclepro.2018.05.033>.
- [5] J. Withers, H. Quesada, R.L. Smith, Bioeconomy survey results regarding barriers to the United States advanced biofuel industry, *BioResources* 12 (2) (2017) 2846–2863, <https://doi.org/10.15376/biores.12.2.2846-2863>.
- [6] J.A. McMahon, M.N. Cardwell, *Research Handbook on EU Agriculture Law*, Edward Elgar Publishing, 2015.
- [7] G. Sorda, M. Banse, C. Kemfert, An overview of biofuel policies across the world, *Energy Policy* 38 (11) (2010) 6977–6988, <https://doi.org/10.1016/j.enpol.2010.06.066>.
- [8] A.P. Saravanan, A. Pugazhendhi, T. Mathimani, A comprehensive assessment of biofuel policies in the BRICS nations: implementation, blending target and gaps, *Fuel* 272 (2020), 117635, <https://doi.org/10.1016/j.fuel.2020.117635>.
- [9] R.N. Acharya, R. Perez-Pena, Role of comparative advantage in biofuel policy adoption in Latin America, *Sustainability* 12 (4) (2020), <https://doi.org/10.3390/su12041411>.
- [10] P. Lamers, C. Hamelinck, M. Junginger, A. Faaij, International bioenergy trade—a review of past developments in the liquid biofuel market, *Renew. Sust. Energ. Rev.* 15 (6) (2011) 2655–2676, <https://doi.org/10.1016/j.rser.2011.01.022>.
- [11] M. Lisowij, M.M. Wright, A review of biogas and an assessment of its economic impact and future role as a renewable energy source, *Rev. Chem. Eng.* 36 (3) (2020) 401–421, <https://doi.org/10.1515/revce-2017-0103>.
- [12] S. Achinas, V. Achinas, G.J.W. Euverink, A technological overview of biogas production from biowaste, *Engineering* 3 (3) (2017) 299–307, <https://doi.org/10.1016/J.ENG.2017.03.002>.
- [13] H.B. Aditiya, T.M.I. Mahlia, W.T. Chong, H. Nur, A.H. Sebayang, Second generation bioethanol production: a critical review, *Renew. Sust. Energ. Rev.* 66 (2016) 631–653, <https://doi.org/10.1016/j.rser.2016.07.015>.
- [14] A.R. Sirajunnisa, D. Surendhiran, Algae – a quintessential and positive resource of bioethanol production: a comprehensive review, *Renew. Sust. Energ. Rev.* 66 (2016) 248–267, <https://doi.org/10.1016/j.rser.2016.07.024>.
- [15] M. Rouhany, H. Montgomery, *Global biodiesel production: The state of the art and impact on climate change*, in: M. Tabatabaei, M. Aghbashlo (Eds.), *Biodiesel: From Production to Combustion*, Springer International Publishing, Cham, 2019, pp. 1–14.
- [16] REN21, *Renewables 2020 global status report* (Paris: REN21 Secretariat). REN21-Renewable energy policy network for the 21st century. https://www.ren21.net/wp-content/uploads/2019/05/grs_2020_full_report_en.pdf, 2020.
- [17] OECD/FAO, *Agricultural Outlook 2018–2027: BIOFUEL - OECD-FAO Agricultural Outlook 2018–2027*, Available at, https://stats.oecd.org/Index.aspx?DataSetCode=HIGH_AGLINK 2016, 2018. Retrieved 24 July 2020.
- [18] D. Singh, D. Sharma, S.L. Soni, S. Sharma, P. Kumar Sharma, A. Jhalani, A review on feedstocks, production processes, and yield for different generations of biodiesel, *Fuel* 262 (2020), 116553, <https://doi.org/10.1016/j.fuel.2019.116553>.
- [19] M.S. Ardi, M.K. Aroua, N.A. Hashim, Progress, prospect and challenges in glycerol purification process: a review, *Renew. Sust. Energ. Rev.* 42 (2015) 1164–1173, <https://doi.org/10.1016/j.rser.2014.10.091>.
- [20] T. Attarbachi, M.D. Kingsley, V. Spallina, New trends on crude glycerol purification: a review, *Fuel* 340 (2023), 127485, <https://doi.org/10.1016/j.fuel.2023.127485>.
- [21] C.A.G. Quispe, C.J.R. Coronado, J.A. Carvalho Jr., Glycerol: production, consumption, prices, characterization and new trends in combustion, *Renew. Sust. Energ. Rev.* 27 (2013) 475–493, <https://doi.org/10.1016/j.rser.2013.06.017>.
- [22] P.S. Kong, M.K. Aroua, W. Daud, H.V. Lee, P. Cognet, Y. Peres, Catalytic role of solid acid catalysts in glycerol acetylation for the production of bio-additives: a review, *RSC Adv.* 6 (73) (2016) 68885–68905, <https://doi.org/10.1039/c6ra10686b>.
- [23] S.A.N.M. Rahim, C.S. Lee, F. Abnisa, M.K. Aroua, W.A.W. Daud, P. Cognet, Y. Pères, A review of recent developments on kinetics parameters for glycerol electrochemical conversion – a by-product of biodiesel, *Sci. Total Environ.* 705 (2020), 135137, <https://doi.org/10.1016/j.scitotenv.2019.135137>.
- [24] M. Pagliaro, M. Rossi, Chapter 1 Glycerol: Properties and production, in: *The Future of Glycerol: New Usages for a Versatile Raw Material*, The Royal Society of Chemistry, 2008, pp. 1–17.
- [25] A. Behr, J. Eilting, K. Irawadi, J. Leschinski, F. Lindner, Improved utilisation of renewable resources: new important derivatives of glycerol, *Green Chem.* 10 (1) (2008) 13–30, <https://doi.org/10.1039/B710561D>.
- [26] C.-H. Zhou, J.N. Beltrami, Y.-X. Fan, G.Q. Lu, Chemoselective catalytic conversion of glycerol as a biorenewable source to valuable commodity chemicals, *Chem. Soc. Rev.* 37 (3) (2008) 527–549, <https://doi.org/10.1039/B707343G>.
- [27] N. Rahmat, A.Z. Abdullah, A.R. Mohamed, Recent progress on innovative and potential technologies for glycerol transformation into fuel additives: a critical review, *Renew. Sust. Energ. Rev.* 14 (3) (2010) 987–1000, <https://doi.org/10.1016/j.rser.2009.11.010>.
- [28] M. Ayoub, A.Z. Abdullah, Critical review on the current scenario and significance of crude glycerol resulting from biodiesel industry towards more sustainable renewable energy industry, *Renew. Sust. Energ. Rev.* 16 (5) (2012) 2671–2686, <https://doi.org/10.1016/j.rser.2012.01.054>.
- [29] H.W. Tan, A.R. Abdul Aziz, M.K. Aroua, Glycerol production and its applications as a raw material: a review, *Renew. Sust. Energ. Rev.* 27 (2013) 118–127, <https://doi.org/10.1016/j.rser.2013.06.035>.
- [30] R. Ciriminna, C.D. Pina, M. Rossi, M. Pagliaro, Understanding the glycerol market, *Eur. J. Lipid Sci. Technol.* 116 (10) (2014) 1432–1439, <https://doi.org/10.1002/ejlt.201400229>.
- [31] J.I. García, H. García-Marín, E. Pires, Glycerol based solvents: synthesis, properties and applications, *Green Chem.* 16 (3) (2014) 1007–1033, <https://doi.org/10.1039/C3GC41857J>.
- [32] Z. Gholami, A.Z. Abdullah, K.-T. Lee, Dealing with the surplus of glycerol production from biodiesel industry through catalytic upgrading to polyglycerols and other value-added products, *Renew. Sust. Energ. Rev.* 39 (2014) 327–341, <https://doi.org/10.1016/j.rser.2014.07.092>.
- [33] P.S. Kong, M.K. Aroua, W.M.A.W. Daud, Conversion of crude and pure glycerol into derivatives: a feasibility evaluation, *Renew. Sust. Energ. Rev.* 63 (2016) 533–555, <https://doi.org/10.1016/j.rser.2016.05.054>.
- [34] X. Luo, X. Ge, S. Cui, Y. Li, Value-added processing of crude glycerol into chemicals and polymers, *Bioresour. Technol.* 215 (2016) 144–154, <https://doi.org/10.1016/j.biortech.2016.03.042>.
- [35] N. Vivek, R. Sindhu, A. Madhavan, A.J. Anju, E. Castro, V. Faraco, A. Pandey, P. Binod, Recent advances in the production of value added chemicals and lipids utilizing biodiesel industry generated crude glycerol as a substrate – Metabolic aspects, challenges and possibilities: an overview, *Bioresour. Technol.* 239 (2017) 507–517, <https://doi.org/10.1016/j.biortech.2017.05.056>.
- [36] A. Almena, L. Bueno, M. Díez, M. Martín, Integrated biodiesel facilities: review of glycerol-based production of fuels and chemicals, *Clean Technol. Environ. Policy* 20 (7) (2018) 1639–1661, <https://doi.org/10.1007/s10098-017-1424-z>.
- [37] C. Len, F. Delbecq, C. Cara Corpas, E. Ruiz Ramos, Continuous flow conversion of glycerol into chemicals: an overview, *Synthesis* 50 (04) (2018) 723–741, <https://doi.org/10.1055/s-0036-1591857>.
- [38] U.I. Nda-Umar, I. Ramli, Y.H. Taufiq-Yap, E.N. Muhamad, An overview of recent research in the conversion of glycerol into biofuels, fuel additives and other bio-based chemicals, *Catalysts* 9 (1) (2019), <https://doi.org/10.3390/catal9010015>.
- [39] M. Anitha, S.K. Kamarudin, N.T. Kofli, The potential of glycerol as a value-added commodity, *Chem. Eng. J.* 295 (2016) 119–130, <https://doi.org/10.1016/j.cej.2016.03.012>.
- [40] M. Checa, S. Nogales-Delgado, V. Montes, J.M. Encinar, Recent advances in glycerol catalytic valorization: a review, *Catalysts* 10 (11) (2020), <https://doi.org/10.3390/catal10111279>.
- [41] N. Tabassum, R. Pothu, A. Pattnaik, R. Boddula, P. Balla, R. Gundeyoyina, P. Challa, R. Rajesh, V. Perugopu, N. Mameda, A.B. Radwan, A.M. Abdullah, N. Al-Qahtani, Heterogeneous catalysts for conversion of biodiesel-waste glycerol into high-added-value chemicals, *Catalysts* 12 (7) (2022) 767, <https://doi.org/10.3390/catal12070767>.
- [42] R. Sedghi, H. Shahbeik, H. Rastegari, S. Rafiee, W. Peng, A.-S. Nizami, V.K. Gupta, W.-H. Chen, S.S. Lam, J. Pan, M. Tabatabaei, M. Aghbashlo, Turning biodiesel glycerol into oxygenated fuel additives and their effects on the behavior of internal combustion engines: a comprehensive systematic review, *Renew. Sust. Energ. Rev.* 167 (2022), 112805, <https://doi.org/10.1016/j.rser.2022.112805>.
- [43] P. Koranian, Q. Huang, A.K. Dalai, R. Sammynaiken, Chemicals production from glycerol through heterogeneous catalysis: a review, *Catalysts* 12 (8) (2022) 897, <https://doi.org/10.3390/catal12080897>.
- [44] A.A. Farias da Costa, A. de Nazaré de Oliveira, R. Esposito, A. Auvigne, C. Len, R. Luque, R.C. Rodrigues Noronha, L.A. Santos do Nascimento, Glycerol and microwave-assisted catalysis: recent progress in batch and flow devices, *Sustain. Energy Fuel* 7 (8) (2023) 1768–1792, <https://doi.org/10.1039/D2SE01647H>.
- [45] Andrzej I. Stankiewicz, Jacob A. Moulijn, *Process intensification: transforming chemical engineering*, *Chem. Eng. Prog.* 96 (1) (2000) 22–34.
- [46] R.C. Wilhoit, J. Chao, K.R. Hall, Thermodynamic properties of key organic oxygen compounds in the carbon range C1 to C4. Part 1. Properties of condensed phases, *J. Phys. Chem. Ref. Data Monogr.* 14 (1) (1985) 1–175, <https://doi.org/10.1063/1.555747>.
- [47] E.D. Nikitin, P.A. Pavlov, P.V. Skripov, Measurement of the critical properties of thermally unstable substances and mixtures by the pulse-heating method, *J. Chem. Thermodyn.* 25 (7) (1993) 869–880, <https://doi.org/10.1006/jcht.1993.1084>.
- [48] W.E. Acree, Thermodynamic properties of organic compounds: enthalpy of fusion and melting point temperature compilation, *Thermochim. Acta* 189 (1) (1991) 37–56, [https://doi.org/10.1016/0040-6031\(91\)87098-H](https://doi.org/10.1016/0040-6031(91)87098-H).
- [49] M. Bastos, S.-O. Nilsson, M.D.M.C. Ribeiro da Silva, M.A.V. Ribeiro da Silva, I. Wadsö, Thermodynamic properties of glycerol enthalpies of combustion and

- vaporization and the heat capacity at 298.15 K. Enthalpies of solution in water at 288.15, 298.15, and 308.15 K, *J. Chem. Thermodyn.* 20 (11) (1988) 1353–1359, [https://doi.org/10.1016/0021-9614\(88\)90173-5](https://doi.org/10.1016/0021-9614(88)90173-5).
- [50] A. Passian, S. Zahrai, A.L. Lereu, R.H. Farahi, T.L. Ferrell, T. Thundat, Nonradiative surface plasmon assisted microscale Marangoni forces, *Phys. Rev. E* 73 (6) (2006), 066311, <https://doi.org/10.1103/PhysRevE.73.066311>.
- [51] J. Esteban, M. Gonzalez-Miquel, Thermodynamic insights on the viscometric and volumetric properties of binary mixtures of ketals and polyols, *J. Mol. Liq.* 263 (2018) 125–138, <https://doi.org/10.1016/j.molliq.2018.04.133>.
- [52] A. Erfani, S. Khosharay, C.P. Aichele, Surface tension and interfacial compositions of binary glycerol/alcohol mixtures, *J. Chem. Thermodyn.* 135 (2019) 241–251, <https://doi.org/10.1016/j.jct.2019.03.014>.
- [53] R.J. Sengwa, Comparative dielectric study of mono, di and trihydric alcohols, *Indian J. Pure Appl. Phys.* 41 (4) (2003) 295–300.
- [54] Y. Gu, F. Jérôme, Glycerol as a sustainable solvent for green chemistry, *Green Chem.* 12 (7) (2010) 1127–1138, <https://doi.org/10.1039/C001628D>.
- [55] M.B. Moghaddam, E.K. Goharshadi, F. Moosavi, Glycerol revisited molecular dynamic simulations of structural, dynamical, and thermodynamic properties, *J. Iran. Chem. Soc.* 14 (1) (2017) 1–7, <https://doi.org/10.1007/s13738-016-0952-5>.
- [56] M. Mokhtarpour, H. Shekaari, M.T. Zafarani-Moattar, S. Golgoun, Solubility and solvation behavior of some drugs in choline based deep eutectic solvents at different temperatures, *J. Mol. Liq.* 297 (2020), 111799, <https://doi.org/10.1016/j.molliq.2019.111799>.
- [57] V.K. Sharma, P.D. Sahare, R.C. Rastogi, S.K. Ghoshal, D. Mohan, Excited state characteristics of acridine dyes: acriflavine and acridine orange, *Spectrochim. Acta Part A* 59 (8) (2003) 1799–1804, [https://doi.org/10.1016/S1386-1425\(02\)00440-7](https://doi.org/10.1016/S1386-1425(02)00440-7).
- [58] F. Reymermier, *Glycerine Market Report, Oleoline, 2020, pp. 1–4*.
- [59] *Oleoline, Crude Glycerine Market Report, 2020*.
- [60] T.I. Market T, S. Your, *Glycerine Market Report, 2020*.
- [61] J.R. Ochoa-Gómez, O. Gómez-Jiménez-Aberasturi, C. Ramírez-López, M. Belsué, A brief review on industrial alternatives for the manufacturing of glycerol carbonate, a green chemical, *Org. Process. Res. Dev.* 16 (3) (2012) 389–399, <https://doi.org/10.1021/op200369v>.
- [62] M.O. Sonnat, S. Amigoni, E.P. Taffin de Givenchy, T. Darmanin, O. Choulet, F. Guittard, Glycerol carbonate as a versatile building block for tomorrow: synthesis, reactivity, properties and applications, *Green Chem.* 15 (2) (2013) 283–306, <https://doi.org/10.1039/C2GC36525A>.
- [63] W.K. Teng, G.C. Ngho, R. Yusoff, M.K. Aroua, A review on the performance of glycerol carbonate production via catalytic transesterification: effects of influencing parameters, *Energy Convers. Manag.* 88 (2014) 484–497, <https://doi.org/10.1016/j.enconman.2014.08.036>.
- [64] P.U. Okoye, B.H. Hameed, Review on recent progress in catalytic carboxylation and acetylation of glycerol as a byproduct of biodiesel production, *Renew. Sust. Energy. Rev.* 53 (2016) 558–574, <https://doi.org/10.1016/j.rser.2015.08.064>.
- [65] Z.I. Ishak, N.A. Sairi, Y. Alias, M.K.T. Aroua, R. Yusoff, A review of ionic liquids as catalysts for transesterification reactions of biodiesel and glycerol carbonate production, *Catal. Rev.* 59 (1) (2017) 44–93, <https://doi.org/10.1080/01614940.2016.1268021>.
- [66] A.R. Trifoi, P.S. Agachi, T. Pap, Glycerol acetals and ketals as possible diesel additives. A review of their synthesis protocols, *Renew. Sust. Energy. Rev.* 62 (2016) 804–814, <https://doi.org/10.1016/j.rser.2016.05.013>.
- [67] A. Cornejo, I. Barrio, M. Campoy, J. Lázaro, B. Navarrete, Oxygenated fuel additives from glycerol valorization. Main production pathways and effects on fuel properties and engine performance: a critical review, *Renew. Sust. Energy. Rev.* 79 (2017) 1400–1413, <https://doi.org/10.1016/j.rser.2017.04.005>.
- [68] P.U. Okoye, A.Z. Abdullah, B.H. Hameed, A review on recent developments and progress in the kinetics and deactivation of catalytic acetylation of glycerol—a byproduct of biodiesel, *Renew. Sust. Energy. Rev.* 74 (2017) 387–401, <https://doi.org/10.1016/j.rser.2017.02.017>.
- [69] R. Estevez, L. Aguado-Deblas, D. Luna, F.M. Bautista, An overview of the production of oxygenated fuel additives by glycerol etherification, either with isobutene or tert-butyl alcohol, over heterogeneous catalysts, *Energies* 12 (12) (2019), <https://doi.org/10.3390/en12122364>.
- [70] Y. Wang, J. Zhou, X. Guo, Catalytic hydrogenolysis of glycerol to propanediols: a review, *RSC Adv.* 5 (91) (2015) 74611–74628, <https://doi.org/10.1039/C5RA11957J>.
- [71] M.R. Nanda, Z. Yuan, W. Qin, C. Xu, Recent advancements in catalytic conversion of glycerol into propylene glycol: a review, *Catal. Rev.* 58 (3) (2016) 309–336, <https://doi.org/10.1080/01614940.2016.1166005>.
- [72] E. Markočič, B. Kramberger, J.G. van Bennekom, H. Jan Heeres, J. Vos, Ž. Knez, Glycerol reforming in supercritical water; a short review, *Renew. Sust. Energy. Rev.* 23 (2013) 40–48, <https://doi.org/10.1016/j.rser.2013.02.046>.
- [73] A. Galadima, O. Muraza, A review on glycerol valorization to acrolein over solid acid catalysts, *J. Taiwan Inst. Chem. Eng.* 67 (2016) 29–44, <https://doi.org/10.1016/j.jtice.2016.07.019>.
- [74] N. Razali, A.Z. Abdullah, Production of lactic acid from glycerol via chemical conversion using solid catalyst: a review, *Appl. Catal. A* 543 (2017) 234–246, <https://doi.org/10.1016/j.apcata.2017.07.002>.
- [75] A.L. Chun Minh, S.P. Samudrala, S. Bhattacharya, Valorisation of glycerol through catalytic hydrogenolysis routes for sustainable production of value-added C3 chemicals: current and future trends, *Sustainable Energy Fuel* 6 (3) (2022) 596–639, <https://doi.org/10.1039/D1SE01333E>.
- [76] E.S. Vasiliadou, A.A. Lemonidou, Glycerol transformation to value added C3 diols: reaction mechanism, kinetic, and engineering aspects, *WIREs Energy Environ.* 4 (6) (2015) 486–520, <https://doi.org/10.1002/wene.159>.
- [77] E. Santacesaria, R. Vitiello, R. Tesser, V. Russo, R. Turco, M. Di Serio, Chemical and technical aspects of the synthesis of chlorohydrins from glycerol, *Ind. Eng. Chem. Res.* 53 (22) (2014) 8939–8962, <https://doi.org/10.1021/ie403268b>.
- [78] N.A. Roslan, S.Z. Abidin, A. Ideris, D.V.N. Vo, A review on glycerol reforming processes over Ni-based catalyst for hydrogen and syngas productions, *Int. J. Hydrog. Energy* 45 (36) (2020) 18466–18489, <https://doi.org/10.1016/j.ijhydene.2019.08.211>.
- [79] J.M. Silva, M.A. Soria, L.M. Madeira, Challenges and strategies for optimization of glycerol steam reforming process, *Renew. Sust. Energy. Rev.* 42 (2015) 1187–1213, <https://doi.org/10.1016/j.rser.2014.10.084>.
- [80] C.A. Schwengber, H.J. Alves, R.A. Schaffner, F.A. da Silva, R. Sequinel, V.R. Bach, R.J. Ferracin, Overview of glycerol reforming for hydrogen production, *Renew. Sust. Energy. Rev.* 58 (2016) 259–266, <https://doi.org/10.1016/j.rser.2015.12.279>.
- [81] A.G. Adeniyi, J.O. Ighalo, A review of steam reforming of glycerol, *Chem. Pap.* 73 (11) (2019) 2619–2635, <https://doi.org/10.1007/s11696-019-00840-8>.
- [82] U.C. Abubakar, Y. Bansod, L. Forster, V. Spallina, C. D'Agostino, Conversion of glycerol to acrylic acid: a review of strategies, recent developments and prospects, *React. Chem. Eng.* 8 (8) (2023) 1819–1838, <https://doi.org/10.1039/D3RE00057E>.
- [83] J. Hu, J. Li, Y. Gu, Z. Guan, W. Mo, Y. Ni, T. Li, G. Li, Oxidative carbonylation of glycerol to glycerol carbonate catalyzed by PdCl₂(phen)/KI, *Appl. Catal. A Gen.* 386 (1) (2010) 188–193, <https://doi.org/10.1016/j.apcata.2010.07.059>.
- [84] J. George, Y. Patel, S.M. Pillai, P. Munshi, Methanol assisted selective formation of 1,2-glycerol carbonate from glycerol and carbon dioxide using nBu₂SnO as a catalyst, *J. Mol. Catal. A Chem.* 304 (1) (2009) 1–7, <https://doi.org/10.1016/j.molcata.2009.01.010>.
- [85] M. Aresta, A. Dibenedetto, F. Nocito, C. Pastore, A study on the carboxylation of glycerol to glycerol carbonate with carbon dioxide: the role of the catalyst, solvent and reaction conditions, *J. Mol. Catal. A Chem.* 257 (1) (2006) 149–153, <https://doi.org/10.1016/j.molcata.2006.05.021>.
- [86] J. Li, T. Wang, Chemical equilibrium of glycerol carbonate synthesis from glycerol, *J. Chem. Thermodyn.* 43 (5) (2011) 731–736, <https://doi.org/10.1016/j.jct.2010.12.013>.
- [87] G.P. Fernandes, G.D. Yadav, Selective glycerolysis of urea to glycerol carbonate using combustion synthesized magnesium oxide as catalyst, *Catal. Today* 309 (2018) 153–160, <https://doi.org/10.1016/j.cattod.2017.08.021>.
- [88] S.E. Kondawar, R.B. Mane, A. Vasishta, S.B. More, S.D. Dhengale, C.V. Rode, Carbonylation of glycerol with urea to glycerol carbonate over supported Zn catalysts, *Appl. Petrochem. Res.* 7 (1) (2017) 41–53, <https://doi.org/10.1007/s13203-017-0177-2>.
- [89] N. Lertlukkanasuk, S. Phiyanalimmat, W. Kiatkittipong, A. Arpornwichanop, F. Aiouache, S. Assabumrungrat, Reactive distillation for synthesis of glycerol carbonate via glycerolysis of urea, *Chem. Eng. Process. Process Intensif.* 70 (2013) 103–109, <https://doi.org/10.1016/j.ccep.2013.05.001>.
- [90] Y. Qing, H.F. Lu, Y.Y. Liu, C.J. Liu, B. Liang, W. Jiang, Production of glycerol carbonate using crude glycerol from biodiesel production with DBU as a catalyst, *Chin. J. Chem. Eng.* 26 (9) (2018) 1912–1919, <https://doi.org/10.1016/j.cjche.2018.01.010>.
- [91] J.R. Ochoa-Gómez, O. Gómez-Jiménez-Aberasturi, B. Maestro-Madurga, A. Pesquera-Rodríguez, C. Ramírez-López, L. Lorenzo-Ibarreta, J. Torrecilla-Soria, M.C. Villarán-Velasco, Synthesis of glycerol carbonate from glycerol and dimethyl carbonate by transesterification: catalyst screening and reaction optimization, *Appl. Catal. A* 366 (2) (2009) 315–324, <https://doi.org/10.1016/j.apcata.2009.07.020>.
- [92] J.R. Ochoa-Gómez, O. Gómez-Jiménez-Aberasturi, C. Ramírez-López, B. Maestro-Madurga, Synthesis of glycerol 1,2-carbonate by transesterification of glycerol with dimethyl carbonate using triethylamine as a facile separable homogeneous catalyst, *Green Chem.* 14 (12) (2012) 3368–3376, <https://doi.org/10.1039/C2GC35992H>.
- [93] G.D. Yadav, P.A. Chandan, A green process for glycerol valorization to glycerol carbonate over heterogeneous hydroxalcalite catalyst, *Catal. Today* 237 (2014) 47–53, <https://doi.org/10.1016/j.cattod.2014.01.043>.
- [94] D. Singh, B. Reddy, A. Ganesh, S. Mahajani, Zinc/lanthanum mixed-oxide catalyst for the synthesis of glycerol carbonate by transesterification of glycerol, *Ind. Eng. Chem. Res.* 53 (49) (2014) 18786–18795, <https://doi.org/10.1021/ie5011564>.
- [95] P. Devi, U. Das, A.K. Dalai, Production of glycerol carbonate using a novel Ti-SBA-15 catalyst, *Chem. Eng. J.* 346 (2018) 477–488, <https://doi.org/10.1016/j.cej.2018.04.030>.
- [96] W.K. Teng, R. Yusoff, M.K. Aroua, G.C. Ngho, Process optimization and kinetics of microwave assisted transesterification of crude glycerol for the production of glycerol carbonate, *Sustain. Energy Fuels* 5 (1) (2021) 274–282, <https://doi.org/10.1039/D0SE01383H>.
- [97] H. Wang, T. Liu, C. Jiang, Y. Wang, J. Ma, Synthesis of glycidol and glycerol carbonate from glycerol and dimethyl carbonate using deep-eutectic solvent as a catalyst, *Chem. Eng. J.* 442 (2022), 136196, <https://doi.org/10.1016/j.cej.2022.136196>.
- [98] J. Esteban, M. Ladero, L. Molinero, F. García-Ochoa, Liquid–liquid equilibria for the ternary systems DMC–methanol–glycerol, DMC–glycerol carbonate–glycerol and the quaternary system DMC–methanol–glycerol carbonate–glycerol at catalytic reacting temperatures, *Chem. Eng. Res. Des.* 92 (12) (2014) 2797–2805, <https://doi.org/10.1016/j.cherd.2014.05.026>.

- [99] J. Esteban, M. Ladero, F. García-Ochoa, Liquid-liquid equilibria for the systems ethylene carbonate+ethylene glycol+glycerol; ethylene carbonate+glycerol carbonate+ethylene glycol+ethylene carbonate+ethylene glycol+glycerol carbonate+glycerol at catalytic reacting temperatures, *Chem. Eng. Res. Des.* 94 (2015) 440–448, <https://doi.org/10.1016/j.cherd.2014.08.024>.
- [100] J. Esteban, E. Fuente, A. Blanco, M. Ladero, F. García-Ochoa, Phenomenological kinetic model of the synthesis of glycerol carbonate assisted by focused beam reflectance measurements, *Chem. Eng. J.* 260 (2015) 434–443, <https://doi.org/10.1016/j.cej.2014.09.039>.
- [101] J. Esteban, M. Ladero, E. Fuente, A. Blanco, F. García-Ochoa, Experimental and modelling approach to the catalytic coproduction of glycerol carbonate and ethylene glycol as a means to valorize glycerol, *J. Taiwan Inst. Chem. Eng.* 63 (2016) 89–100, <https://doi.org/10.1016/j.jtice.2016.03.031>.
- [102] J. Esteban, E. Domínguez, M. Ladero, F. García-Ochoa, Kinetics of the production of glycerol carbonate by transesterification of glycerol with dimethyl and ethylene carbonate using potassium methoxide, a highly active catalyst, *Fuel Process. Technol.* 138 (2015) 243–251, <https://doi.org/10.1016/j.fuproc.2015.06.012>.
- [103] J. Esteban, E. Fuente, M. González-Miquel, A. Blanco, M. Ladero, F. García-Ochoa, Sustainable joint solventless coproduction of glycerol carbonate and ethylene glycol via thermal transesterification of glycerol, *RSC Adv.* 4 (95) (2014) 53206–53215, <https://doi.org/10.1039/C4RA11209A>.
- [104] J. Esteban, A.J. Vorholt, Obtaining glycerol carbonate and glycols using thermomorphic systems based on glycerol and cyclic organic carbonates: kinetic studies, *J. Ind. Eng. Chem.* 63 (2018) 124–132, <https://doi.org/10.1016/j.jiec.2018.02.008>.
- [105] M. Schrimpf, J. Esteban, T. Rösler, A.J. Vorholt, W. Leitner, Intensified reactors for gas-liquid-liquid multiphase catalysis: from chemistry to engineering, *Chem. Eng. J.* 372 (2019) 917–939, <https://doi.org/10.1016/j.cej.2019.03.133>.
- [106] A. Cornejo, M. Campoy, I. Barrio, B. Navarrete, J. Lázaro, Solketal production in a solvent-free continuous flow process: scaling from laboratory to bench size, *React. Chem. Eng.* 4 (10) (2019) 1803–1813, <https://doi.org/10.1039/C9RE00083F>.
- [107] F.M. Perez, N. Nichio, F. Pompeo, Thermodynamic assessment of chemical equilibrium for the synthesis of solketal in the liquid phase, *Chem. Eng. Technol.* 44 (8) (2021) 1356–1363, <https://doi.org/10.1002/ceat.202000435>.
- [108] M.R. Nanda, Z. Yuan, W. Qin, H.S. Ghaziaskar, M.-A. Poirier, C.C. Xu, Thermodynamic and kinetic studies of a catalytic process to convert glycerol into solketal as an oxygenated fuel additive, *Fuel* 117 (2014) 470–477, <https://doi.org/10.1016/j.fuel.2013.09.066>.
- [109] M.N. Moreira, R.P.V. Faria, A.M. Ribeiro, A.E. Rodrigues, Solketal production from glycerol ketalization with acetone: catalyst selection and thermodynamic and kinetic reaction study, *Ind. Eng. Chem. Res.* 58 (38) (2019) 17746–17759, <https://doi.org/10.1021/acs.iecr.9b03725>.
- [110] J.A. Vannucci, N.N. Nichio, F. Pompeo, Solketal synthesis from ketalization of glycerol with acetone: a kinetic study over a sulfated zirconia catalyst, *Catal. Today* 372 (2021) 238–245, <https://doi.org/10.1016/j.cattod.2020.10.005>.
- [111] Y. Ji, T. Zhang, X. Gui, H. Shi, Z. Yun, Solventless ketalization of glycerol to solketal with acetone over the ionic liquid [P(C4H9)3C14H29][TsO], *Chin. J. Chem. Eng.* 28 (1) (2020) 158–164, <https://doi.org/10.1016/j.cjche.2019.07.019>.
- [112] R.P.V. Faria, C.S.M. Pereira, V.M.T.M. Silva, J.M. Loureiro, A.E. Rodrigues, Glycerol valorisation as biofuels: selection of a suitable solvent for an innovative process for the synthesis of GEA, *Chem. Eng. J.* 233 (2013) 159–167, <https://doi.org/10.1016/j.cej.2013.08.035>.
- [113] J. Esteban, A.J. Vorholt, A. Behr, M. Ladero, F. García-Ochoa, Liquid-liquid equilibria for the system acetone + solketal + glycerol at (303.2, 313.2, and 323.2) K, *J. Chem. Eng. Data* 59 (9) (2014) 2850–2855, <https://doi.org/10.1021/je500469a>.
- [114] I. Agirre, I. García, J. Requies, V.L. Barrio, M.B. Güemez, J.F. Cambra, P.L. Arias, Glycerol acetals, kinetic study of the reaction between glycerol and formaldehyde, *Biomass Bioenergy* 35 (8) (2011) 3636–3642, <https://doi.org/10.1016/j.biombioe.2011.05.008>.
- [115] A. Hasabnis, S. Mahajani, Acetalization of glycerol with formaldehyde by reactive distillation, *Ind. Eng. Chem. Res.* 53 (31) (2014) 12279–12287, <https://doi.org/10.1021/ie501577q>.
- [116] I. Agirre, M.B. Güemez, A. Ugarte, J. Requies, V.L. Barrio, J.F. Cambra, P.L. Arias, Glycerol acetals as diesel additives: kinetic study of the reaction between glycerol and acetaldehyde, *Fuel Process. Technol.* 116 (2013) 182–188, <https://doi.org/10.1016/j.fuproc.2013.05.014>.
- [117] M.B. Güemez, J. Requies, I. Agirre, P.L. Arias, V.L. Barrio, J.F. Cambra, Acetalization reaction between glycerol and n-butyraldehyde using an acidic ion exchange resin. Kinetic modelling, *Chem. Eng. J.* 228 (2013) 300–307, <https://doi.org/10.1016/j.cej.2013.04.107>.
- [118] J. Esteban, M. Ladero, F. García-Ochoa, Kinetic modelling of the solventless synthesis of solketal with a sulfonic ion exchange resin, *Chem. Eng. J.* 269 (2015) 194–202, <https://doi.org/10.1016/j.cej.2015.01.107>.
- [119] V. Rossa, Y.D.S.P. Pessanha, G.C. Díaz, L.D.T. Câmara, S.B.C. Pergher, D.A. G. Aranda, Reaction kinetic study of solketal production from glycerol ketalization with acetone, *Ind. Eng. Chem. Res.* 56 (2) (2017) 479–488, <https://doi.org/10.1021/acs.iecr.6b03581>.
- [120] L. Roldán, R. Mallada, J.M. Fraile, J.A. Mayoral, M. Menéndez, Glycerol upgrading by ketalization in a zeolite membrane reactor, *Asia Pac. J. Chem. Eng.* 4 (3) (2009) 279–284, <https://doi.org/10.1002/apj.243>.
- [121] J.S. Clarkson, A.J. Walker, M.A. Wood, Continuous reactor technology for ketal formation: an improved synthesis of solketal, *Org. Process. Res. Dev.* 5 (6) (2001) 630–635, <https://doi.org/10.1021/op000135p>.
- [122] G.L. Catuzo, C.V. Santilli, L. Martins, Hydrophobic-hydrophilic balance of ZSM-5 zeolites on the two-phase ketalization of glycerol with acetone, *Catal. Today* 381 (2021) 215–223, <https://doi.org/10.1016/j.cattod.2020.07.008>.
- [123] M. Pagliaro, Chapter 3 - Esters, ethers, polyglycols, and polyesters, in: M. Pagliaro (Ed.), *Glycerol*, Elsevier, 2017, pp. 59–90.
- [124] P. Mukhopadhyay, R. Chakraborty, S. Singh, Triacetin additive in biodiesel to reduce air pollution: a review, *Environ. Chem. Lett.* 20 (2022) 32, <https://doi.org/10.1007/s10311-021-01362-0>.
- [125] L. Zhou, T.-H. Nguyen, A.A. Adesina, The acetylation of glycerol over amberlyst-15: kinetic and product distribution, *Fuel Process. Technol.* 104 (2012) 310–318, <https://doi.org/10.1016/j.fuproc.2012.06.001>.
- [126] L. Hermida, A.Z. Abdullah, A.R. Mohamed, Synthesis of monoglyceride through glycerol esterification with lauric acid over propyl sulfonic acid post-synthesis functionalized SBA-15 mesoporous catalyst, *Chem. Eng. J.* 174 (2) (2011) 668–676, <https://doi.org/10.1016/j.cej.2011.09.072>.
- [127] M. Ravelo, J. Esteban, M. Ladero, F. García-Ochoa, Enzymatic synthesis of ibuprofen monoglycerides catalyzed by free *Candida antarctica* lipase B in a toluene-glycerol biphasic medium, *RSC Adv.* 6 (73) (2016) 69658–69669, <https://doi.org/10.1039/C6RA15480H>.
- [128] D. Singh, P. Patidar, A. Ganesh, S. Mahajani, Esterification of oleic acid with glycerol in the presence of supported zinc oxide as catalyst, *Ind. Eng. Chem. Res.* 52 (42) (2013) 14776–14786, <https://doi.org/10.1021/ie401636v>.
- [129] J.J. Tamayo, M. Ladero, V.E. Santos, F. García-Ochoa, Esterification of benzoic acid and glycerol to α -monobenzoate glycerol in solventless media using an industrial free *Candida antarctica* lipase B, *Process Biochem.* 47 (2) (2012) 243–250, <https://doi.org/10.1016/j.procbio.2011.10.037>.
- [130] L. Molinero, J. Esteban, F. Sanchez, F. García-Ochoa, M. Ladero, Solventless esterification of glycerol with p-methoxycinnamic acid catalyzed by a novel sulfonic acid mesoporous solid: reaction kinetics, *J. Ind. Eng. Chem.* 109 (2022) 442–452, <https://doi.org/10.1016/j.jiec.2022.02.034>.
- [131] A.J. Martín, S. Mitchell, C. Mondelli, S. Jaydev, J. Pérez-Ramírez, Unifying views on catalyst deactivation, *Nat. Catal.* 5 (10) (2022) 854–866, <https://doi.org/10.1038/s41929-022-00842-y>.
- [132] H. Li, J. Li, X. Li, X. Gao, Esterification of glycerol and acetic acid in a pilot-scale reactive distillation column: experimental investigation, model validation, and process analysis, *J. Taiwan Inst. Chem. Eng.* 89 (2018) 56–66, <https://doi.org/10.1016/j.jtice.2018.05.009>.
- [133] D. Zhang, D. Zhou, X. Wei, J. Liang, X. Chen, L. Wang, Green catalytic conversion of hydrogenated rosin to glycerol esters using subcritical CO₂ in water and the associated kinetics, *J. Supercrit. Fluids* 125 (2017) 12–21, <https://doi.org/10.1016/j.supflu.2017.01.009>.
- [134] S.B. More, J.T. Waghmare, P.R. Gogate, Ultrasound pretreatment as a novel approach for intensification of lipase catalyzed esterification of tricaprilyn, *Ultrason. Sonochem.* 36 (2017) 253–261, <https://doi.org/10.1016/j.ultrsonch.2016.11.036>.
- [135] L. Molinero, M. Ladero, J.J. Tamayo, F. García-Ochoa, Homogeneous catalytic esterification of glycerol with cinnamic and methoxycinnamic acids to cinnamate glycerides in solventless medium: kinetic modeling, *Chem. Eng. J.* 247 (2014) 174–182, <https://doi.org/10.1016/j.cej.2014.02.079>.
- [136] M. Ladero, M. de Gracia, J.J. Tamayo, I.L.D. Ahumada, F. Trujillo, F. García-Ochoa, Kinetic modelling of the esterification of rosin and glycerol: application to industrial operation, *Chem. Eng. J.* 169 (1) (2011) 319–328, <https://doi.org/10.1016/j.cej.2011.03.012>.
- [137] L. Molinero, M. Ladero, J.J. Tamayo, J. Esteban, F. García-Ochoa, Thermal esterification of cinnamic and p-methoxycinnamic acids with glycerol to cinnamate glycerides in solventless media: a kinetic model, *Chem. Eng. J.* 225 (2013) 710–719, <https://doi.org/10.1016/j.cej.2013.04.016>.
- [138] I. Banu, G. Bumbac, D. Bombos, S. Velea, A.-M. Gălan, G. Bozga, Glycerol acetylation with acetic acid over Purolite CT-275. Product yields and process kinetics, *Renew. Energy* 148 (2020) 548–557, <https://doi.org/10.1016/j.renene.2019.10.060>.
- [139] D.M. Reinoso, D.E. Boldrini, Kinetic study of fuel bio-additive synthesis from glycerol esterification with acetic acid over acid polymeric resin as catalyst, *Fuel* 264 (2020), 116879, <https://doi.org/10.1016/j.fuel.2019.116879>.
- [140] M.S. Khayoon, S. Triwahyono, B.H. Hameed, A.A. Jalil, Improved production of fuel oxygenates via glycerol acetylation with acetic acid, *Chem. Eng. J.* 243 (2014) 473–484, <https://doi.org/10.1016/j.cej.2014.01.027>.
- [141] M. Srivastava, P. Mukhopadhyay, R. Chakraborty, Efficient monooleoyl glycerol synthesis employing hybrid ultrasonic-infrared-wave promoted reactor: concurrent catalytic and noncatalytic esterification kinetics, *Int. J. Chem. Kinet.* 52 (1) (2020) 61–73, <https://doi.org/10.1002/kin.21330>.
- [142] D. Unlu, N. Durmaz Hilmioglu, Production of fuel bioadditive “triacetin” using a phosphomolybdic-acid-loaded PVA membrane in a pervaporation catalytic membrane reactor, *Energy Fuel* 33 (3) (2019) 2208–2218, <https://doi.org/10.1021/acs.energyfuels.8b03344>.
- [143] J. Liu, Z. Zhang, P. Zhang, B. Yang, On the kinetics of multiphase etherification of glycerol with isobutene, *Chem. Eng. J.* 375 (2019), 122037, <https://doi.org/10.1016/j.cej.2019.122037>.
- [144] M.P. Pico, S. Rodríguez, A. Santos, A. Romero, Etherification of glycerol with benzyl alcohol, *Ind. Eng. Chem. Res.* 52 (41) (2013) 14545–14555, <https://doi.org/10.1021/ie402026t>.
- [145] M.P. Pico, A. Romero, S. Rodríguez, A. Santos, Etherification of glycerol with tert-butyl alcohol: kinetic model, *Ind. Eng. Chem. Res.* 51 (28) (2012) 9500–9509, <https://doi.org/10.1021/ie300481d>.
- [146] C. Cannilla, G. Giacoppo, L. Frusteri, S. Todaro, G. Bonura, F. Frusteri, Techno-economic feasibility of industrial production of biofuels by glycerol etherification

- reaction with isobutene or tert-butyl alcohol assisted by vapor-permeation membrane, *J. Ind. Eng. Chem.* 98 (2021) 413–424, <https://doi.org/10.1016/j.jiec.2021.03.023>.
- [147] M.A. Jaworski, S. Rodríguez Vega, G.J. Siri, M.L. Casella, A. Romero Salvador, A. Santos López, Glycerol etherification with benzyl alcohol over sulfated zirconia catalysts, *Appl. Catal. A* 505 (2015) 36–43, <https://doi.org/10.1016/j.apcata.2015.04.027>.
- [148] A.A. Al-Rabiah, R.K. Al Darwish, A.E. Alqahtani, D.M. Chaves, M.J. da Silva, Production of biofuel additives using catalytic bioglycerol etherification: kinetic modelling and reactive distillation design, *Catalysts* 12 (11) (2022) 1332, <https://doi.org/10.3390/catal12111332>.
- [149] G.D. Yadav, P.A. Chandan, N. Gopalaswami, Green etherification of bioglycerol with 1-phenyl ethanol over supported heteropolyacid, *Clean Technol. Environ. Policy* 14 (1) (2012) 85–95, <https://doi.org/10.1007/s10098-011-0380-2>.
- [150] W. Kiatkittipong, P. Intaracharoen, N. Laosiripojana, C. Chaisuk, P. Praserttham, S. Assabumrungrat, Glycerol ethers synthesis from glycerol etherification with tert-butyl alcohol in reactive distillation, *Comput. Chem. Eng.* 35 (10) (2011) 2034–2043, <https://doi.org/10.1016/j.compchemeng.2011.01.016>.
- [151] N.N. Pandhare, S.M. Pudi, S. Mondal, K. Pareta, M. Kumar, P. Biswas, Development of kinetic model for hydrogenolysis of glycerol over Cu/MgO catalyst in a slurry reactor, *Ind. Eng. Chem. Res.* 57 (1) (2018) 101–110, <https://doi.org/10.1021/acs.iecr.7b03684>.
- [152] S. Mondal, H. Malviya, P. Biswas, Kinetic modelling for the hydrogenolysis of bioglycerol in the presence of a highly selective Cu–Ni–Al₂O₃ catalyst in a slurry reactor, *React. Chem. Eng.* 4 (3) (2019) 595–609, <https://doi.org/10.1039/C8RE00138C>.
- [153] S. Mondal, P. Biswas, Conversion of bio-glycerol to propylene glycol over basic oxides (MgO, La₂O₃, MgO-La₂O₃, CaO, and BaO₂) supported Cu–Zn bimetallic catalyst: a reaction kinetic study, *Environ. Technol. Innov.* 27 (2022), 102367, <https://doi.org/10.1016/j.eti.2022.102367>.
- [154] J. Yuan, S. Li, L. Yu, Y. Liu, Y. Cao, Efficient catalytic hydrogenolysis of glycerol using formic acid as hydrogen source, *Chin. J. Catal.* 34 (11) (2013) 2066–2074, [https://doi.org/10.1016/S1872-2067\(12\)60656-1](https://doi.org/10.1016/S1872-2067(12)60656-1).
- [155] Y. Liu, C.T.Q. Mai, F.T.T. Ng, Glycerol hydrogenolysis with in situ hydrogen produced via methanol steam reforming: the promoting effect of Pd on a Cu/ZnO/Al₂O₃ catalyst, *Catalysts* 11 (1) (2021) 110, <https://doi.org/10.3390/catal11010110>.
- [156] V.L. Yfanti, D. Ipsakis, A.A. Lemonidou, Kinetic study of liquid phase glycerol hydrodeoxygenation under inert conditions over a Cu-based catalyst, *React. Chem. Eng.* 3 (4) (2018) 559–571, <https://doi.org/10.1039/C8RE00061A>.
- [157] D.K. Pandey, N.N. Pandhare, P. Biswas, Production of propylene glycol (propane-1,2-diol) in vapor phase over Cu–Ni/γ-Al₂O₃ catalyst in a down flow tubular reactor: effect of catalyst calcination temperature and kinetic study, *React. Kinet. Mech. Catal.* 127 (1) (2019) 523–542, <https://doi.org/10.1007/s11144-019-01582-0>.
- [158] M.N. Gatti, F. Pompeo, N.N. Nichio, G.F. Santori, Crude glycerol hydrogenolysis to bio-propylene glycol: effect of its impurities on activity, selectivity and stability, *Processes* 11 (6) (2023) 1731, <https://doi.org/10.3390/pr11061731>.
- [159] T. Rajkhowa, G.B. Marin, J.W. Thybaut, Quantifying the dominant factors in Cu catalyst deactivation during glycerol hydrogenolysis, *J. Ind. Eng. Chem.* 54 (2017) 270–277, <https://doi.org/10.1016/j.jiec.2017.05.040>.
- [160] A.-H. Zhang, S.-Y. Huang, X.-Y. Zhuang, K. Wang, C.-Y. Yao, B.-S. Fang, A novel kinetic model to describe 1,3-propanediol production fermentation by *Clostridium butyricum*, *AIChE J.* 65 (6) (2019) e16587, <https://doi.org/10.1002/aic.16587>.
- [161] L. He, X. Zhao, K. Cheng, Y. Sun, D. Liu, Kinetic modeling of fermentative production of 1,3-propanediol by *Klebsiella pneumoniae* HR526 with consideration of multiple product inhibitions, *Appl. Biochem. Biotechnol.* 169 (1) (2013) 312–326, <https://doi.org/10.1007/s12010-012-9984-1>.
- [162] C. Zhu, B. Fang, S. Wang, Effects of culture conditions on the kinetic behavior of 1,3-propanediol fermentation by *Clostridium butyricum* with a kinetic model, *Biotechnol. Bioinform.* 212 (2016) 130–137, <https://doi.org/10.1016/j.biotech.2016.04.028>.
- [163] A. Rodriguez, V.E. Santos, E. Gomez, F. Garcia-Ochoa, Influence of fluid dynamic conditions on 1,3-propanediol production from glycerol by *Shimwellia blattae*: carbon flux and cell response, *J. Chem. Technol. Biotechnol.* 92 (8) (2017) 2050–2059, <https://doi.org/10.1002/jctb.5200>.
- [164] A. Rodriguez, M. Wojtusik, F. Masca, V.E. Santos, F. Garcia-Ochoa, Kinetic modeling of 1,3-propanediol production from raw glycerol by *Shimwellia blattae*: influence of the initial substrate concentration, *Biochem. Eng. J.* 117 (2017) 57–65, <https://doi.org/10.1016/j.bej.2016.09.018>.
- [165] D.-T. Pan, X.-D. Wang, H.-Y. Shi, D.-C. Yuan, Z.-L. Xiu, Dynamic flux balance analysis for microbial conversion of glycerol into 1,3-propanediol by *Klebsiella pneumoniae*, *Bioprocess Biosyst. Eng.* 41 (12) (2018) 1793–1805, <https://doi.org/10.1007/s00449-018-2002-4>.
- [166] D.T. Pan, X.D. Wang, H.Y. Shi, D.C. Yuan, Z.L. Xiu, Ensemble optimization of microbial conversion of glycerol into 1,3-propanediol by *Klebsiella pneumoniae*, *J. Biotechnol.* 301 (2019) 68–78, <https://doi.org/10.1016/j.jbiotec.2019.06.001>.
- [167] M. Dalil, D. Carnevali, J.-L. Dubois, G.S. Patience, Transient acrolein selectivity and carbon deposition study of glycerol dehydration over WO₃/TiO₂ catalyst, *Chem. Eng. J.* 270 (2015) 557–563, <https://doi.org/10.1016/j.cej.2015.02.058>.
- [168] A. Talebian-Kiakalaieh, N.A.S. Amin, Kinetic modeling, thermodynamic, and mass-transfer studies of gas-phase glycerol dehydration to acrolein over supported silicotungstic acid catalyst, *Ind. Eng. Chem. Res.* 54 (33) (2015) 8113–8121, <https://doi.org/10.1021/acs.iecr.5b02172>.
- [169] A. Talebian-Kiakalaieh, N.A.S. Amin, Thermo-kinetic and diffusion studies of glycerol dehydration to acrolein using HSiW-γ-Al₂O₃ supported ZrO₂ solid acid catalyst, *Renew. Energy* 114 (2017) 794–804, <https://doi.org/10.1016/j.renene.2017.07.096>.
- [170] Q. Xie, T. Pan, G. Zheng, Y. Zhou, S. Yu, Y. Duan, Y. Nie, Microwave fixed-bed reactor for gas-phase glycerol dehydration: experimental and simulation studies, *Ind. Eng. Chem. Res.* 61 (30) (2022) 10723–10735, <https://doi.org/10.1021/acs.iecr.2c01176>.
- [171] Q. Xie, S. Li, R. Gong, G. Zheng, Y. Wang, P. Xu, Y. Duan, S. Yu, M. Lu, W. Ji, Y. Nie, J. Ji, Microwave-assisted catalytic dehydration of glycerol for sustainable production of acrolein over a microwave absorbing catalyst, *Appl. Catal. B* 243 (2019) 455–462, <https://doi.org/10.1016/j.apcatb.2018.10.058>.
- [172] H. Park, Y.S. Yun, T.Y. Kim, K.R. Lee, J. Baek, J. Yi, Kinetics of the dehydration of glycerol over acid catalysts with an investigation of deactivation mechanism by coke, *Appl. Catal. B* 176–177 (2015) 1–10, <https://doi.org/10.1016/j.apcatb.2015.03.046>.
- [173] I. Martinuzzi, Y. Azizi, O. Zahraa, J.-P. Leclerc, Deactivation study of a heteropolyacid catalyst for glycerol dehydration to form acrolein, *Chem. Eng. Sci.* 134 (2015) 663–670, <https://doi.org/10.1016/j.ces.2015.05.060>.
- [174] S. Thanasilp, J.W. Schwank, V. Meeyoo, S. Pengpanich, M. Hunsom, One-pot oxydehydration of glycerol to value-added compounds over metal-doped SiW/HZSM-5 catalysts: effect of metal type and loading, *Chem. Eng. J.* 275 (2015) 113–124, <https://doi.org/10.1016/j.cej.2015.04.010>.
- [175] R. Vitiello, V. Russo, R. Turco, R. Tesser, M. Di Serio, E. Santacesaria, Glycerol chlorination in a gas-liquid semibatch reactor: new catalysts for chlorohydrin production, *Chin. J. Catal.* 35 (5) (2014) 663–669, [https://doi.org/10.1016/S1872-2067\(14\)60069-3](https://doi.org/10.1016/S1872-2067(14)60069-3).
- [176] A. Medina, J.I. Abad, P. Tolvanen, C. de Araujo Filho, T. Salmi, Revisiting the kinetics and mechanism of glycerol hydrochlorination in the presence of homogeneous catalysts, *Ind. Eng. Chem. Res.* 61 (37) (2022) 13827–13840, <https://doi.org/10.1021/acs.iecr.2c01805>.
- [177] C.A. de Araujo Filho, K. Eränen, J.-P. Mikkola, T. Salmi, A comprehensive study on the kinetics, mass transfer and reaction engineering aspects of solvent-free glycerol hydrochlorination, *Chem. Eng. Sci.* 120 (2014) 88–104, <https://doi.org/10.1016/j.ces.2014.08.043>.
- [178] R. Tesser, M. Di Serio, R. Vitiello, V. Russo, E. Ranieri, E. Speranza, E. Santacesaria, Glycerol chlorination in gas-liquid semibatch reactor: an alternative route for chlorohydrins production, *Ind. Eng. Chem. Res.* 51 (26) (2012) 8768–8776, <https://doi.org/10.1021/ie201629z>.
- [179] Z.-H. Luo, X.-Z. You, H.-R. Li, A kinetic model for glycerol chlorination in the presence of acetic acid catalyst, *Korean J. Chem. Eng.* 27 (1) (2010) 66–72, <https://doi.org/10.1007/s11814-009-0329-x>.
- [180] S.-J. Wang, D.S.-H. Wong, S.-S. Jang, S.-H. Huang, Novel plant-wide process design for producing dichlorohydrin by glycerol hydrochlorination, *J. Taiwan Inst. Chem. Eng.* 73 (2017) 50–61, <https://doi.org/10.1016/j.jtice.2016.05.055>.
- [181] S. Guo, L. Guo, J. Yin, H. Jin, Supercritical water gasification of glycerol: intermediates and kinetics, *J. Supercrit. Fluids* 78 (2013) 95–102, <https://doi.org/10.1016/j.supflu.2013.03.025>.
- [182] C.K. Cheng, S.Y. Foo, A.A. Adesina, Glycerol steam reforming over bimetallic Co–Ni/Al₂O₃, *Ind. Eng. Chem. Res.* 49 (21) (2010) 10804–10817, <https://doi.org/10.1021/ie100462t>.
- [183] A. Desgagnés, M.C. Iliuta, Kinetic study of glycerol steam reforming catalyzed by a Ni-promoted metallurgical residue, *Chem. Eng. J.* 429 (2022), 132278, <https://doi.org/10.1016/j.cej.2021.132278>.
- [184] H.D. Demsash, K.V.K. Kondamudi, S. Upadhyayula, R. Mohan, Ruthenium doped nickel-alumina-ceria catalyst in glycerol steam reforming, *Fuel Process. Technol.* 169 (2018) 150–156, <https://doi.org/10.1016/j.fuproc.2017.09.017>.
- [185] S. Bepari, N.C. Pradhan, A.K. Dalai, Selective production of hydrogen by steam reforming of glycerol over Ni/Fly ash catalyst, *Catal. Today* 291 (2017) 36–46, <https://doi.org/10.1016/j.cattod.2017.01.015>.
- [186] B. Dou, C. Wang, Y. Song, H. Chen, Y. Xu, Activity of Ni–Cu–Al based catalyst for renewable hydrogen production from steam reforming of glycerol, *Energy Convers. Manag.* 78 (2014) 253–259, <https://doi.org/10.1016/j.enconman.2013.10.067>.
- [187] J.P.D.S.Q. Menezes, R.L. Manfro, M.M.V.M. Souza, Hydrogen production from glycerol steam reforming over nickel catalysts supported on alumina and niobia: deactivation process, effect of reaction conditions and kinetic modeling, *Int. J. Hydrog. Energy* 43 (32) (2018) 15064–15082, <https://doi.org/10.1016/j.ijhydene.2018.06.048>.
- [188] Y. Liu, A. Lawal, Kinetic study of autothermal reforming of glycerol in a dual layer monolith catalyst, *Chem. Eng. Process. Process Intensif.* 95 (2015) 276–283, <https://doi.org/10.1016/j.cep.2015.07.008>.
- [189] A. Odoom, M. Fabrik, A. Salama, E. Shirif, H. Ibrahim, Mechanistic kinetic modelling framework for the conversion of waste crude glycerol to value-added hydrogen-rich gas, *Catalysts* 12 (2) (2022) 200, <https://doi.org/10.3390/catal12020200>.
- [190] M.S. Macedo, M.A. Soria, L.M. Madeira, Process intensification for hydrogen production through glycerol steam reforming, *Renew. Sust. Energy Rev.* 146 (2021) 111151, <https://doi.org/10.1016/j.rser.2021.111151>.
- [191] R. Moreira, F. Bimbela, L.M. Gandía, A. Ferreira, J.L. Sánchez, A. Portugal, Oxidative steam reforming of glycerol. A review, *Renew. Sust. Energy Rev.* 148 (2021) 111299, <https://doi.org/10.1016/j.rser.2021.111299>.
- [192] S.J. Yoon, Y.M. Yun, M.W. Seo, Y.K. Kim, H.W. Ra, J.-G. Lee, Hydrogen and syngas production from glycerol through microwave plasma gasification, *Int. J. Hydrog. Energy* 38 (34) (2013) 14559–14567, <https://doi.org/10.1016/j.ijhydene.2013.09.001>.

- [193] S. Wang, X. Yang, S. Xu, K. Zhang, B. Li, Assessment of sorption-enhanced crude glycerol steam reforming process via CFD simulation, *Int. J. Hydrog. Energy* 43 (32) (2018) 14996–15004, <https://doi.org/10.1016/j.ijhydene.2018.06.053>.
- [194] X. Yang, S. Wang, S. Liu, Y. He, CFD analysis on sorption-enhanced glycerol reforming in a membrane-assisted fluidized bed reactor, *Int. J. Hydrog. Energy* 44 (39) (2019) 21424–21433, <https://doi.org/10.1016/j.ijhydene.2019.06.088>.
- [195] S. Yang, H. Sun, S. Yang, J. Hu, H. Wang, Investigation of sorption-enhanced hydrogen production by glycerol steam reforming in bubbling fluidized bed, *Fuel* 349 (2023), 128731, <https://doi.org/10.1016/j.fuel.2023.128731>.
- [196] J.A. Diaz, E. Skrzynska, S. Zaid, J.S. Girardon, M. Capron, F. Dumeignil, P. Fongarland, Kinetic modelling of the glycerol oxidation in the liquid phase: comparison of Pt, Au and Ag AS active phases, *J. Chem. Technol. Biotechnol.* 92 (9) (2017) 2267–2275, <https://doi.org/10.1002/jctb.5296>.
- [197] S.A. Zavrzhnov, A.L. Esipovich, S.Y. Zlobin, A.S. Belousov, A.V. Vorotyntsev, Mechanism analysis and kinetic modelling of Cu NPs catalysed glycerol conversion into lactic acid, *Catalysts* 9 (3) (2019), <https://doi.org/10.3390/catal9030231>.
- [198] R. Abdullah, S.N. Mohamed Saleh, K. Embong, A.Z. Abdullah, Recent developments and potential advancement in the kinetics of catalytic oxidation of glycerol, *Chem. Eng. Commun.* 207 (9) (2020) 1298–1328, <https://doi.org/10.1080/00986445.2019.1641699>.
- [199] X. Hu, J. Lu, Y. Liu, L. Chen, X. Zhang, H. Wang, Sustainable catalytic oxidation of glycerol: a review, *Environ. Chem. Lett.* 21 (5) (2023) 2825–2861, <https://doi.org/10.1007/s10311-023-01608-z>.
- [200] H. Yin, H. Yin, A. Wang, L. Shen, Catalytic conversion of glycerol to lactic acid over graphite-supported nickel nanoparticles and reaction kinetics, *J. Ind. Eng. Chem.* 57 (2018) 226–235, <https://doi.org/10.1016/j.jiec.2017.08.028>.
- [201] A. Namdeo, J.H. Jhaveri, S.M. Mahajani, A.K. Suresh, Palladium catalyzed liquid phase oxidation of glycerol under alkaline conditions - Kinetic analysis and modelling, *Chem. Eng. J.* 438 (2022), 135424, <https://doi.org/10.1016/j.cej.2022.135424>.
- [202] B. Katryniok, H. Kimura, E. Skrzyńska, J.-S. Girardon, P. Fongarland, M. Capron, R. Ducoulombier, N. Mimura, S. Paul, F. Dumeignil, Selective catalytic oxidation of glycerol: perspectives for high value chemicals, *Green Chem.* 13 (8) (2011) 1960–1979, <https://doi.org/10.1039/C1GC15320J>.
- [203] N. Kondamudi, M. Misra, S. Banerjee, S. Mohapatra, S. Mohapatra, Simultaneous production of glyceric acid and hydrogen from the photooxidation of crude glycerol using TiSi₂, *Appl. Catal. B* 126 (2012) 180–185, <https://doi.org/10.1016/j.apcatb.2012.05.006>.
- [204] Y. Ma, J. Gan, M. Pan, Y. Zhang, W. Fu, X. Duan, W. Chen, D. Chen, G. Qian, X. Zhou, Reaction mechanism and kinetics for Pt/CNTs catalyzed base-free oxidation of glycerol, *Chem. Eng. Sci.* 203 (2019) 228–236, <https://doi.org/10.1016/j.ces.2019.03.068>.
- [205] A. Wang, Q. Xu, H. Yin, Synthesis of lactic acid starting from glycerol catalyzed by CaO-supported CuO and metallic Cu catalysts in Ca(OH)₂ aqueous solution, *React. Kinet. Mech. Catal.* 135 (6) (2022) 3205–3221, <https://doi.org/10.1007/s11144-022-02328-1>.
- [206] E. Kano, T. Aihara, I.T. Ghampson, T. Nogami, H. Miura, T. Shishido, Continuous production of lactic acid from glycerol over bifunctional catalysts under base-free conditions using a liquid-phase flow reactor, *ACS Sustain. Chem. Eng.* 10 (37) (2022) 12072–12081, <https://doi.org/10.1021/acssuschemeng.2c00129>.
- [207] M.M.H. Coelho, N.W.S. Morais, T.J.T. Ferreira, F.S.S. Silva, E.L. Pereira, A.B. dos Santos, Carboxylic acids production using residual glycerol as a substrate in anaerobic fermentation: a kinetic modeling study, *Biomass Bioenergy* 143 (2020), 105874, <https://doi.org/10.1016/j.biombioe.2020.105874>.
- [208] C. Li, Y. Xiao, Z. Sang, Z. Yang, T. Xu, X. Yang, J. Yan, C.S.K. Lin, Inhibition kinetics of bio-based succinic acid production by the yeast *Yarrowia lipolytica*, *Chem. Eng. J.* 442 (2022), 136273, <https://doi.org/10.1016/j.cej.2022.136273>.
- [209] Paul Anastas, John Warner, *Green Chemistry: Theory and Practice*, Oxford University Press, New York, 2008.
- [210] A. Sandid, J. Esteban, C. D'Agostino, V. Spallina, Process assessment of renewable-based acrylic acid production from glycerol valorisation, *J. Clean. Prod.* 418 (2023), 138127, <https://doi.org/10.1016/j.jclepro.2023.138127>.
- [211] G.M. Lari, G. Pastore, M. Haus, Y. Ding, S. Papadokonstantakis, C. Mondelli, J. Pérez-Ramírez, Environmental and economical perspectives of a glycerol biorefinery, *Energy Environ. Sci.* 11 (5) (2018) 1012–1029, <https://doi.org/10.1039/C7EE03116E>.
- [212] X. Ge, H. Li, M. Liu, Z. Zhao, X. Jin, X. Fan, X. Gao, Microwave-assisted catalytic alcoholysis of fructose to ethoxymethylfurfural (EMF) over carbon-based microwave-responsive catalyst, *Fuel Process. Technol.* 233 (2022), 107305, <https://doi.org/10.1016/j.fuproc.2022.107305>.
- [213] K. Köhnke, N. Wessel, J. Esteban, J. Jin, A.J. Vorholt, W. Leitner, Operando monitoring of mechanisms and deactivation of molecular catalysts, *Green Chem.* 24 (5) (2022) 1951–1972, <https://doi.org/10.1039/D1GC04383H>.
- [214] A. Chakrabarti, M.E. Ford, D. Gregory, R.R. Hu, C.J. Keturakis, S. Lwin, Y.D. Tang, Z. Yang, M.H. Zhu, M.A. Banares, I.E. Wachs, A decade plus of operando spectroscopy studies, *Catal. Today* 283 (2017) 27–53, <https://doi.org/10.1016/j.cattod.2016.12.012>.